eman ta zabal zazu

Universidad del País Vasco
Euskal Herriko Unibertsitatea

SYNTHESIS AND CHARACTERIZATION OF HYBRID NANOMATERIALS BASED ON BLOCK COPOLYMERS AND MAGNETIC NANOPARTICLES

IRATI BARANDIARAN OLAETXEA

PhD PROGRAM RENEWABLE MATERIALS ENGINEERING

Chemical and Environmental Engineering Department

"Materials + Technologies" Group

Engineering College
Gipuzkoa

Directed by Galder Kortaberria

Donostia 2016

Azkenean tontorra,

Pasa dira urte batzuk mendi honen igoerari ekin niola, inguruan bidelagun ugariren laguntzarekin. Zaila da esatea noiz hasi zen bidea, baina badirudi tontorrera heldu naizela. Bide honen hasiera tesia burutzeko beka lortzearekin lotzea ere pasa zait burutik, baina horrek lagun, erabaki, une, etab. luze bat bidetik kanpo uztea ekarriko luke, eta ez nuke ez inor ez ezer bide honetatik kanpo utzi nahi.

Bidean zehar momentu gazi-gozoak egon dira eta tontorrera iritsi naizen honetan ez nuke hauetako bakarra ere ahaztu nahi, pasatako une guztiek egiten baitute berezi une hau.

Barne gogoeta ttiki honen ondoren heldu da eskerrak emateko unea ere.

Hasteko, eskerrak eman Galder Kortaberria doktoreari tesi hau burutu ahal izateko egindako gidari lanari esker; eskainitako laguntza, pazientzia eta denboragatik. Baita GMT taldeari ere, tesia burutzerakoan nire esku utzitako baliabide pertsonal, material eta tekniko guztiengatik. Aldi berean, ezin ahaztu Iñaki Mondragon zenak talde honetan sartzeko emandako aukera. Eta nola ez lau urte hauetan ondoan edukitako kideak ere (Eskerrik asko!, ¡Muchas Gracias!, Dziękuję!), emandako laguntza, gomendio eta ideiengatik, eta baita konpartitutako tertuliengatik ere.

Eskerrak eman nahiko nizkioke Euskal Herriko Unibertsitateari ere doktoretza tesia burutu ahal izateko emandako finantziazioagatik. Baita Technische Universität München (TUM)-eri ere, egonaldia bertan egiteko aukera emateagatik, eta bereziki Peter Müller-Buschbaum irakasle doktoreari, bere ikerketa taldean onartzeagatik eta emandako irakaspenengatik, eta E13 taldeko kide guztiei egonaldia esperientzia ahaztezin bilakatzeagatik (Danke!).

Eskerrak ere lagunei, hainbeste momentu on, anekdota, xelebrekeri, parranda, tertuli, etab.-engatik. Tesia zerren ingurukoa zen galdetzen zenidatenean, nire

azalpenak interes aurpegia jarriz entzuteagatik. Eskerrik asko! (atal honetan nahiago izenik ez aipatzea, asko zarete, eta ez nuke inor ahaztu nahi)

Zuei ere eskerrik asko, etxekoei, honaino iristen laguntzeagatik. Zuei eskerrik beroenak. Eskainitako pazientzia, laguntza, ulermen, babes, maitasun, etab. luze batengatik; sostengu izateagatik momentu zailetan, eta poztasunak elkarbanatzeagatik momentu alaietan: ama eta atte, Aratz eta Alaine, Ziortza eta Aingeru, eta nola ez azken aldian gure irribarre askoren protagonista izan den Onekari ere, eskerrik asko! Ezin ahaztu ere gainontzeko familiakoak, bereziki Txomin, Mari Mar eta Jone, partekatutako momentu guztiengatik. Lerro hauek ez nituzke amaitu nahi bidai honen amaieran izandako bidaidea ere aipatu gabe, eskerrik asko zuri ere Eñaut.

Badirudi iritsi naizela tontor honetara, bideak askotarako eman du, hurrengo tontorrerako bideak ere honek bezain beste emanen duelakoan, eskerrok asko denoi.

Zuekin beti oroitzen bainaiz
ahaztu naizenik ez pentsa
sentimenduak esaten baina
ez da hain gauza erreza

Badira hiru aste (Mikel Urdangarin)

SUMMARY

The aim of this work is to contribute to the development of nanotechnology in the generation of new nanocomposites based on block copolymers and magnetic nanoparticles. Several nanocomposites have been prepared, using different block copolymers as matrix and maghemite nanoparticles, modified with polymer brushes by different grafting methods, as fillers.

This work has been divided into 8 chapters. In Chapter 1 motivations and main objectives have been summarized. In Chapter 2 a bibliographic overview has been done in order to briefly introduce the main topics of this thesis: nanotechnology and nanomaterials, organic/inorganic nanocomposites, block copolymers, magnetic nanoparticles and polymer brushes.

In Chapter 3 nanocomposites based on PS-*b*-PCL copolymer and magnetic nanoparticles modified with PMMA-*b*-PCL by *grafting to* method have been synthesized and characterized.

In Chapter 4 nanocomposites based on PS-*b*-P4VP copolymer and magnetic nanoparticles modified with PS brushes by *grafting through* method have been prepared and characterized.

With the same grafting method, PMMA-modified magnetic nanoparticles have been dispersed in PS-*b*-PMMA copolymer, generating and characterizing obtained nanocomposites, as it is shown in Chapter 5. In this chapter nanocomposites with silanized nanoparticles have also been prepared in order to compare the effect of polymer brushes on dispersion level and morphology.

In Chapter 6 nanocomposites based on SBM triblock copolymer and PS- or PMMA-modified magnetic nanoparticles, obtained by *grafting through* method have been synthesized and characterized.

Grafting from method has been the method used for modifying magnetic nanoparticles with PMMA brushes in Chapter 7. Nanostructures generated by two different PI-*b*-PMMA copolymers with different annealing treatments have been analyzed, preparing nanocomposites with the selected one.

Finally, in Chapter 8 main conclusions extracted from this research have been summarized, possible future works related to this research have been recommended, and the list of scientific publications and conferences derived from this work have been included.

TABLE OF CONTENTS

Apendix

Chapter 1

MOTIVATION AND OBJECTIVES

1.1. MOTIVATION AND OBJECTIVES

Nanomaterials have attracted great interest in the last decades due to their potential application in many fields, resulting in an exponential increase of the research in this area. Among nanomaterials, those with magnetic properties have attracted special attention due to their applicability in different fields such as magnetic fluids, magnetic resonance imaging and data storage, among others.

Moreover, organic/inorganic nanocomposites based on block copolymer and inorganic nanoparticles are excellent candidates to cover the requirements of novel application fields such as nanoelectronics, photonics, energy-storing, catalysis, coatings and others.

For the synthesis and preparation of those nanocomposites, the precise control of the dispersion and localization of inorganic nanoparticles at nanoscale is a key point to reach the desired properties at the macroscale. Block copolymers are good matrixes to prepare this type of nanocomposites, due to their ability to self-assembly into nanometric scale. The possibility to form nanostructures is a helpful property to prepare organic/inorganic nanocomposites, as it can help the dispersion of the inorganic part. Moreover, for preparing nanocomposites with selectively placed inorganic nanoparticles, their functionalization with polymer brushes for increasing the compatibility with one of the copolymer domains is one of the efficient and used methods.

The main objectives of the investigation work related to this thesis are the following.

- Functionalization of magnetic nanoparticles with polymer brushes by three different methods: *grafting to*, *grafting through* and g*rafting from*

- Preparation of organic/inorganic nanocomposites based on block copolymers and magnetic nanoparticles, obtaining good dispersion and selective placement of nanoparticles into desired domains

- Transference of magnetic properties from nanoparticles to nanocomposites

Chapter 2

INTRODUCTION

2.1. NANOTECHNOLOGY AND NANOMATERIALS

Nanotechnology has attracted great attention all over the world, exciting the imagination of countless scientists. Interest in the subject has increased remarkably during the last years because of the potential scientific and technological applications, and also commercial interests (Romig et al. 2007). Nanotechnology can be seen in our daily lives, car tires, tennis rackets, solar cells, fuel cells and many more commercial and consume items. Nanotechnology has the potential to become the promising technological advancement of this century, offering remarkable potential in terms of applications and economic benefits. It is an interdisciplinar subject, a cross-disciplinary research where different science disciplines brings together as it can be seen in the Figure 2.1 (Tarafdar et al. 2013). This promising science encompasses different areas of general interest, like nanobiotechnology and allied science sectors; chemistry, environment and energy; or industries and engineering.

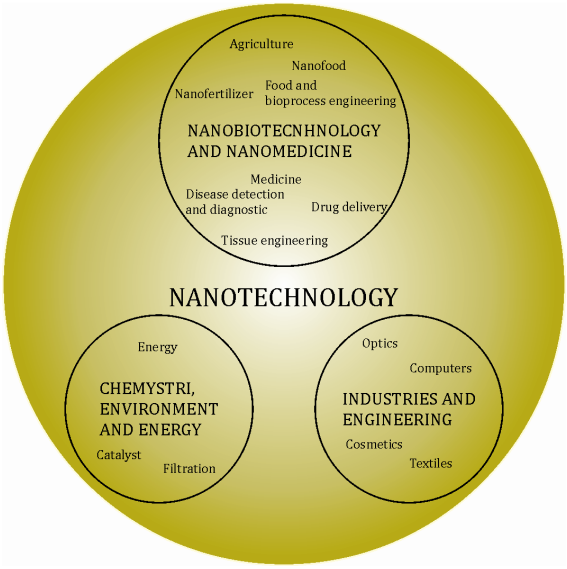

Figure 2.1. Interdisciplinarity of nanotecnhology

Trying to find a definition for nanotechnology is a controversial subject. In literature different definitions can be found for nanotechnology, being the

following an approach to include all the aspects: the design, characterization, production, and application of structures, devices, and systems by controlled manipulation of size and shape at nanometer scale (atomic, molecular, and macromolecular scale) that produces structures, devices, and systems with at least one novel/superior characteristic or property (Bawa et al. 2005).

Nanomaterials are categorized as those having structured components with at least one dimension less than 100 nm, and they can be classified depending on their geometry (Asmatulu 2013). Materials which have one dimension (1D) in the nanometer scale are generally referred as nanolayers, nanosheets, nanoflakes or nanoplatelets. The ones with two dimensions (2D) in the nanometer scale and a third dimension that could be in micro- or macroscale, form an elongated structure and are generally referred as nanotubes, nanorods or whiskers. Finally nanomaterials that have three dimensions (3D) in nanometer scale are generally referred as nanoparticles (NP), nanogranules or nanocrystals.

2.2. NANOCOMPOSITES

Nanocomposites are multiphase solid materials in which one of the phases has one, two or three dimensions of less than 100 nm, or structures having nano-scale repeating distances between the different phases that make up the material.

Different types of nanocomposites can be found. Depending on the presence of polymers as matrices they can be classified in two main groups: polymer-based nanocomposites and non-polymer based nanocomposites. The second group can be divided into: ceramic matrix and metal matrix nanocomposites. Ceramic nanocomposites have exceptional mechanical strength, toughness at room temperature and retention of high strength at elevated temperatures. Si_3N_4–SiC, Al_2O_3–SiC, Al_2O_3–Si_3N_4, Al_2O_3–TiC, B_4C–TiC, B_4C–TiB_2, MgO–SiC, CNT–ceramic, etc., are some of the important classes of ceramic nanocomposites (Maitra 2014).

On the other hand, composites with metallic matrix reinforced by nanoparticles are also promising materials, suitable for a large number of applications. Nanoparticles can improve the base material in terms of wear resistance, damping properties and mechanical strength. Different kinds of metals, predominantly Al, Mg and Cu, have been employed for the production of composites reinforced by ceramic nanoparticles such as carbides, nitrides, oxides as well as carbon nanotubes (Casati 2014).

2.2.1. ORGANIC/INORGANIC NANOCOMPOSITES

These nanocomposites are hybrid materials based on polymeric matrices (homopolymer or copolymer) that constitute the organic part, with nanoparticles or nanofillers dispersed on them. The addition of inorganic functional nanoparticles endows the nanocomposites with specific advantageous optical, conductive, electric, or magnetic properties (Gutierrez et al. 2009a, Xia et al. 2011, Etxeberria et al. 2014), for various fields of application such as photonic band gap materials, solar cells, sensors, and high-density magnetic storage devices (Bockstaller et al. 2005, Darling et al. 2005, Park et al. 2009, Jang et al. 2012). Among them, hybrid nanocomposites based on block copolymers can be underlayed.

The ability of block copolymers (BCP) to self-assemble into continuous nanostructures such as lamellar, cylindrical or spherical, among others, makes them excellent candidates for engineering the self-assembly of inorganic nanoparticles within nanodomains, in order to design periodic arrangements for materials with enhanced properties at the nanometer scale (Hoheisel et al. 2015). In the last years different works have been done related to nanocomposites based on block copolymer matrix and inorganic nanoparticles. Vural et al. produced stretchable elastic conductive fibers based on polystyrene-*block*-polyisoprene-*block*-polystyrene (SIS) block copolymer and silver nanoparticles (Ag) (Vural et al.

2015). Song et al. prepared nanocomposites based on block copolymers and gold nanoparticles (Au). They obtain well-ordered functional nanocomposites containing high loadings of large NPs with core diameters of over 15 nm (Song et al. 2015a), and also large volume of highly ordered arrays (single grains) on the order of millimeters in scale can be rapidly created through a unique innate guiding mechanism of brush block copolymers (BBCPs,) and long-range order was maintained in the presence of high loadings of functional additives such as gold NPs (Song et al. 2015b). Xu et al. prepared semiconducting organic/inorganic nanocomposites for potential applications in thermoelectric based on amphiphilic star-like PAA-*b*-PEDOT (poly(acrylic acid)-*block*-poly(3,4-ethylene dioxythiophene)) diblock copolymers as template for monodispersing PEDOT-functionalized telluride (PbTe) nanoparticles (Xu et al. 2015). Davidi and Shenhar placed disk-shaped nanoparticles into microphase separated polystyrene-*block*-poly(2-vinyl pyridine) (PS-*b*-P2VP) by confining metal precursors inside hierarchically-structured polymeric matrices (Davidi and Shenhar 2015). Magnetic inks stable over time, made of L10-ordered FePt nanoparticles, thiol-ended poly(ethylene glycol) methyl ether (mPEO-SH) compatibilizing macromolecules and asymmetric polystyrene-*block*-poly(ethylene oxide) (PS-*b*-PEO) copolymers as a subsequent self-organizing medium, were also prepared (Basly et al. 2015). Our group also has published different works on this topic; Garcia et al., for example, prepared self-assembled nanomaterials based on iron oxide magnetic nanoparticles modified by polystyrene (PS) brushes on polystyrene-*block*-polybutadiene-*block*-polystyrene (SBS) block copolymer (Garcia et al. 2008a), Etxeberria et al. modified CdSe nanoparticles with PS brushes to achieve a good placement of nanoparticles into SBS block copolymer (Etxeberria et al. 2013a), and Gutierrez et al. prepared nanocomposites based on polystyrene-*block*-poly(methyl methacrylate) (PS-*b*-PMMA) and TiO_2 by sol-gel process (Gutierrez et al. 2009b).

As it can be seen, research about organic/hybrid nanocomposites based on block copolymers and nanoparticles is still challenging and matter of many investigations.

2.3. BLOCK COPOLYMERS

Copolymers are macromolecules that consist on more than one sequence of monomer units with different chemical composition that are covalently bonded. When synthesizing copolymers different architectures such as random, di- or tri-block, graft, or star copolymer can be created (Figure 2.2).

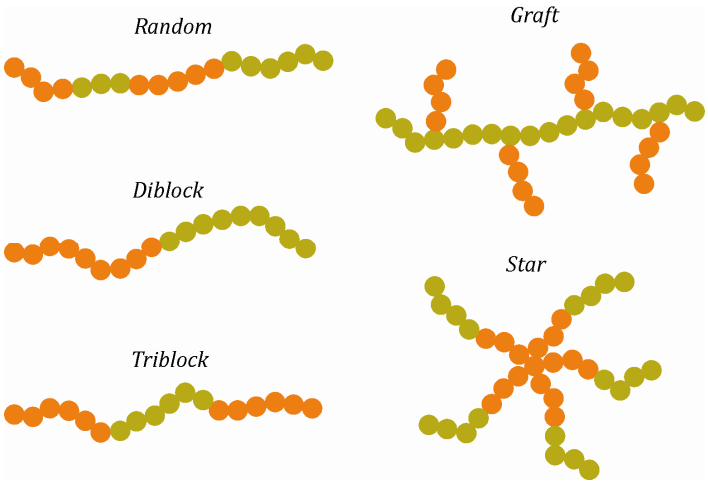

Figure 2.2. Different copolymer architectures

Due to the thermodynamic incompatibility between blocks that form the block copolymer, they can self-assemble in a wide variety of nanostructures, covalent linkage among blocks preventing the phase separation at macroscopic scale (Leibler 1980, Bates and Fredickson 1990, Hadjichristidis et al. 2003). This self-assembling capability has increased the scientific interest in block copolymers during the last years (Luo and Epps 2013, Singh et al. 2015, Yoo et al. 2015).

Morphologies of self-assembled block copolymers depend on several parameters such as copolymer composition (*f*), Flory-Huggins interaction parameter among blocks (χ) and polymerization degree of the copolymer (*N*). Most common morphologies obtained for diblock copolymers either in bulk or in thin films (Figure 2.3) are spheres, cylinders, gyroids and lamellas (Balsara 1999, Castelletto and Hamley 2004, Matsen and Bates 1996, Fasolka and Mayes 2001).

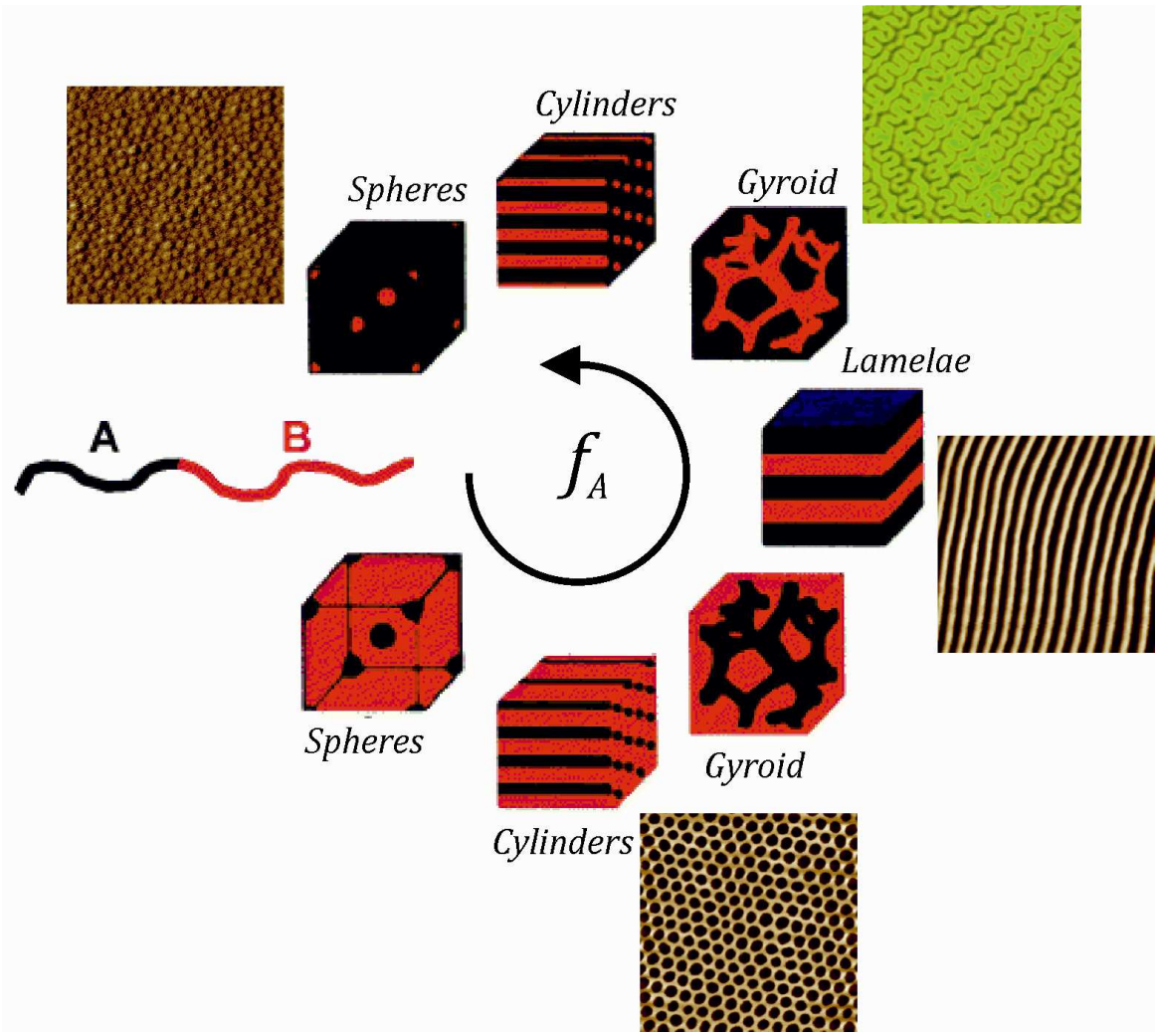

Figure 2.3. Diblock copolymer morphologies as a function of volume fraction of each segment (Adapted with permission from {Wu et al. 2015}. Copyright {2015} American Chemical Society)

The control of the long-range order and the orientation of the nanostructures in thin films have attracted much attention, as they could be used as templates for

nanoparticle deposition, nanolithography or nanopatterned materials (Lazzari and López-Quintela 2003, Jeong et al. 2013, Luo and Epps 2013, Sarkar and Alexandridis 2015). In order to obtain long-order nanostructured block copolymer thin films different techniques like thermal annealing, graphoepitaxy, electric field, spin-coating under in situ annealing, direct immersion, control of the molecular architecture or solvent vapor annealing (SVA) have been used (Shi et al. 2015, Jang et al. 2015, Kathrein et al. 2015, Modi et al. 2015, Jung et al. 2015, Wu et al. 2015, Baruth et al. 2014, Qian et al. 2014). Shi et al. used thermal annealing to obtain long-range ordering of body centered cubic (BCC) spheres with poly(dimethylsiloxane)-*block*-poly{2,5-bis[(4-butoxyphenyl) oxycarbonyl styrene]} (PDMS-*b*-PBPCS) diblock copolymer. Kathrein et al. used combined effect of the simultaneously applied graphoepitaxy and electric field on the self-assembly of cylinder forming polystyrene-*block*-poly(dimethylsiloxane) block copolymer thin film. One of the most investigated block copolymers have been PS-*b*-PMMA. Different methods have been studied to obtain the desired ordering of this block copolymer. Jung et al. used a procedure based on the spin-coating of a block copolymer solution in a low volatile solvent while thermal annealing with an halogen lamp in order to obtain well-ordered lamellar patterns; Modi et al. used direct immersion annealing, PS-*b*-PMMA block copolymer films were immersed in carefully selected mixtures of good and marginal solvents that can impart enhanced polymer mobility, while inhibiting film dissolution, enabling to obtain stable morphologies. Jang et al. obtained ordered nanostructures by controlling the molecular architecture of the block copolymer, using star-shaped PS-*b*-PMMA block copolymer to obtain vertically oriented lamellar and cylindrical nanodomains on various substrates. SVA is another promising method to obtain nanostructured block copolymer thin films. Recent year different works have demonstrated that SVA is a simple and good method for self-assembling block copolymers that overcomes some problems attached to thermal annealing, such as thermal degradation or slow dynamics due to high molar masses. For example, Baruth et al. used tetrahydrofuran (THF) vapors for annealing cylinder-forming

polystyrene-*block*-polylactide (PS-*b*-PLA) thin films, Qian et al. combined SVA method with soft shear to obtain aligned nanostructures with various BCP thin films, and Wu et al. examined the morphological evolution of gyroid-forming polystyrene-*block*-poly(*L*-lactide) (PS-*b*-PLLA) copolymer thin film with a solvent partially selective for PS.

For nanostructuring thin films by SVA, solvent election is of crucial importance. The solubility of both blocks in the solvent determines generated morphologies (Huang et al. 2012, Gotrik et al. 2012). The solubility of a non-polar polymer in a solvent is determined by the Flory-Huggins interaction parameter (equation 2.1), which can be obtained by the solubility parameter (equation 2.2) of the components. A polymer is considered to be soluble in a solvent if $\chi \leq 0.5$ (Van Krevelen 1989).

$$\chi \approx 0.34 + \frac{V}{RT}(\delta_P - \delta_S)^2 \tag{2.1}$$

$$\delta = \sqrt{\frac{E_{coh}}{V}} = \sqrt{\frac{\Delta H_V - RT}{V}} \tag{2.2}$$

Where R is ideal gas constant, T temperature, δ solubility parameter, E_{coh} cohesive energy and ΔH_V vaporization enthalpy. In the SVA method, BCP thin film can be exposed to neutral or selective solvent vapors. A solvent is considered neutral when it solves both blocks, while it is selective when it solves one of them. The exposure of a block copolymer thin film to solvent vapors has several effects on the block copolymer (and consequently on the generated morphologies), including an increase in volume and diffusivity, a decrease in the effective χ proportional to the amount of solvent, and a change in the effective f that depends on the swelling of each block by the solvent (Huang et al. 1998, Hanley et al. 2000). As it has been compiled in those lines, the effect of selective or neutral solvent on generated morphologies has been studied by several authors,

concluding that different domain orientations can be obtained depending on the solvent.

2.4. MAGNETIC NANOPARTICLES

Research related to nanoparticles attracts great interest. A bulk material should have constant physical properties regardless of its size, but at nano-scale size-dependent properties are often observed. Thus, properties of materials change as their size approaches the nanoscale and the percentage of atoms at the surface becomes significant.

Due to the size effect, nanoparticles often posses unexpected properties, like optical ones, as they are small enough to confine their electrons and produce quantum effects: quantum confinement in semiconductor particles (Nirmal and Brus 1998, Smith and Nie 2010), surface plasmon resonance in some metallic particles (Zhan et al. 2015, Song et al. 2013) and superparamagnetism in magnetic materials (Zucolotto et al. 2015, Kralj and Makovec 2015).

Magnetic nanoparticles (MNP) have attracted great interest for researchers from a wide range of disciplines, including magnetic fluids (Munoz-Menendez 2015), catalysis (Zhao and Liu 2015), biotechnology (Aseri et al. 2015), magnetic resonance imaging (Sun et al. 2008), data storage (Galloway et al. 2015), and environmental remediation (Mirshahghassemi and Lead 2015). Below a critical diameter value nanoparticles improve their performance; this value depends on the material. Below this value each nanoparticle becomes a single magnetic domain and shows superparamagnetic behavior when the temperature is above the blocking temperature (T_B). Individual nanoparticles have large constant magnetic moment (M) and behave like a giant paramagnetic atom with a fast response to applied magnetic fields with negligible remanence (M_R) (residual

magnetism) and coercivity (H_C) (the field required to bring the magnetization to zero).

The most studied **finite-size effects** in nanoparticles are the single-domain and superparamagnetic limit (Figure 2.4). Large magnetic particles have a multidomain structure, where regions of uniform magnetization are separated by domain walls. The formation of domain walls is a process driven by the balance between the magnetostatic energy (ΔE_{MS}), which increases proportionally to the volume of the materials, and the domain-wall energy (E_{dw}), which increases proportionally to the interfacial area between domains. If sample size is reduced, there is a critical volume below which more energy is needed to create a domain wall than for supporting the external magnetostatic energy (stray field) of the single-domain state. This critical diameter typically lies in the range of a few tens of nanometers and depends on the material.

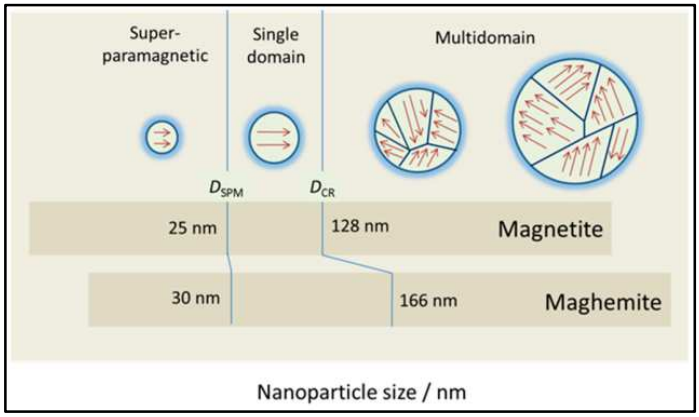

Figure 2.4. Magnetic regimes of magnetite and maghemite as a function of their size (superparamagnetic, single domain, multidomain) (Estelrich et al. 2015)

The critical diameter of a spherical particle (D_c), below which it exists in a single-domain state, is reached when $\Delta E_{MS}=E_{dw}$, which implies that $D_c \approx 18\frac{\sqrt{AK_{eff}}}{\mu_0 M_S^2}$, where A is the exchange constant, K_{eff} is anisotropy constant, μ_0 is the vacuum permeability, and M_s is the saturation magnetization.

The second phenomenum is the superparamagnetism. In order to understand the superparamagnetism, the behavior of a well-isolated singledomain particle should be considered. The magnetic anisotropy energy per particle, which is responsible for holding the magnetic moments along a certain direction, can be expressed by $E(\theta) = K_{eff} V \sin^2 \theta$, where V is the particle volume, K_{eff} anisotropy constant and θ is the angle between the magnetization and the easy axis.

The relaxation time of the moment of a particle, τ, is given by the Néel-Brown expression (equation 2.3), where k_B is the Boltzmann's constant, and $\tau_0 = 10^{-9} s$.

$$\tau = \tau_0 exp\left(\frac{K_{eff} V}{k_B T}\right) \tag{2.3}$$

If the particle magnetic moment reverses at shorter times than the experimental time scales, the system is in a superparamagnetic state and if not, it is in the blocked one. The temperature which separates both regimes is the blocking temperature, and can be calculated by considering the time window of the measurement. For example, the experimental measuring time with a magnetometer (roughly 100 s) results in a $T_B = \frac{K_{eff} V}{30 k_B}$. From this equation it is concluded that the blocking temperature depends on the effective anisotropy constant, the size of the particles, the applied magnetic field, and the experimental measuring time.

The blocking temperature can be calculated by direct current (DC) magnetometry measurements, with zero-field-cooled/field-cooled (ZFC/FC) procedure. The sample is first cooled from room temperature without magnetic field, then a small magnetic field is applied (about 100 Oe) and the magnetization is recorded on warming and in a magnetic field (ZFC). When room temperature is reached, maintaining the magnetic field the sample is again cooled, and the magnetization is recorded on warming again (FC). As temperature increases, the thermal energy disturbs the system and more moments acquire the energy to be aligned with the

external field direction. The number of unblocked, aligned moments reaches a maximum at T_B. Above the blocking temperature the thermal energy is strong enough to randomize the magnetic moments leading to a decrease in magnetization.

Another important parameter of magnetic nanoparticles that has to be analyzed is the **surface effect**. As the particles size decreases, a higher percentage of all the atoms in a nanoparticle are surface-atoms, which implies that surface and interface effects become more important. Owing to this large surface atoms/bulk atoms ratio, the surface spins make an important contribution to the magnetization. This local breaking of the symmetry might lead to changes in the band structure, lattice constant or/and atom coordination. Under these conditions, some surface and/or interface related effects occur, such as surface anisotropy and, under certain conditions, core-surface exchange anisotropy.

Various types of MNPs have been synthesized with different compositions and phases, including iron oxides (Pang et al. 2015), pure metals such as Fe and Co (Yang et al 2015, Abel et al. 2015), spinel-type ferromagnets such as $MgFe_2O_4$, $MnFe_2O_4$, and $CoFe_2O_4$ (Wan and Li 2015, Ibrahim et al. 2015), as well as alloys, such as $CoPt_3$ and FePt (Bahmanrokh et al. 2014, Jha et al. 2015). In the last decade, quite many investigations with different iron oxides as Fe_3O_4 (magnetite, $FeIIFeIII_2O_4$), α-Fe_2O_3 (hematite), γ-Fe_2O_3 (maghemite), FeO (wüstite,), ε-Fe_2O_3 or β-Fe_2O_3 (Teixeira et al. 2012), have been carried out in the field of MNPs. Among them magnetite and maghemite are the most promising and popular candidates. In this work **maghemite nanoparticles** have been used.

It is a technological challenge to control size, shape, stability, and dispersability of NPs in desired solvents. Magnetic iron oxide nanoparticles have a large surface-to-volume ratio and therefore possess high surface energies. Consequently, they tend to aggregate to minimize the surface energies. Therefore, providing a proper

surface coating and developing some effective protection strategies to keep the stability of magnetic iron oxide NPs becomes of crucial importance.

Also when preparing organic/inorganic nanocomposites based on block copolymer matrix the dispersion and placement of the nanoparticles into the desired nanodomains is crucial. To overcome the problem of the tendency of nanoparticles to aggregate and to facilitate their dispersion in a selected domain of a block copolymer different routes have been used. One of them is the use of surfactants. In that way, Ocando et al. used dodecanothiol as surfactant to get well dispersed nanocomposites based on SBS block copolymer and Ag nanoparticles (Ocando et al. 2011). The electrophoretic deposition of nanoparticles has been other of the used methods. In this way, Zhang et al. placed CdSe nanoparticles in diblock copolymer templates (Zhang et al. 2005). Also the so-called *in situ* approach (nanoparticles are directly synthesized within a block copolymer domain from metal precursors) has been used for incorporating inorganic nanoparticles into block copolymer nanostructures. Boontongkong and Cohen prepared nanocomposites based on polystyrene-*block*-poly(acrylic acid) (PS-*b*-PAA) copolymer and metallic nanoparticles of Pd, Cu, Au and Ag following this method (Boontongkong and Cohen 2002).

Another method to disperse and place nanoparticles into the desired nanodomain of a block copolymer is the use of polymer brushes on the surface of nanoparticles. In that way Kim et al. prepared nanocomposites based on PS-*b*-P2VP copolymer and Au nanoparticles. They investigated the effect of the grafting density of PS brushes on the nanoparticle surface in the placement of the nanoparticles on the copolymeric matrix. At low grafting densities nanoparticles tended to locate at the interfaces, while at higher graft density they were placed at polystyrene domain (Kim et al. 2006). Our group also has used polymer brushes to place different nanoparticles into desired domains of the BCP (Etxeberria et al. 2013a, Garcia et al. 2008a).

2.5. POLYMER BRUSHES

Polymer brushes consist on polymer molecules attached by one or some anchor points to a surface, in such a way that the grafting density of the polymers is high enough for the surface attached chains becoming crowded and stretched away from the surface (Advincula et al. 2004).

Polymer brushes can be classified regarding different criteria. The first classification depends on the substrate; one dimension, two dimension and three dimension polymer brushes, correspond to brushes grafted on linear polymer chains, planar surfaces or spherical particles, respectively. Another classification is based on chemical composition and architectures; homopolymer brushes, mixed homopolymer brushes, block copolymer brushes, and branched polymer brushes. Figure 2.5 shows different polymer brushes that can be generated onto different surfaces.

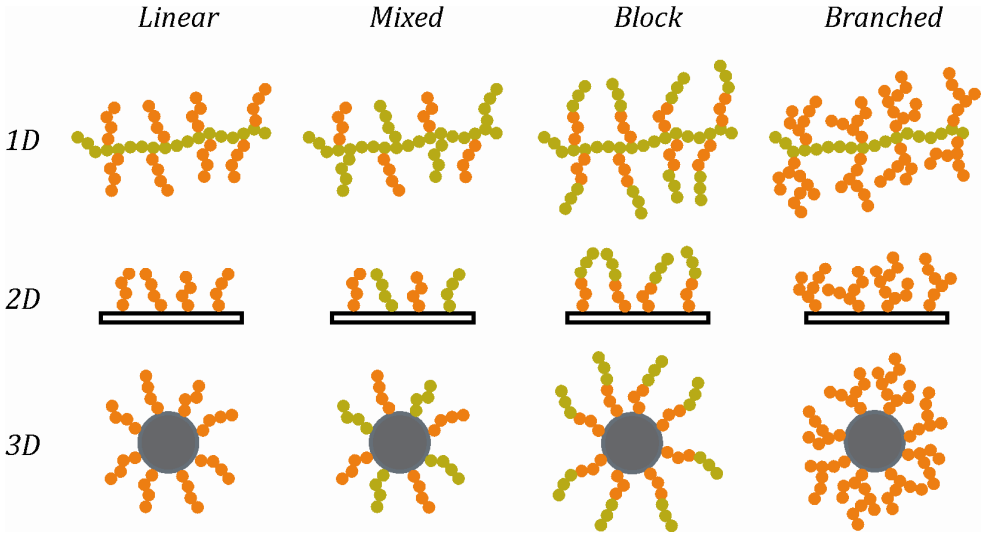

Figure 2.5. Different architectures of polymer brushes

Physisorption and chemical bonding are the most common techniques used to generate polymer brushes (Zhao and Brittain 2000). Physisorption consists of two component polymer chains, in which one part strongly adheres to the interface

while the other one extends to generate the polymer layer (Mittal 2012). In order to generate polymer brushes by physisorption functionalized polymer chains or diblock copolymers have been used (Yang et al. 2013). It is a reversible process due to its physical nature. The brushes are rendered thermally and solvolitically unstable.

On the other hand, different methods have been proposed to chemically bond a polymer to a surface (Figure 2.6) (Minko et al. 2002). So generated brushes are thermally and solvolitically stable. The first method is known as *grafting to*: polymers with suitable end-functional groups react with appropriate surface sites on the inorganic nanoparticles (Duwea et al. 2006, Sawal et al. 2004). This technique has a limitation on the choice of functional groups available for incorporating into the polymer because functional groups on the polymer can compete with the anchor moieties for surface sites. This point has important relevance if the aim is to immobilize functional polymers containing highly polar or charged groups onto polar surface, as the adsorption of functional groups into the surface can be strong and competes with chemisorption process (Minko et al. 2003). Another limitation is the thickness of the film, and accordingly the number of functional groups per surface area that can be obtained by using this approach. The rate of attachment reaction levels off rather quickly and further polymer is linked to the substrate only at an extremely slow rate due to the kinetic hindrance. Due to the inability of large polymer chains to diffuse to the reactive surface sites, they are sterically hindered by the surrounding bounded chains (Advincula et al. 2004).

The second method, *grafting through*, is a surface copolymerization through a covalently linked monomer. In this route the inorganic phase is incorporated inside the polymer chains (Rozes et al. 2005, Trabelsi et al. 2005, Etxeberria et al. 2013b, Henze at al. 2014). For a polymer layer generation through this method, the growth of polymer chains is initiated in solution. During propagation,

occasionally a surface-bound monomer unit can be integrated into the growing chains, which directly results in a permanent anchoring of the polymer chains. After that, chain growth can proceed and further free or surface attached units can be added to the growing chain. Despite the fact that such processes are widely applied, even in industrial applications mostly for adhesion promotion, from a scientific point of view *grafting through* approach has not been extensively explored and the details of the mechanism are not well understood.

In the third method, known as *grafting from*, polymer chains grow *in situ* from initiator molecules that have been pre-grafted onto the surface of the nanoparticles or from a surfactant (Pyun and Matyjaszewski 2001, Radhakrishnan et al. 2006, Garcia et al. 2008b, Xu et al. 2006).

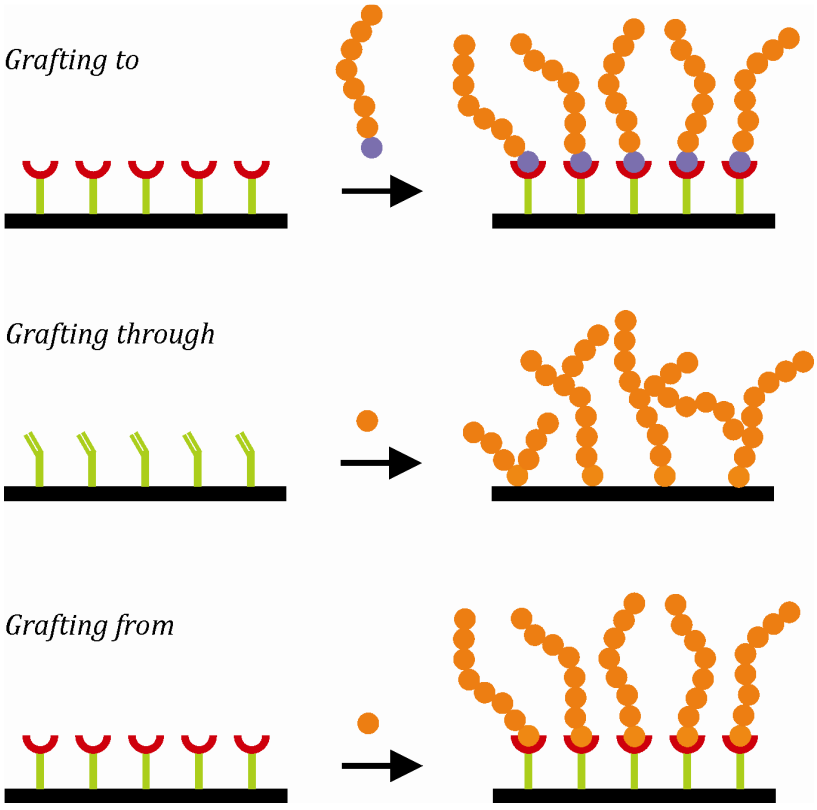

Figure 2.6. Different techniques for polymer brush grafting

To functionalize planar or nanoparticle surfaces following the *grafting from* method different polymerization techniques such as controlled radical

polymerization (CRP), ionic living polymerization or ring-opening polymerization have been used (Ilgach et al. 2014, Zhang et al. 2012, Li et al. 2014). But some issues like, poor control of molecular weight, polydispersity, end functionality, chain architecture and composition in the case of the CRP (Matyjaszewski and Davis 2002, Matyjaszewski 1996, Hsieh and Quirk 1996) or, stringent conditions and the small number of monomers that can be polymerized in ionic living polymerization method (Zhou et al. 2001, Sudo et al. 1999), are disadvantages that should be overcome. Following the aim of improving the CRP technique, controlled living radical polymerization methods have been developed, such as atom transfer radical polymerization (ATRP) (Kanhakeaw et al. 2015, Mao et al. 2015, Qin et al. 2015, Sun et al. 2015), reversible addition-fragmentation chain transfer (RAFT) (Ranka et al. 2015, Rossner et al. 2015) or nitroxide-mediated polymerization (NMP) (Mazurowski et al. 2013, Robbes et al. 2012, Chen et al. 2010).

It should be mentioned that in this work, three of the methods mentioned above have been used to functionalize nanoparticle surface, *grafting to*, *grafting from* and *grafting through*. For those iron oxide nanoparticles functionalized by *grafting from* method, ATRP has been used. ATRP is based on a multicomponent system, that is constituted by the monomer, initiator with a transferable (pseudo)halogen, and a catalyst (composed of a transition metal with a suitable ligand). Both activating and deactivating components of catalytic system must be simultaneously present (Hong et al. 2003). ATRP can be carried out in bulk or in solution (Li et al. 2004, Johnson et al. 2000). One of the most important advantages of ATRP is the large number of monomers that can be polymerized. ATRP has been used for the controlled polymerization of vinyl monomers such as styrenes (Xiaowei et al. 2012), acrylates (Cao et al. 2015), methacrylates (Junior et al. 2014), and other monomers which contain substituents capable of stabilizing propagation radicals.

2.6. REFERENCES

Abel F.M., Tzitzios V. and Hadjipanayis G.C., New approach for direct chemical synthesis of hexagonal Co nanoparticles. *Journal of Magnetism and Magnetic Materials* **2016,** 400, 286-289

Advincula R., Ruehe J., Brittain W. and Caster K., Polymer Brushes. Eds. VCH Wiley, Weinheim, **2004**

Aseri A., Garg S.K., Nayak A., Trivedi S.K. and Ahsan J., Magnetic Nanoparticles: Magnetic Nano-technology Using Biomedical Applications and Future Prospects. *Int. J. Pharm. Sci. Rev. Res* **2015**, 31, 119-131

Asmatulu R., Nanotechnology Safety. Elsevier, Amsterdam, **2013**

Bahmanrokh G., Hashim M., Matori K.A., Navasery M., Soltani N., Vaziri P., Kanagesan S., Sabbaghizadeh R. and Shafie M.S.E., Recording-media-related morphology and magnetic properties of crystalline CoPt3 and CoPt3-Au core-shell nanoparticles synthesized via reverse microemulsion. *Journal of Applied Physics* **2014**, 116, 093907

Balsara N.P., Kinetics of phase transitions in block copolymers. *Current Opinion in Solid State & Material Science* **1999**, 4, 553-558

Baruth A., Seo M., Lin C.H., Walster K., Shankar A., Hillmyer M.A. and Leighton C., Optimization of Long-Range Order in Solvent Vapor Annealed Poly(styrene)-*block*-poly(lactide) Thin Films for Nanolithography *ACS Appl. Mater. Interfaces* **2014**, 6, 13770-13781

Basly B., Alnasser T., Aissou K., Fleury G., Pecastaings G., Hadziioannou G., Duguet E., Goglio G. and Mornet S., Optimization of Magnetic Inks Made of L10-Ordered FePt Nanoparticles and Polystyrene-*block*-Poly(ethylene oxide) Copolymers. *Langmuir* **2015**, 31, 6675-6680

Bates F.S. and Fredickson G.H., Block copolymer thermodynamic: theory and experiment. *Annu Rev Phys Chem* **1990**, 41, 525-557

Bawa R., Bawa S.R., Maebius S.B., Flynn T. and Wei C., Protecting new ideas and inventions in nanomedicine with patents *Nanomedicine: Nanotechnology, biology and medicine* **2005**, 1, 150-158

Bockstaller M.R., Mickiewicz R.A. and Thomas E.L., Block copolymer nanocomposites: perspectives for tailored functional materials. *Adv. Mater.* **2005**, 17, 1331-1349

Boontongkong Y. and Cohen R. E., Cavitated block copolymer thin films. Lateral arrays on open nanoreactors. *Macromolecules* **2002**, 35, 3647-3652

Cao Y., Xu Y., Zhang J., Yang D. and Liu J., Well-controlled atom transfer radical polymerizations of acrylates using recyclable niobium complex nanoparticle as photocatalyst under visible light irradiation. *Polymer* **2015**, 61, 198-203

Casati R. and Vedani M., Metal Matrix Composites Reinforced by Nano-Particles-A Review. *Metals* **2014**, 4, 65-83

Castelletto V. and Hamley I.W., Morphologies of block copolymer melts. *Current Opinion in*

Solid State & Material Science **2004**, 8, 426-438

Chen Z., Yang Q., Peng K. and Guo Y., Surface-Initiated Nitroxide-Mediated Radical Polymerization of 4-Vinylpyridine on Magnetite Nanoparticles. J*ournal of Applied Polymer Science* **2011**, 119, 3582-3590

Darling S.B., Yufa N.A., Cisse A.L., Bader S.D. and Sibener S.J., Self-organization of FePt nanoparticles on photochemically modified diblock copolymer templates. *Adv. Mater.* **2005**, 17, 2446-2450

Davidi I. and Shenhar R., Synthesis of disk-shaped nanoparticle aggregates organized in hierarchical structures in block copolymer matrixes. *Polymer* **2015**, 64, 39-45

Duwez A.-S., Guillet P., Colard C., Gohy J.-F. and Fustin C.A., Dithioesters and Trithiocarbonates as Anchoring Groups for the "Grafting-To" Approach. *Macromolecules* **2006**, 39, 2729-2731

Estelrich J., Escribano E., Queralt J. and Busquets M.A., Iron Oxide Nanoparticles for Magnetically-Guided and Magnetically-Responsive Drug Delivery. *Int. J. Mol. Sci.* **2015**, 16, 8070-8101

Etxeberria H., Tercjak A., Mondragon I., Eceiza A. and Kortaberria G., Electrostatic force microscopy measurements of CdSe-PS nanoparticles and CdSe-PS/poly(styrene-b-butadiene-b-styrene) nanocomposites. *Collod Polym Sci* **2014**, 292, 229-234

Etxeberria H., Zalakain I., Fernandez R., Kortaberria G. and Mondragon I., Controlled placement of polystyrene-grafted CdSe nanoparticles in self-assembled block copolymers. *Colloid Polym Sci* **2013a**, 291, 633-640

Etxeberria H., Zalakain I., Mondragon I., Eceiza A. and Kortaberria G., Generation of nanocomposites based on polystyrene-grafted CdSe nanoparticles by grafting through and block copolymer. *Colloid Polym Sci* **2013b**, 291, 1881-1886

Fasolka M.J. and Mayes A.M., Block copolymer thin films: physics and applications. *Annu Rev Mater Res* **2001**, 31, 323-355

Galloway J.M., Talbot J.E., Critchley K., Miles J.J. and Bramble J.P., Developing Biotemplated Data Storage: Room Temperature Biomineralization of $L1_0$ CoPt Magnetic Nanoparticles. *Adv. Funct. Mater.* **2015**, 25, 4590-4600

Garcia I., Tercjak A., Gutierrez J., Rueda L. and Mondragon I., Nanostructuration via Solvent Vapor Exposure of Poly(2-vinyl pyridine-b-methyl methacrylate) Nanocomposites Using Modified Magnetic Nanoparticles. *J. Phys. Chem. C* **2008b**, 112, 14343-14347

García I., Tercjak A., Rueda L. and Mondragon I., Self-Assembled Nanomaterials Using Magnetic Nanoparticles Modified with Polystyrene Brushes and Poly(styrene-*b*-butadiene-*b*-styrene). *Macromolecules* **2008a**, 41, 9295-9298

Gotrik K.W., Hannon A.F., Son J.G., Keller B., Alexander-Katz A. and Ross C.A., Morphology control in block copolymer films using mixed solvent vapors. *AcsNano* **2012**, 6, 8052-8059

Gutierrez J., Tercjak A., Garcia I. and Mondragon I., The effect of thermal and vapor annealing treatments on the self-assembly of TiO2/PS-b-PMMA nanocomposites generated via the sol–gel process. *Nanotechnology* **2009b**, 20, 225603 (9pp)

Gutierrez J., Tercjak A., Peponi L. and Mondragon I., Conductive Properties of Inorganic

and Organic TiO2/Polystyrene-block-Poly(ethylene oxide) Nanocomposites. *J. Phys. Chem. C* **2009a**, 113, 8601-8605

Hadjichristidis N., Pispas S. and Fluodas G.A., Block copolymers: synthetic strategies, physical properties, and applications. Wiley-interscience, New Jersey, **2003**

Hanley K.J., Lodge T.P. and Huang C.-I., Phase behavior of a block copolymer in solvents of varying selectivity. *Macromolecules* **2000**, 33, 5918-5931

Henze M., Mädge D., Prucker O. and Rühe J., "Grafting Through": Mechanistic Aspects of Radical Polymerization Reactions with Surface-Attached Monomers. *Macromolecules* **2014**, 47, 2929-2937

Hoheisel T.N., Hur K. and Wiesner U.B., Block copolymer-nanoparticle hybrid self-assembly. *Progress in Polymer Science* **2015**, 40, 3-32

Hong S.H., Lutz J.-F., Inoue Y., Strissel C., Nuyken O. and Matyjaszewski K., Use of an Immobilized/Soluble Hybrid ATRP Catalyst System for the Preparation of Block Copolymers, Random Copolymers, and Polymers with High Degree of Chain End Functionality. *Macromolecules* **2003**, 36, 1075-1082

Hsieh H.L. and Quirk R.P., Anionic polymerization, principles and practical applications. Marcel Dekker, New York, **1996**

Huang C.-I, Chapman B.R., Lodge T.P. and Balsara N.P., Quantifying the "neutrality" of good solvents for block copolymers: poly(styrene-b-isoprene) in toluene, benzene, and THF. *Macromolecules* **1998**, 31, 9384-9386

Huang W.-H., Chen P.-Y. and Tung S.-H., Effects of annealing solvents on the morphology of block copolymer-based supramolecular thin films. *Macromolecules* **2012**, 45, 1562-1569

Ibrahim I., Ali I.O., Salamaa T.M., Bahgat A.A. and Mohamed M.M., Synthesis of magnetically recyclable spinel ferrite (MFe_2O_4, M = Zn, Co, Mn) nanocrystals engineered by sol gel-hydrothermal technology: High catalytic performances for nitroarenes reduction. *Applied Catalysis B: Environmental* **2016**, 181, 389-402

Ilgacha D.M., Meleshkoa T.K. and Yakimansky A.V., Methods of Controlled Radical Polymerization for the Synthesis of Polymer Brushes. *Polymer Science, Ser. C* **2015**, 57, 3-19

Jang S., Lee K., Moon H.C., Kwak J., Park J., Jeon G., Lee W.B. and Kim J.K., Vertical Orientation of Nanodomains on Versatile Substrates through Self-Neutralization Induced by Star-Shaped Block Copolymers. *Adv. Funct. Mater.* **2015**, 25, 5414-5419

Jang Y.H., Xin X., Byun M., Jang Y.J., Lin Z. and Kim D.H., An Unconventional Route to High-Efficiency Dye-Sensitized Solar Cells via Embedding Graphitic Thin Films into TiO_2 Nanoparticle Photoanode. *Nano Lett.* **2012**, 12, 479-485

Jeong S.-J., Kim J.Y., Kim B.H., Moon H.-S. and Kim S.O., Directed self-assembly of block copolymers for next generation nanolithography. *Materials Today* 16, **2013**, 468-476

Jha D.K., Varadarajan K.S., Patel A.B. and Deb P., Direct synthesis of water dispersible superparamagnetic TGA capped FePt nanoparticles: One pot, one shot. *Materials Chemistry and Physics* **2015**, 156, 247-253

Johnson R.M., Corbin P.S., Ng C. and Fraser C.L., Poly(methyl methacrylates) with

Ruthenium Tris(bipyridine) Cores via $NiBr_2(PR_3)_2$-Catalyzed Atom Transfer Radical Polymerization (ATRP). *Macromolecules* **2000**, 33, 7404-7412

Jung H., Woo S., Choe Y., Ryu D.Y., Huh J. and Bang J., Single Step Process for Self-Assembled Block Copolymer Patterns via in Situ Annealing during Spin-Casting. *ACS Macro Lett.* **2015**, 4, 656-660

Junior W.S., Emmler T., Abetz C., Handge U.A., dos Santos J.F., Amancio-Filho S.T. and Abetz V., Friction spot welding of PMMA with PMMA/silica and PMMA/silica-g-PMMA nanocomposites functionalized via ATRP. *Polymer* **2014,** 55, 5146-5159

Kanhakeaw P., Rutnakornpituk B., Wichai U. and Rutnakornpituk M., Surface-Initiated Atom Transfer Radical Polymerization of Magnetite Nanoparticles with Statistical Poly(tert-butyl acrylate)-poly(poly(ethylene glycol) methyl ether methacrylate) Copolymers. *Journal of Nanomaterials* **2015**, 2015, 121369

Kathrein C.C., Bai W., Currivan-Incorvia J.A., Liontos G, Ntetsikas K., Avgeropoulos A., Böker A., Tsarkova L. and Ross C.A., Combining Graphoepitaxy and Electric Fields toward Uniaxial Alignment of Solvent-Annealed Polystyrene-b-Poly(dimethylsiloxane) Block Copolymers. *Chem. Mater.* **2015**, 27, 6890-6898

Kim B. J., Bang J., Hawker C.J. and Kramer E.J., Effect of Areal Chain Density on the Location of Polymer-Modified Gold Nanoparticles in a Block Copolymer Template. *Macromolecules* **2006**, 39, 4108-4114

Kralj S. and Makovec D., Magnetic Assembly of Superparamagnetic Iron Oxide Nanoparticle Clusters into Nanochains and Nanobundles. *ACSNano* **2015**, 9, 9700-9707

Lazzari M. and López-Quintela M.A., Block copolymer as a tool for nanomaterial fabrication. *Adv. Mater.* **2003**, 15, 1583-1594

Leibler L., Theory of Microphase Separation in Block Copolymers. *Macromolecules* **1980**, 13, 1602-1617

Li M., Jahed N.M., Min K. and Matyjaszewski K., Preparation of Linear and Star-Shaped Block Copolymers by ATRP Using Simultaneous Reverse and Normal Initiation Process in Bulk and Miniemulsion. *Macromolecules* **2004**, 37, 2434-2441

Li W., Bao C., Wright R.A.E. and Zhao B., Synthesis of mixed poly(ε-caprolactone)/ polystyrene brushes from Y-initiatorfunctionalized silica particles by surface-initiated ring-opening polymerization and nitroxidemediated radical polymerization. *RSC Adv.* **2014**, 4, 18772-18781

Luo M. and Epps T.H., Directed Block Copolymer Thin Film Self-Assembly: Emerging Trends in Nanopattern Fabrication. *Macromolecules* **2013**, 46, 7567-7579

Maitra S., Nanoceramic matrix composites: types, processing and applications (Chapter 3) Advances in Ceramic Matrix Composites. Woodhead Publishing Limited, Cambridge, **2014**

Mao X., Sun H., He X., Chen L. and Zhang Y., Well-defined sulfamethazine-imprinted magnetic nanoparticles via surface-initiated atom transfer radical polymerization for highly selective enrichment of sulfonamides in food samples. *Anal. Methods*, **2015**, 7, 4708-4716

Matsen M.W. and Bates F.S., Unifying weak- and strong-segregation block copolymer

theories. *Macromolecules* **1996**, 29, 1091-1098

Matyjaszewski K. and Davis T.P., Handbook of Radical Polymerization Eds. VCHWiley: Weinheim. **2002**

Matyjaszewski K., Cationic polymerizations: mechanisms, synthesis and applications. Marcel Dekker, New York, **1996**

Mazurowski M., Sondergeld K., Elbert J., Kim C.J., Junyu Li , Frielinghaus H., Gallei M., Stühn B. and Rehahn M., Polystyrene Brushes on Fully Deuterated Organic Nanoparticles by Surface-Initiated Nitroxide-Mediated Radical Polymerization. *Macromol. Chem. Phys.* **2013**, 214, 1094-1106

Minko S., Müller M., Motornov M., Nitschke M., Grundke K. and Stamm M., Two-Level Structured Self-Adaptive Surfaces with Reversibly Tunable Properties. *J. Am. Chem. Soc.* **2003**, 125, 3896-3900

Minko S., Patil S., Datsyuk V., Simon F., Eichhorn K.-J., Motornov M., Usov D., Tokarev I. and Stamm M., Synthesis of Adaptive Polymer Brushes via "Grafting To" Approach from Melt. *Langmuir* **2002**, 18, 289-296

Mirshahghassemi S. and Lead J.R., Oil Recovery from Water under Environmentally Relevant Conditions Using Magnetic Nanoparticles. *Environ. Sci. Technol*. **2015**, 49, 11729-11736

Mittal V., Polymer Brushes: Substrates, Technologies and Properties. Taylor & Francis, Boca Raton, **2012**

Modi A., Bhaway S.M., Vogt B.D., Douglas J.F., Al-Eniz A., Elzatahry A., Sharma A. and Karim A., Direct Immersion Annealing of Thin Block Copolymer Films. *ACS Applied Materials & Interfaces* **2015**, 39, 21639-21645

Munoz-Menendez C., Conde-Leboran I., Baldomir D., Chubykalo-Fesenkob O. and Serantes D.,The role of size polydispersity in magnetic fluid hyperthermia: average vs. local infra/over-heating effects. *Phys. Chem. Chem. Phys.* **2015,** 17, 27812-27820

Nirmal M. and Brus L., Luminescence Photophysics in Semiconductor Nanocrystals. *Acc. Chem. Res*. **1999**, 32, 407-414

Pang Y.L., Lim S., Ong H.C. and Chong W.T., Research progress on iron oxide-based magnetic materials: Synthesis techniques and photocatalytic applications. *Ceramics International* **2016,** 42, 9-34

Park S., Lee D.H., Xu J., Kim B., Hong S.W., Jeong U., Xu T. and Russell T.P., Macroscopic 10-Terabit–per– Square-Inch Arrays from Block Copolymers with Lateral Order. *Science* **2009**, 323, 1030-1033

Pyun J. and Matyjaszewski K., Synthesis of Nanocomposite Organic/Inorganic Hybrid Materials Using Controlled/"Living" Radical Polymerization. *Chem. Mater.* **2001**, 13, 3436-3448

Qin L., Xu Y., Han H., Liu M., Chen K., Wang S., Wang J., Xu J., Li L. and Guo X., β-Lactoglobulin (BLG) binding to highly charged cationic polymer-grafted magnetic nanoparticles: Effect of ionic strength. *Journal of Colloid and Interface Science* **2015**, 460, 221-229

Radhakrishnan B., Ranjan R. and Brittain W.J., Surface initiated polymerizations from silica nanoparticles. *Soft Matter* **2006**, 2, 386-396

Ranka K., Brown P. and Hatton T.A., Responsive Stabilization of Nanoparticles for Extreme Salinity and High-Temperature Reservoir Applications. *ACS Appl. Mater. Interfaces* **2015**, 7, 19651-19658

Robbes A.-S., Cousin F., Meneau F., Chevigny C., Gigmes D., Fresnais J., Schweinse R. and Jestin J., Controlled grafted brushes of polystyrene on magnetic γ-Fe_2O_3 nanoparticles *via* nitroxide-mediated polymerization. *Soft Matter* **2012**, 8, 3407-3418

Romig Jr. A.D., Baker A.B., Johannes J., Zipperian T., Eijkel K., Kirchhoff B., Mani H.S., Rao C.N.R., and Walsh S., An introduction to nanotechnology policy: Opportunities and constraints for emerging and established economies. *Technological Forecasting & Social Change* **2007**, 74, 1634-1642

Rossner C., Glatter O., Saldanha O., Köster S. and Vana P., The Structure of Gold-Nanoparticle Networks Cross-Linked by Diand Multifunctional RAFT Oligomers. *Langmuir* **2015**, 31, 10573-10582

Rozes L., Fornasieri G., Trabelsi S., Creton C., Zafeiropoulos N.E., Stamm M. and Sanchez C.,Reinforcement of polystyrene by covalently bonded oxo-titanium clusters. *Progress in Solid State Chemistry* **2005,** 33, 127-135

Sarkar B. and Alexandridis P., Block copolymer–nanoparticle composites: Structure, functional properties, and processing. *Progress in Polymer Science* **2015**, 40, 33-62

Sawall D.D., Villahermosa R.M., Lipeles R.A. and Hopkins A.R., Interfacial Polymerization of Polyaniline Nanofibers Grafted to Au Surfaces. *Chem. Mater.* **2004**, 16, 1606-1608

Shi L.-Y., Li H., Lei W.-W., Ni W., Ran R., Pan Y., Fanb X.-H. and Shen Z., Extraordinary Boundary Morphologies of Large-Scale Ordered Domains of Spheres in Thin Films of a Narrowly Dispersed Diblock Copolymer via Thermodynamic Control. *Nanoscale* **2015**, 7, 17756-17763

Singh A.N., Thake R.D., More J.C., Sharma P.K. and Agrawal J.C., Block copolymer nanostructures and their applications: a review. *Polymer-Plastics Technology and Engineering* **2015**, 54, 1077-1095

Smith A.M. and Nie S., Semiconductor Nanocrystals: Structure, Properties, and Band Gap Engineering. *Acc. Chem. Res* **2010**, 43, 190-200

Song D.-P., Li C., Colella N.S., Xie W., Li S., Lu X., Gido S., Lee J.-H. and Watkins J.J.,Large-Volume Self-Organization of Polymer/Nanoparticle Hybrids with Millimeter-Scale Grain Sizes Using Brush Block Copolymers. *J. Am. Chem. Soc*. **2015**b, 137, 12510-12513

Song D.-P., Lin Y., Gai Y., Colella N.S., Li C., Liu X.-H., Gido S. and Watkins J.J., Controlled Supramolecular Self-Assembly of Large Nanoparticles in Amphiphilic Brush Block Copolymers. *J. Am. Chem. Soc.* **2015**a, 137, 3771-3774

Song J., Roh J., Lee I. and Jang J., Low temperature aqueous phase synthesis of silver/silver chloride plasmonic nanoparticles as visible light photocatalysts. *Dalton Trans*. **2013**, 42, 13897-13904

Sudo A., Uchino S. and Endo T., Development of a Living Anionic Polymerization of

Ethylphenylketene: A Novel Approach to Well-Defined Polyester Synthesis. *Macromolecules* **1999**, 32, 1711-1713

Sun C., Lee J.S.H. and Zhang M., Magnetic nanoparticles in MR imaging and drug delivery. *Advanced Drug Delivery Reviews* **2008**, 60, 1252-1265

Sun N., Meng X. and Xiao Z., Functionalized Si_3N_4 nanoparticles modified with hydrophobic polymer chains by surface-initiated atom transfer radical polymerization (ATRP). *Ceramics International* **2015**, 41, 13830-13835

Tarafdar J.C., Sharma S. and Raliya R., Nanotechnology: Interdisciplinary science of applications. *African Journal of Biotechnology* **2013**, 12, 219-226

Teixeira A.P.C., Tristão J.C., Araujo M.H., Oliveira L.C.A., Moura F.C.C., Ardisson J.D., Amorimd C.C. and Lago R.M., Iron: a Versatile Element to Produce Materials for Environmental Applications. *J. Braz. Chem. Soc*. **2012**, 23, 1579-1593

Trabelsi S., Janke A., Hässler R., Zafeiropoulos N.E., Fornasieri G., Bocchini S., Rozes L., Stamm M., Gérard J.-F. and Sanchez C., Novel Organo-Functional Titanium-oxo-cluster-Based Hybrid Materials with Enhanced Thermomechanical and Thermal Properties. *Macromolecules* **2005**, 38, 6068-6078

Van Krevelen D.W., Properties of Polymers. Elsevier Scientific Publishing Sons, New York, **1989**

Vural M., Behrens A.M., Ayyub O.B., Ayoub J.J. and Kofinas P., Sprayable Elastic Conductors Based on Block Copolymer Silver Nanoparticle Composites. *ACS NANO* **2015**, 9, 336-344

Wan C. and Li J., Synthesis of well-dispersed magnetic $CoFe_2O_4$ nanoparticles in cellulose aerogels via a facile oxidative co-precipitation method. *Carbohydrate Polymers* **2015**, 134, 144-150

Wu Y.-H., Lo T.-Y., She M.-S. and Ho R.-M., Morphological Evolution of Gyroid-Forming Block Copolymer Thin Films with Varying Solvent Evaporation Rate. *ACS Appl. Mater. Interfaces* 2**015**, 7, 16536-16547

Xia X., Metwalli E., Ruderer M.A., Körstgens V., Busch P., Böni P. and Müller-Buschbaum P., Nanostructured diblock copolymer films with embedded magnetic nanoparticles. *J. Phys.: Condens. Matter* **2011**, 23, 254203 (9pp)

Xiaowei Y., Yanwei Z., Tongxiang C. and Zhenxing H, Preparation of (Ba,Sr)TiO3@polystrene core-shell nanoparticles by solvent-free surface-initiated atom transfer radical polymerization. *Applied Surface Science* **2012**, 258, 7365-7371

Xu C., Ohno K., Ladmiral V. and Composto R.J., Dispersion of polymer grafted magnetic nanoparticles in homopolymers and block copolymers. *Polymer* **2008**, 49, 3568-3577

Xu H., Pang X., He Y., He M., Jung J., Xia H. and Lin Z., An Unconventional Route to Monodisperse and Intimately Contacted Semiconducting Organic/inorganic Nanocomposites. *Angew. Chem. Int. Ed.* **2015**, 54, 4636-4640

Yang Y., Zuo C.C., Zuo Y.X., Yu Y., Formation of Polymer Brushes with Diblock Copolymers on a Planar Surface. *Advanced Materials Research* **2013**, 705, 143-149

Yoo H.G., Byun M., Jeong C.K. and Lee K.J., Performance Enhancement of Electronic and

Energy Devices via Block Copolymer Self-Assembly. *Adv. Mater.* **2015**, 27, 3982-3998

Zhan Z., Xu R., Mi Y., Zhao H. and Lei Y., Highly Controllable Surface Plasmon Resonance Property by Heights of Ordered Nanoparticle Arrays Fabricated via a Nonlithographic Route. *ACSNano* **2015**, 9, 4583-4590

Zhang N., Luxenhofer R. and Jordan R., Thermoresponsive Poly(2-oxazoline) Molecular Brushes by Living Ionic Polymerization: Kinetic Investigations of Pendant Chain Grafting and Cloud Point Modulation by Backbone and Side Chain Length Variation. *Macromol. Chem. Phys.* **2012**, 213, 973-981

Zhang Q., Xu T., Butterfield D., Misner M. J., Ryu D. Y., Emrick T. and Russel T. P., Controlled placement of CdSe nanoparticles in diblock copolymer templates by electrophoretic deposition. *Nano Lett* **2005**, 5, 357-361

Zhao B. and Brittain W.J., Polymer brushes: surface-immobilized macromolecules. *Prog. Polym. Sci.* **2000**, 24, 677-710

Zhao X. and Liu X., A novel magnetic $NiFe_2O_4$@graphene–Pd multifunctional nanocomposite for practical catalytic application. *RSC Adv.* **2015**, 5, 79548-79555

Zhou Q., Fan X., Xia C., Mays J. and Advincula R., Living Anionic Surface Initiated Polymerization (SIP) of Styrene from Clay Surfaces. *Chemistry of Materials* **2001**, 13, 3057-3057

Zucolotto B., Pla Cid C.C., Isoppo E.A., Pasa A.A., Duque J.G.S. and Folly W.S.D., Reliable evaluation of magnetic properties of nanoparticle systems. *Appl. Phys.* **2015**, 118, 113903

Chapter 3

SYNTHESIS AND CHARACTERIZATION OF PS-*b*-PCL/Fe_2O_3-*g*-(PMMA-*b*-PCL) NANOCOMPOSITES: *grafting to* method

3.1. INTRODUCTION

Research about nanocomposites based on magnetic nanoparticles and BCP matrix have attracted great attention in the last years. Even if there are few works on other magnetic nanoparticles like cobalt oxide ones for example, with which Ahmed et al. prepared nanocomposites based on BCP analyzing their magnetic properties and morphology (Ahmed et al. 2004), most of the works related to block copolymer/magnetic nanoparticle nanocomposites are based on iron oxide or iron-containing nanoparticles. Following this current, Garcia et al. prepared nanocomposites based on poly(2-vinyl pyridine)-*block*-poly(methyl methacrylate) (P2VP-*b*-PMMA) and magnetite nanoparticles, obtaining nanostructured nanocomposites by solvent vapor annealing (Garcia et al. 2008). Xu et al. also used magnetite nanoparticles to prepare nanocomposites with PS-*b*-PMMA matrix. They analyzed the effect of the molecular weight of the poly(methyl methacrylate) (PMMA) brushes on the dispersion of nanoparticles through the BCP (Xu et al. 2008). Yao et al. investigated the effect of maghemite nanoparticle concentration on the morphology of polystyrene-*block*-poly(N-isopropylacrylamide) (PS-*b*-PNIPAM). In this system the addition of nanoparticles modified the nanostructure of the BCP, and when NPs were added in excess they accumulate at film surface (Yao et al. 2015). Aissou et al prepared nanocomposites based on PS-*b*-PEO and $L1_0$-ordered FePt nanoparticles, where nanoparticles were located at the spherical poly(ethylene oxide) PEO domains (Aissou et al 2013). Following this work, magnetic stable inks were prepared (Basly et al 2015) based on those systems. The size of nanoparticles has been found to have effect on their dispersion (Wu et al. 2014); they concluded that the dispersion state strongly depends on the ratio of the particle diameter to the lamellar thickness (l) of the polybutadiene (PB) domains, which further changes the phase separation of SBS. When $D_c/l \sim 0.5$, most of the nanoparticles were located at PB domains; if $D_c/l \sim 1$, NPs aggregate to form clusters of 100 to 300 nm in size, but within the clusters nanoparticles were

still selectively dispersed in PB domains instead of forming macroscopic phase separation. When D_c was larger than l, NPs were macroscopically separated from the SBS matrix to form clusters of hundreds of nanometers to several micrometers.

Polystyrene-*block*-poly(ε-caprolactone) (PS-*b*-PCL) is a versatile block copolymer that have attracted the interest of various authors. Zhang et al. analyzed the crystal growth of a symmetric PS-*b*-PCL (amorphous-crystaline) diblock copolymer (Zhang et al 2003). The crystallization of di and triblock copolymers based on poly(ε-caprolactone) (PCL) and PS with different configurations were investigated by Nakawaga et al. (Nakagawa et al. 2015). Copolymers based on PCL and PS are interesting on the formation of nanophases in epoxy thermosets via reaction induced microphase separation (RIPS) approach. Yu et al. studied different morphologies formed in epoxy thermosets by this copolymer, analyzing the effect of copolymer architecture on them (Yu et al. 2012). Xia et al. also studied the influence of PS-*b*-PCL block copolymer on the RIPS of epoxy/polyetherimide (PEI) blends (Xia et al. 2014).

As it was pointed out in Chapter 2, one of the techniques used for modifying nanoparticles with polymer brushes is the *grafting to*. Several works have been published on the use of this technique for nanoparticle modification. Wang et al. followed this method for grafting P(PEGMA)-*co*-PNIPAAm (poly(ethylene glycol) monomethacrylate (PEGMA)-*co*-N-isopropylacrylamide monomer) copolymer brushes to magnetic nanoparticle surfaces (Wang et al. 2008). Duwez et al. grafted presynthesized PS brushes to Au surfaces following this method (Duwez et al. 2006), while Sawal et al. grafted polyaniline nanofibers onto Au surfaces (Sawal et al. 2004). Also Hailu et al. used this technique to functionalize TiO_2 nanoparticles with PMMA-*b*-PS copolymer and analyzed their dispersion in PS or PMMA homopolymers, and PS-*b*-PMMA block copolymer. They obtained good dispersion in PMMA and PS-*b*-PMMA films, in contrast to poor dispersion in PS films. They

concluded that it could be because of the PMMA outer corona of the functionalized nanoparticles (Hailu et al. 2015).

The main objectives of the work described in this chapter are the following. Firstly, the complete characterization of the nanoparticles; then their functionalization with PMMA-*b*-PCL brushes by *grafting to* technique together with their characterization; and last, preparation and characterization of nanocomposites based on PS-*b*-PCL block copolymer and functionalized magnetic nanoparticles. Neat nanoparticles were characterized by Mössbauer spectroscopy and X-ray diffraction (XRD). Their functionalization was analyzed by Fourier transform infrared spectroscopy (FTIR), thermogravimetric analysis (TGA) and transmission electron microscopy (TEM). The morphology of obtained nanocomposites was studied by atomic force microscopy (AFM).

3.2. MATERIALS AND METHODS

3.2.1. MATERIALS

In this work maghemite (γ-Fe_2O_3) nanoparticles were used as inorganic filler. These nanoparticles have a nominal size of 10 nm and a polydispersity of 1.08. They were purchased from Integram Technologies. The silane used to be the link between the nanoparticles and the anchored copolymer brushes has been the 3-aminopropyl tryethoxysilane (APTS) one, purchased from Sigma-Aldrich, with a purity of 99 %. Poly(methyl methacrylate)-*block*-poly(ε-caprolactone) block copolymer with terminal chlorine group (*Cl*-PMMA-*b*-PCL) was used for grafting to the nanoparticles surface. This copolymer was synthesized by ATRP with a molecular weight per number (M_n) of 21,500 g/mol (f_{PMMA}= 0.7 and f_{PCL}= 0.3) and a polydispersity of 1.35. PS-*b*-PCL copolymeric matrix (f_{PS}= 0.7 and f_{PCL}= 0.3) was purchased from Polymer Source, Inc.. The molecular weights of PS and PCL blocks were 27,000 and 10,000 g/mol, respectively, with a polydispersity index of 1.25.

Chemical structures of silane, *Cl*-PMMA-*b*-PCL and PS-*b*-PCL can be seen in Scheme 3.1. Solvents used were toluene and THF, both purchased from Aldrich.

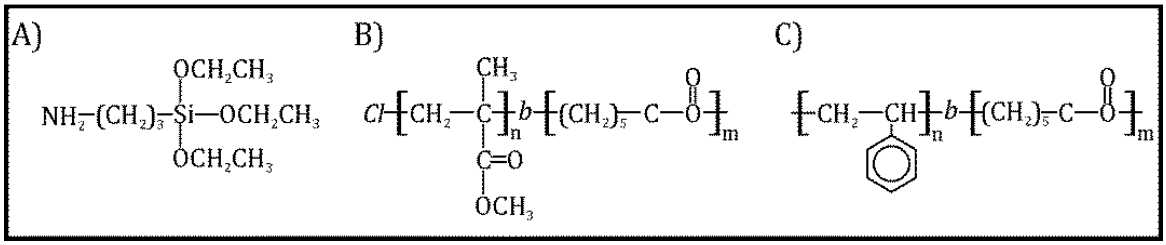

Scheme 3.1. Chemical structure of A) APTS, B) *Cl*-PMMA-*b*-PCL and C) PS-*b*-PCL copolymer

3.2.2. METHODS

3.2.2.1. Nanoparticle functionalization

Nanoparticle modification was carried out in two steps: first silanization process and then PMMA-*b*-PCL copolymer grafting to the silanized surface.

3.2.2.1.1. Silanization process

Fe_2O_3 magnetic nanoparticles were first modified with APTS. Scheme 3.2 shows the reaction of nanoparticles with silane. This reaction implies a nucleophilic attack of hydroxyl groups (-OH) at nanoparticle surface to the silicon (Si) atoms of APTS. In order to carry out the reaction extradry toluene, APTS and nanoparticles were mixed under sonication at inert atmosphere for 3 h at room temperature. After this, nanoparticles were subsequently washed six times with THF (assuring the complete removal of non-attached silane by FTIR) and then dried in vacuum at 40 °C for a period of 2 days. In order to obtain the best coverage different OH/APTS molar ratios were investigated: 1:1, 1:2, 1:3 and 1:5. As the highest silane grafting density was obtained for 1:3 ratio (as it will be shown below with TGA measurements), so modified nanoparticles were subsequently used for the grafting process.

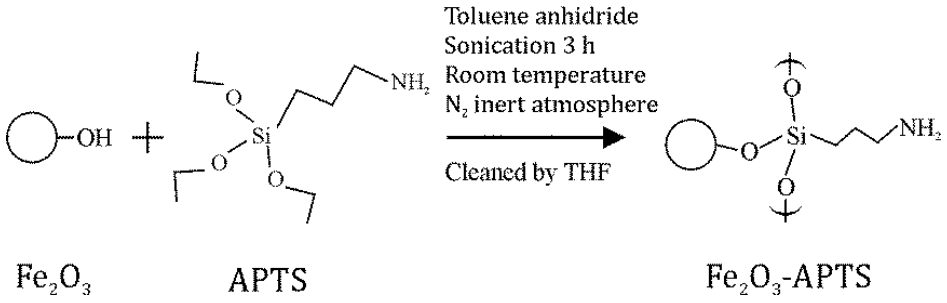

Scheme 3.2. APTS silanization reaction

3.2.2.1.2. Attachment of PMMA-*b*-PCL brushes by *grafting to* method

To finish with the functionalization of nanoparticle surface PMMA-*b*-PCL block copolymer was anchored to it by *grafting to* method. Scheme 3.3 shows the reaction of silanized nanoparticles with *Cl*-PMMA-*b*-PCL. The covalent linking among silanized nanoparticles and PMMA-*b*-PCL block copolymer (with terminal *Cl*- group) was carried out by an alkylation reaction of amine groups present at the surface of nanoparticles. Reaction was realized by preparing a solution with extradry toluene, silanized nanoparticles and copolymer. The grafting reaction was carried out at room temperature for 6 h with reflux. Functionalized nanoparticles were then cleaned repeatedly with THF (assuring the complete removal of non-grafted copolymer by FTIR) by centrifugation and then dried in vacuum at room temperature for 2 days. In order to obtain the highest grafting density different copolymer/silane molar ratios of 8, 11, 15 and 22 % were investigated. The highest grafting density was obtained for 15 % ratio, as it will be shown below with TGA measurements.

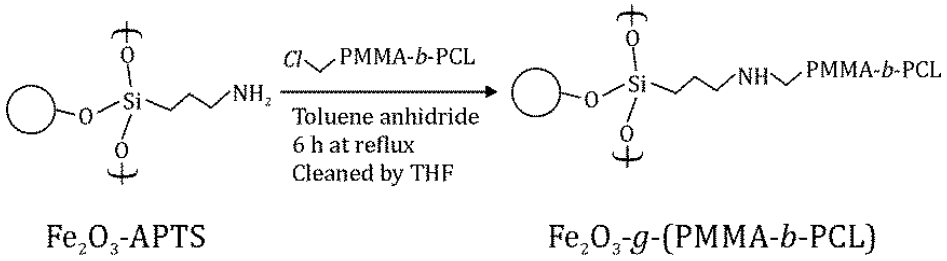

Scheme 3.3. PMMA-*b*-PCL copolymer anchoring by *grafting to* reaction

3.2.2.2. Nanocomposite preparation

To prepare PMMA-*b*-PCL-grafted iron oxide nanoparticles (Fe_2O_3-*g*-(PMMA-*b*-PCL)) and PS-*b*-PCL block copolymer-based nanocomposites, first the nanoparticles were dispersed into toluene. For this propose a mixture of nanoparticles and toluene was sonicated for 2 h. Once nanoparticles were dispersed, PS-*b*-PCL block copolymer was added to the solution. Then both neat block copolymer and organic/inorganic nanocomposites thin films were prepared by spin-coating onto silicon wafers (Si(100), from Si-Mat) at 2000 rpm for 120 s using a spin-coater P6700 from Specialty Coating Systems Inc.. Obtained neat block copolymer and nanocomposites films, were annealed at different temperatures under vacuum. Nanocomposites were prepared with 2 and 5 wt% of nanoparticles.

3.2.2.3. Characterization techniques

3.2.2.3.1. Mössbauer spectroscopy

Mössbauer spectroscopy is a versatile technique that can give very precise information about the chemical, structural, magnetic and time-dependent properties of a material. The key for the success of this technique is the discovery of recoilless γ-ray emission and absorption, referred as *Mössbauer Effect*. When the emitting and absorbing nuclei are bound in a solid, a certain fraction of γ-rays are emitted and absorbed with negligible energy loss due to recoil. This could be understood in the following way: the nucleus can behave as if it was rigidly bound to the solid such that the recoil is taken up by the entire solid. When this happens in both the source and absorber, the condition for resonant absorption of γ-rays is satisfied. The energy of nuclear transition must be large enough to give useful γ-ray photon, but not enough to cause recoil effect.

Nuclei in atoms undergo a variety of energy level transitions, often associated with the emission or absorption of a γ-ray. These energy levels are influenced by their surrounding environment, both electronic and magnetic, which can change or split them. These changes in the energy levels can provide information about the atom's local environment within a system and ought to be observed using resonance-fluorescence.

Resonance only occurs when the transition energy of the emitting and absorbing nuclei match exactly the effect of specific isotope. The relative number of recoil-free events (and hence the strength of the signal) is strongly dependent upon the γ-ray energy and so the Mössbauer effect is only detected in isotopes with very low lying excited states. Similarly the resolution is dependent upon the lifetime of the excited state. These two factors limit the number of isotopes that can be used successfully for Mössbauer spectroscopy. The most used is ^{57}Fe, which has both very low energy γ-ray and long-lived excited state, matching both requirements.

Mössbauer spectra were obtained in transmission geometry with a standard electromechanical spectrometer using a sinusoidal velocity waveform and a source of ^{57}Co in rhodium. The measurement was performed at 4.2 K in a liquid He bath cryostat, with the source and the absorber kept at the same temperature.

In this work Mössbauer spectroscopy was used to characterize the iron oxide nanoparticles, to determine the iron oxide type, Fe_3O_4 or Fe_2O_3.

3.2.2.3.2. XRD

XRD measurements were performed to identify the crystalline phases of the iron oxide nanoparticles. XRD is a useful technique for the fingerprint characterization of crystalline materials and the determination of their structure. Each crystalline solid has its unique characteristic X-ray powder pattern which may be used as a "fingerprint" for its identification. Once the material has been identified, X-ray

crystallography may be used to determine its structure, i.e. how the atoms pack together in the crystalline state and what the interatomic distance and angle are.

XRD was carried out on PANalytical Xpert PRO diffractometer, equipped with a copper tube ($\lambda Cu_{K\alpha average}$=1,5418 Å, $\lambda Cu_{K\alpha 1}$=1,54060 Å y $\lambda Cu_{K\alpha 2}$=1,54439 Å), vertical goniometer (Bragg-Brentano geometry), programmable divergence slit, automatic sample exchanger, secondary graphite monochromer and PixCel detector. Source was set to 40 kV and 20 mA and the samples were examined over the angular range (2θ) of 5 to 70°. The obtained patterns were compared to the diffraction dataset cards from the Joint Committee on Powder Diffraction Standards (JCPDS).

3.2.2.3.3. FTIR

FTIR was used to verify if the iron oxide nanoparticles had been modified properly. Infrared spectra were carried out in a Nicolet Nexus 670 Spectrometer.

The infrared portion of the electromagnetic spectrum is divided into three regions; the near-, mid- and far-infrared, named for their relation to the visible spectrum. The far-infrared, (approx. 400-10 cm^{-1}) lying adjacent to the microwave region, has low energy and may be used for rotational spectroscopy. The mid-infrared (approx. 4000-400 cm^{-1}) may be used to study the fundamental vibrations and associated rotational-vibration structure, whilst the higher energy near-infrared (14000-4000 cm^{-1}) can excite overtone or harmonic vibrations. Infrared spectroscopy works because chemical bonds have specific frequencies at which they vibrate corresponding to energy levels. The resonant frequencies or vibration frequencies are determined by the shape of the molecular potential energy surfaces, the masses of the atoms and, eventually by the associated vibronic coupling. In order to a vibration mode in a molecule to be infrared active, it must be associated with changes in the permanent dipole. Complex molecules

may have many bonds, and vibrations can be conjugated, leading to infrared absorptions at characteristic frequencies that may be related to chemical groups. In order to measure a sample, a beam of infrared light is passed through the sample, and the amount of energy absorbed at each wavelength is recorded. This may be done by scanning through the spectrum with a monochromatic beam, which changes in wavelength over time, or by using a Fourier transform instrument to measure all wavelengths at once. From this, a transmittance or absorbance spectrum may be plotted, which shows at which wavelengths the sample absorbs the infrared radiation, and allows the interpretation of which bonds are present.

In this work the nanoparticles were pressed together with KBr to form pellets that were analyzed through the signal averaging 32 scans at a resolution of 2 cm^{-1} in a wavenumber range from 4000 to 400 cm^{-1}.

3.2.2.3.4. TGA

TGA was used to determine the hydroxyl density of the nanoparticle surface, the amount of the grafted silane and grafted copolymer brushes. TGA analysis results were obtained using a TGA/SDTA-851e equipment scanning from 25 to 800 °C at a heating rate of 10 °C/min under N_2 atmosphere for avoiding the atmospheric oxidation.

3.2.2.3.5. TEM

TEM measurements were used to analyze the nanoparticles, before and after modification. TEM is a microscopy technique in which a beam of electrons is transmitted through an ultra-thin specimen, interacting with it as it passes through. An image is formed from the interaction of the electrons transmitted through the specimen; the image is magnified and focused onto an imaging device.

In this work a drop of nanoparticle solution was laid on a copper formvard and dried. The used equipment was a Philips Tecnai 20 transmission electron microscopy operating at 200 kV with a resolution of 2.5 Å.

3.2.2.3.6. AFM

The morphologies of neat block copolymers and PS-*b*-PCL/Fe_2O_3-*g*-(PMMA-*b*-PCL) nanocomposite thin films were studied at room temperature by AFM. It is a subdivision of a more general group of scanning force microscopy (SFM) methods in which a sample surface is scanned with a probe and interactions between probe and sample are monitored (Magonov et al. 1997; Veeco Manual 2005). The probe of the AFM is a flexible cantilever (100 to 200 μm long) with a tip (couple of microns long) attached to its underside. Additionally, this technique allows investigating the properties of materials since Van der Waals, friction, electrostatic and magnetic forces interactions can be sensed using AFM. AFM measurements can be performed in three different modes: contact mode (CM), tapping mode (TM) and noncontact mode. To choose adequate AFM mode the surface characteristics and the hardness/stickiness of the investigated materials should be taken into account.

Figure 3.1 illustrates the working concept of an atomic force microscope. A cantilever with a sharp tip is positioned above a surface. Depending on this separation distance, long range or short range forces dominate the interaction. Those forces are measured by the bending of the cantilever by an optical lever technique: a laser beam is focused on the back of a cantilever and follows all their movements reflecting them into a photodetector. Small forces between the tip and sample cause lower deflection than higher forces. The tip scans across the surface recording the change in forces as a function of position. Consequently, a map of surface topography and other properties can be detected.

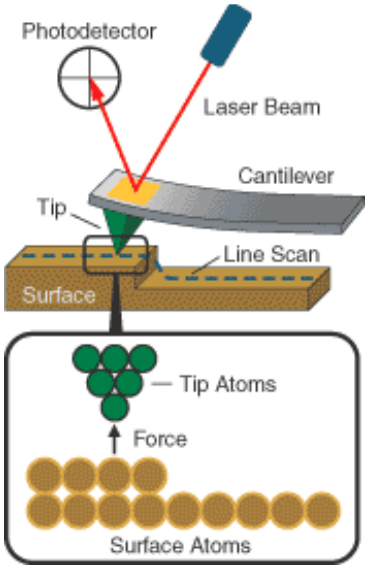

Figure 3.1. Schematic model AFM

In this study AFM measurements were performed in tapping mode using a Bruker's Dimension Icon Nanoscope V. This operating method is usually applied for analyzing the morphology of soft materials. Additionally, the primary advantage of the TM is that the lateral forces between the tip and the sample can be eliminated, which greatly improves the image resolution.

In this mode the tip is scanned over the sample surface maintaining a distance of 1-10 nm between them. Consequently, the cantilever oscillates close to its resonance frequency maintaining constant oscillation amplitude. An electronic feedback loop ensures that the oscillation amplitude remains constant; as a result constant tip-sample interactions are maintained during scanning. Forces that act between the sample and the tip can not only cause a change in the oscillation amplitude, but also a change in the resonance frequency and phase of the cantilever. The oscillation amplitude is used as a feedback signal and the vertical adjustments (changes in coordinate z) of the piezo driver allow taking the topographic (height) image. The phase lag of the cantilever oscillation, related with the signal sent to the piezo driver of the cantilever allows the simultaneous monitoring of the phase images. This phase shift can be correlated with specific material properties that affect the tip/sample interaction. Consequently, the phase

shift can be used to differentiate areas on a sample with different friction, adhesion, or viscoelasticity properties (Veeco Manual 2005).

In this investigation, etched single beam cantilevers (110-140 μm length) composed by silicon nitride probes having a tip with nominal radius of 10 nm were used. Scan rates were ranged from 0.7 to 1.2 Hz/s. Measurements were performed with 512 scan lines and target amplitude around 0.9 V. Height and phase images were recorded simultaneously. Different regions of the specimens were scanned to ensure that the morphology of the investigated material was the representative one.

3.3. RESULTS AND DISCUSSION

3.3.1. NANOPARTICLE CHARACTERIZATION

In this thesis the first step is the characterization of the nanoparticles that will be used during all work. The proper characterization of the nanoparticles is vital for the right evolution of the thesis. Nanoparticles were characterized by Mössbauer spectroscopy and XRD.

Mössbauer spectroscopy measurements were carried out to determine the structure and type of iron oxide magnetic nanoparticle, whether the nanoparticles are Fe_2O_3 or Fe_3O_4 type.

The structure of iron oxides can be described as ABO_x. In Fe_2O_3 both A and B are trivalent (Fe^{3+}) iron, but in the case of Fe_3O_4 A is also Fe^{3+}, but B is a mixture of di and trivalent (Fe^{2+} and Fe^{3+}) iron. By Mössbauer spectroscopy (Figure 3.2) it is possible to determine if the analyzed sample has only trivalent iron ion or has a mixture of di and trivalent ions; what would determine if nanoparticles are Fe_2O_3 or Fe_3O_4.

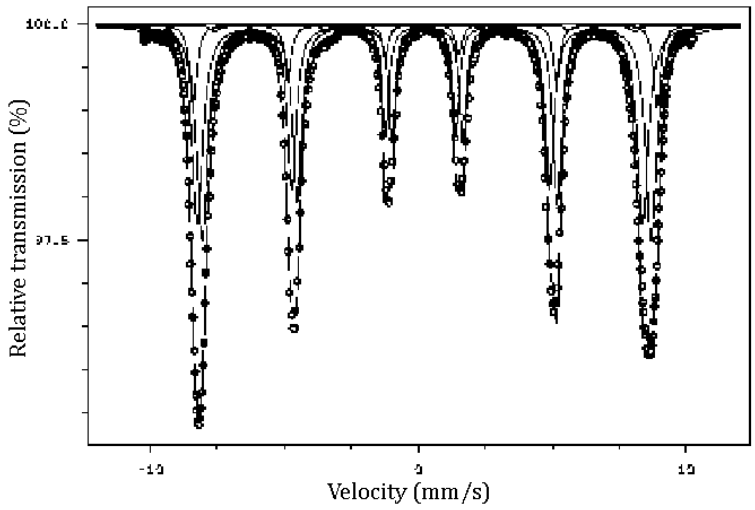

Figure 3.2. Mössbauer spectroscopy of Fe_2O_3 nanoparticle

Mössbauer spectrum exhibits a magnetic sextet, which matches the standard feature of γ-Fe_2O_3, and thereby allows for a distinct identification of the type of iron oxide nanoparticle. The measured spectrum (dots) has been fitted by the software Mos90 with two Lorentzian distribution lines. The two Lorentzian distribution curves indicate two different Fe^{3+} lattice constructions of octahedral and tetrahedral individually, not showing any curve indicating the presence of Fe^{2+}.

In Figure 3.3 the XRD diffraction patterns of the iron oxide nanoparticles are represented. These results have been superimposed with the best match patterns found in the International Center for Diffraction Data.

X-ray diffraction analysis revealed that the iron oxide magnetic nanoparticles are γ-Fe_2O_3 ones, as the diffraction peaks at 2θ=30.29°, 35.72°, 53.90°, 57.45° and 63.07°, corresponding to the reflection of the (220), (311), (400), (422), (511) and (440) planes, respectively, match with the characteristic peaks of the maghemite.

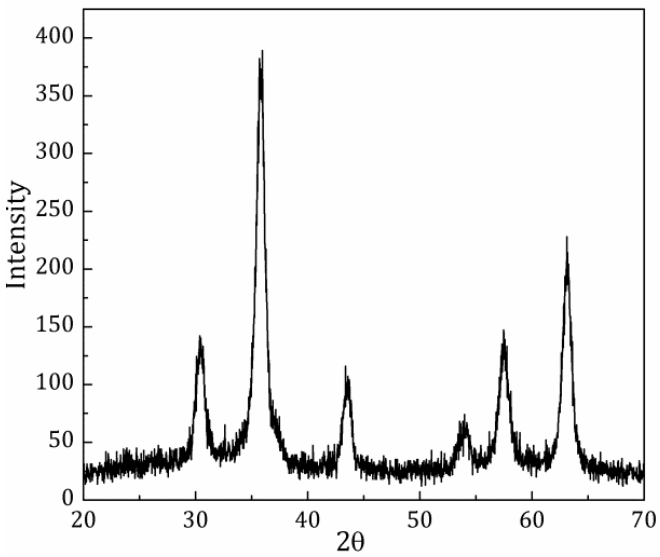

Figure 3.3. XRD patter of γ-Fe_2O_3 nanoparticles

3.3.2. CHARACTERIZATION OF FUNCTIONALIZED NANOPARTICLES

The surface functionalization of the iron oxide nanoparticles have been analyzed by FTIR, TGA and TEM.

In Figure 3.4 the FTIR spectra of pristine nanoparticles, silanized and PMMA-*b*-PCL copolymer-grafted nanoparticles can be seen. The broad peaks around 3400 cm^{-1} can be attributed to O-H bonds of nanoparticle hydroxyl groups (Sabuncu and Çulha 2015, George et al. 2015). The other two peaks at 633 and 558 cm^{-1}, which can be found in the three spectra, are due to the Fe-O bond (Jing 2006, Abboud et al. 1997). As it can be seen, there is a complete absence of any carbon-related peaks, this showing that nanoparticles are surfactant-free.

The success of the reaction between the hydroxyl groups and APTS has also been confirmed by FTIR. In the infrared spectrum of silanized nanoparticles at Figure 3.4, the characteristic absorption bands of the aminopropyl groups can be seen, bending of -NH_2 at 1635 cm^{-1} (Chen and Yakovlev 2010), the stretching vibration of Fe-O (633 and 558 cm^{-1}) and Si-O bonds (1103 and 1024 cm^{-1}) together with the bands related to aliphatic C-H bonds (1461 cm^{-1}) (Marutani et al. 2004). These

experimental findings strongly suggest that APTS indeed reacted with the surface OH groups. However, the presence of the peak related with O-H bonds for modified nanoparticles seems to indicate that not all hydroxyl groups have reacted, as has been determined by TGA and will be shown below.

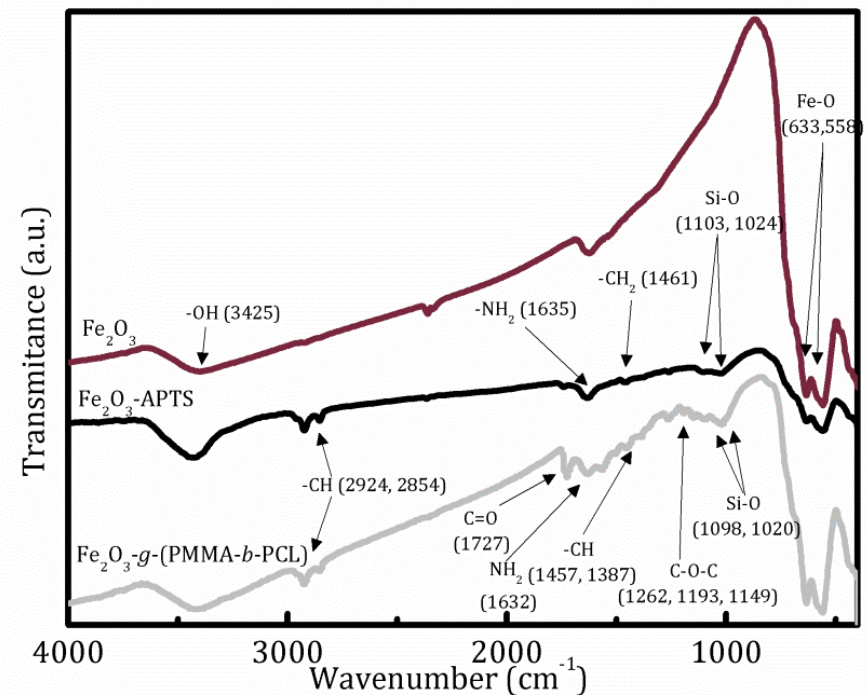

Figure 3.4. FTIR spectra of pristine, silanized and PMMA-*b*-PCL-grafted nanoparticles

The grafting of the PMMA-*b*-PCL copolymer to the surface of the nanoparticle through the previously anchored silane has also been demonstrated. In the infrared spectrum of copolymer-grafted nanoparticles, the presence of the band related to the stretching vibrations of carbonyl group at 1727 cm^{-1} (George et al. 2015), and that corresponding to C-O-C single bond stretching deformation vibration at 1262, 1193 and 1149 cm^{-1} (Shingo et al. 2012) present in both PMMA and PCL blocks can be seen, suggesting that copolymer has been successfully grafted to the silanized nanoparticle surface.

Figure 3.5 shows the weight loss of pristine, silanized and copolymer-grafted Fe_2O_3 nanoparticles as obtained from TGA measurements. The weight loss of the unmodified nanoparticles is related to physisorbed water and the hydroxyl groups

present at their surface. The physisorbed water is lost between 25 and 150 °C, while the hydroxyl groups are degraded between 150 and 850 °C (Cosio-Castañeda et al. 2014). For silanized nanoparticles, a significant weight loss starts at around 300 °C, related with the decomposition of the aminopropil group of silane (Marutani et al. 2004), this weight loss has been used for the determination of APTS surface density. When the copolymer is anchored to the nanoparticle, different weight loss steps are observed. Besides silane decomposition, thermal decomposition of copolymer can be seen: the decomposition of PCL block occurs in a single step between 200 and 350 °C (Galeotti et al. 2011), while main thermal decomposition for PMMA occurs at around 400 and 600 °C (Rana et al. 2009).

The quantity of hydroxyl groups on the surface has been determined using TGA results, according to the method of Abboud et al. (Abboud et al. 1997). The specific surface area of magnetic nanoparticles measured by Brunauer Emmett and Teller (BET) method has been estimated to be 102 m^2/g. The surface density of hydroxyl groups was found to be 5.5 OH/nm^2. After modification, the amount of grafted silane has been determined by TGA (Bartholome et al. 2003). The surface density of the silane is about 1.9 $molecules/nm^2$. A direct comparison of the surface density of hydroxyl groups and that of the silane on the surface yield a reaction efficiency of 35.8 %. Those data were measured for nanoparticles modified with 1:3 OH/APTS molar ratio, which has given the highest silane density and efficiency. For this reason, 1:3 ratio have been chosen for nanoparticle silanization. TGA measurements have been also used to quantify the grafting density of PMMA-*b*-PCL anchored to nanoparticles (Ohno et al. 2002). The highest graft density (0.04 $chains/nm^2$) was found for 15 % copolymer/APTS molar ratio, while the rest of molar ratios used gave lower densities. So the nanoparticles with the highest grafting density of 0.04 $chains/nm^2$ have been used for nanocomposite preparation.

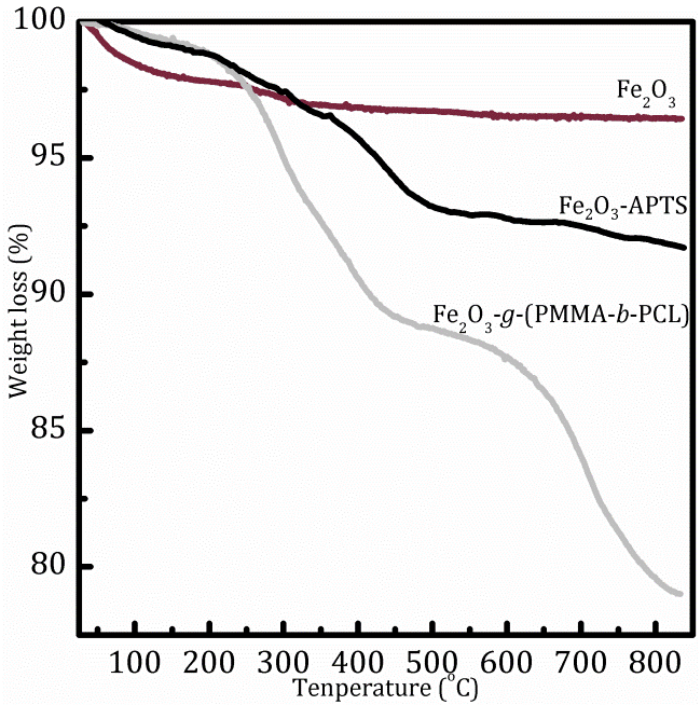

Figure 3.5. TGA thermograms of pristine, silanized and PMMA-*b*-PCL-grafted nanoparticles

TEM measurements have been also used for nanoparticle characterization before and after modification reactions. Figure 3.6 shows TEM images of both unmodified and copolymer-grafted nanoparticles. It can be seen that during grafting process nanoparticles tend to aggregate and the modification does not occur around a single nanoparticle but around small aggregates, around which the copolymer can be seen. The average size of aggregates is between 20 and 40 nm.

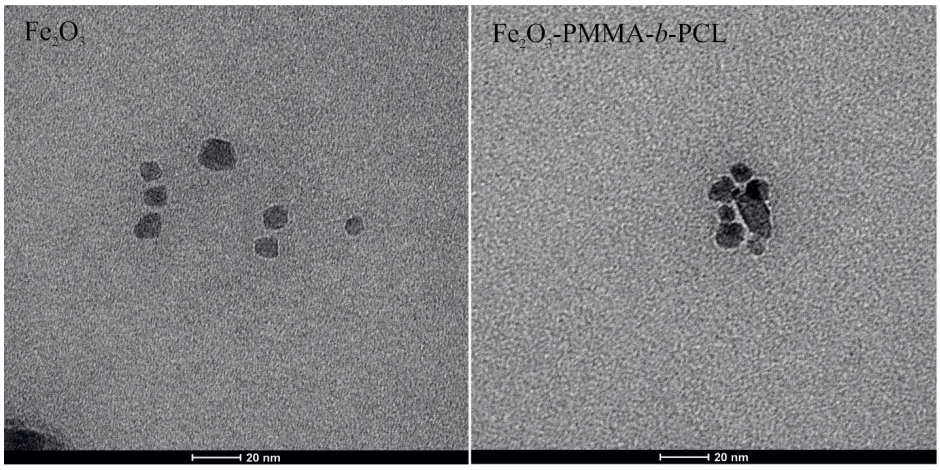

Figure 3.6. TEM micrograph modified and unmodified nanoparticles

3.3.3. MORPHOLOGICAL CHARACTERIZATION OF NANOCOMPOSITES

Neat BCP and nanocomposite thin films have been thermal annealed at 80, 100 and 120 °C for 72 h. Obtained morphologies have been analyzed in terms of AFM. In Figure 3.7 morphologies achieved for those films can be seen.

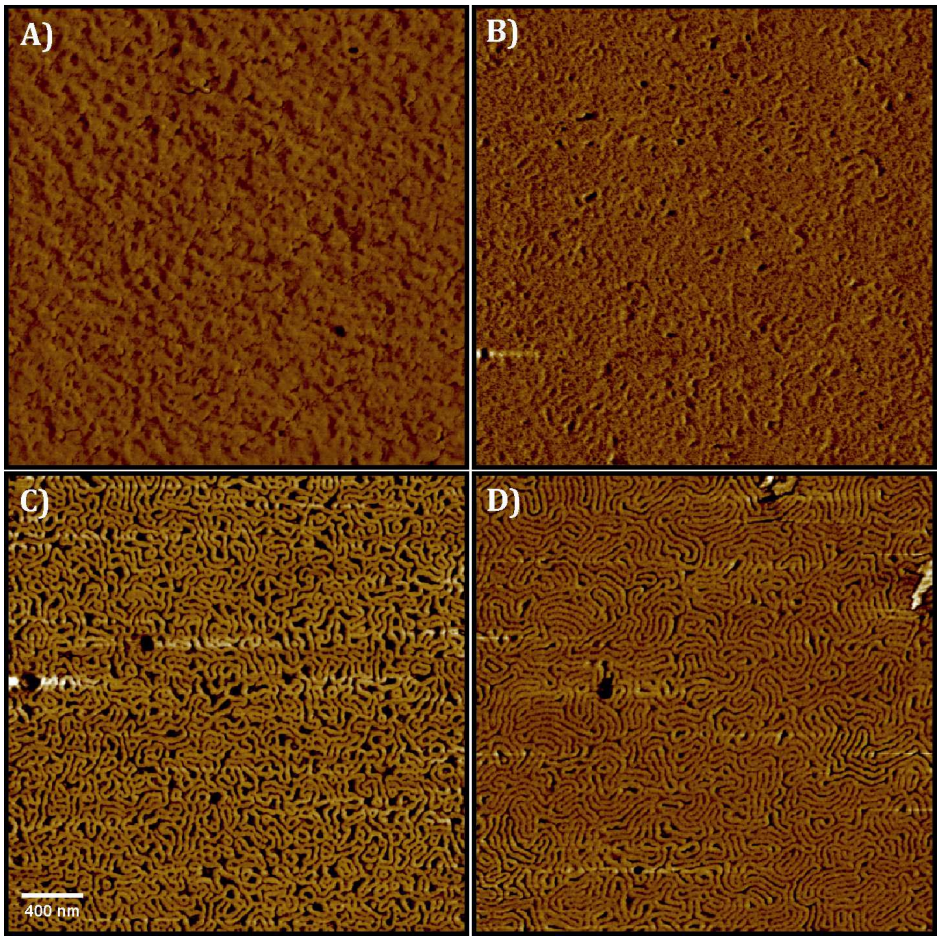

Figure 3.7. AFM phase images of the PS-*b*-PCL block copolymer, A) spin coated film, thermal annealed at B) 80 °C, C) 100 °C and D) 120 °C

As it is shown in Figure 3.7 when BCP films have been prepared by spin coating without any annealing treatment, although soft microphase separation is observed, no ordered microstructure is formed. When these films have been annealed at 80 °C for 72 h any remarkable difference is not appreciated, observing a very similar soft microphase separation than that of samples without annealing. Films annealed at 100 °C show worm-like morphology, in which bright domains

correspond to PS block, as it is the hardest phase (Demirel et al. 2004). When annealing temperature is 120 °C a lamellar morphology can be clearly seen. It is worth to note that PCL crystalline domains are not observed in the images. In fact, as it was measured by differential scanning calorimetry (DSC) (not shown here), crystallization degree of PCL block (only 30 % of copolymer) was below 5 % in both cases. Furthermore, for nanocomposites crystallization degrees are even lower than 1 %.

Figure 3.8 shows AFM images of nanocomposites with 2 and 5 wt% of nanoparticles annealed at 100 and 120 °C.

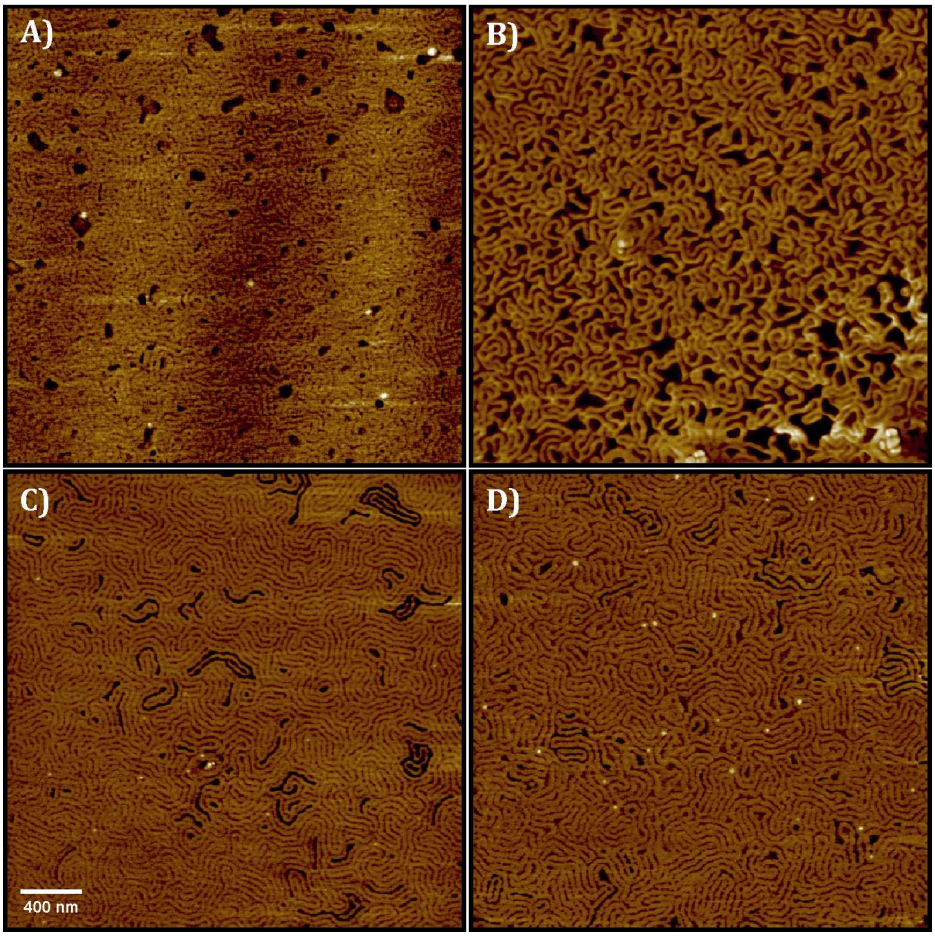

Figure 3.8. AFM phase images of PS-*b*-PCL/Fe_2O_3-*g*-(PMMA-*b*-PCL) nanocomposites annealed at different temperatures and nanoparticle amounts, A) 100 °C and 2 wt%, B) 100 °C and 5 wt%, C) 120 °C and 2 wt% and D) 120 °C and 5 wt%

As it can be seen in Figure 3.8 the addition of Fe_2O_3 nanoparticles grafted with the copolymer does not modify the morphology of block copolymer. Samples annealed at 100 °C present a warm-like morphology very similar to that of neat copolymer, while those annealed at 120 °C present nanostructured lamellar morphology similarly to neat copolymer. Bright points observed in images of Figure 3.8 can be attributed to Fe_2O_3 nanoparticles; the amount of points obviously increases with nanoparticle content. Although small nanoparticle aggregates have been formed during grafting process, functionalized nanoparticles are well dispersed in the copolymer. The grafting of nanoparticles with PMMA-*b*-PCL copolymer seems to increase compatibility with matrix, improving their dispersion; they are mainly located at the interface between dark PCL and bright PS domains without breaking copolymer nanostructure. This fact could be due to the low grafting density (0.04 chain/nm^2) of the copolymer on the nanoparticle surface; other authors pointed out that when the grafting density is low NP tends to locate at the interfaces (Kim et al. 2006).

For comparison, Figure 3.9 shows AFM image of nanocomposite with 5 wt% of unmodified nanoparticles. Bigger aggregates are formed, as nanoparticles tend to aggregate due to their low compatibility with the matrix. Formation of aggregates is avoided by increasing the compatibility of nanoparticles via grafting process.

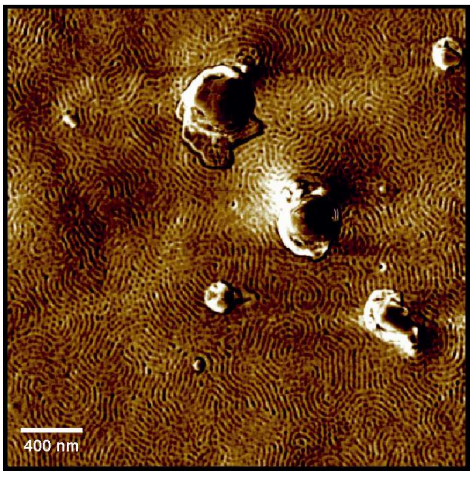

Figure 3.9. AFM phase image of PS-*b*-PCL/Fe_2O_3 nanocomposites with 5 wt% of nanoparticles, annealed at 120 °C for 72 h

Size distribution of modified nanoparticles in the nanocomposites has also been analyzed by AFM. As an example, size distribution of Fe_2O_3-*g*-(PMMA-*b*-PCL) in the nanocomposites annealed at 120 °C is shown in Figure 3.10. Average sizes of 22 and 38 nm are obtained for 2 and 5 wt% nanoparticle amount, respectively. Very similar results are obtained for nanocomposites annealed at 100 °C. It has to be noted that the size of those aggregates is very similar to that obtained for Fe_2O_3-*g*-(PMMA-*b*-PCL) nanoparticles after modification, suggesting that aggregates are formed mainly during modification and not during nanocomposites preparation, as it have been seen by TEM characterization previously.

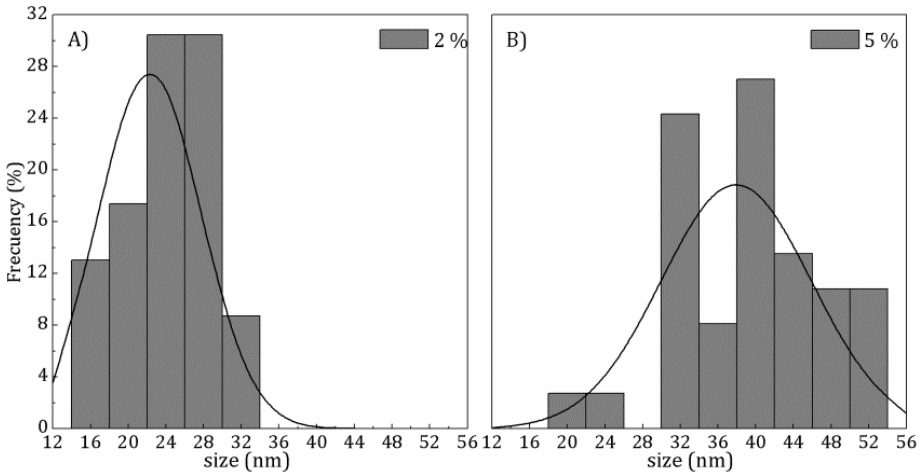

Figure 3.10 Fe_2O_3-*g*-(PMMA-*b*-PCL) size distribution in the nanocomposite annealed at 120 °C with: A) 2 wt% and B) 5 wt% of nanoparticles

3.4. CONCLUSIONS

From this chapter different conclusions can be extracted. Mössbauer spectroscopy and XRD measurements showed that nanoparticles used in this work are γ-Fe_2O_3 ones. These nanoparticles have been successfully functionalized, both by silanization and subsequent copolymer grafting, as demonstrated by FTIR and TGA. This functionalization seems to increase compatibility with copolymer, leading to good nanoparticle dispersion in the nanocomposites, without altering

nanostructure generated by BCP self-assembly. Nanoparticles are mainly located at the interface between both blocks. During functionalization process, nanoparticles tend to create small aggregates surrounded by a copolymeric shell, as it was corroborated by TEM. Those small aggregates are very similar in size that those found in the nanocomposites, suggesting that aggregates have been formed during functionalization and not during nanocomposites preparation. The dispersion of modified nanoparticles in the copolymer has been clearly improved when comparing to that of unmodified ones.

3.5. REFERENCES

Abboud M., Turner M., Duguet E. and Fontanille M., PMMA-based composite materials with reactive ceramic fillers. Part 1. Chemical modification and characterization of nanoparticles. *J Mater Chem* **1997**, 7, 1527-1532

Ahmed S.R. and Kofinas P., Magnetic properties and morphology of block copolymer-cobalt oxide nanocomposites. *Journal of Magnetism and Magnetic Materials* **2005**, 288, 219-223

Aissou K., Alnasser T., Pecastaings G., Goglio G., Toulemonde O., Mornet S., Fleury G. and Hadziioannou G., Hierarchical assembly of magnetic $L1_0$-ordered FePt nanoparticles in block copolymer thin films. *J. Mater. Chem. C* **2013**, 1, 1317-1321

Bartholome C., Beyou E., Bourgeat-Lami E., Chaumont P. and Zydowicz N., Nitroxide-mediated polymerizations from silica nanoparticle surfaces: ''graft from'' polymerization of styrene using a triethoxysilyl-terminated alkoxyamine initiator. *Macromolecules* **2003**, 36, 7946-7952

Basly B., Alnasser T., Aissou K., Fleury G., Pecastaings G., Hadziioannou G., Duguet E., Goglio G. and Mornet S., Optimization of Magnetic Inks Made of $L1_0$-Ordered FePt Nanoparticles and Polystyrene-block-Poly(ethylene oxide) Copolymers. *Langmuir* **2015**, 31, 6675-6680

Chen Q. and Yakovlev N.L., Adsorption and interaction of organosilanes on TiO_2 nanoparticles. *Applied Surface Science* **2010**, 257, 1395-1400

Cosio-Castaneda C., Martinez-Garcia R. and Socolovsky L.M., Synthesis of silanized maghemite nanoparticles onto reduced graphene sheets composites. *Solid State Sci* **2014**, 30, 17–20

Demirel A.L., Degirmenci M. and Yagcı Y. Atomic force microscopy investigation of asymmetric diblock copolymer morphologies in thin films. *European Polymer Journal* **2004**, 40, 1371-1379

Duwez A.-S., Guillet P., Colard C., Gohy J.-F. and Fustin C.-A., Dithioesters and Trithiocarbonates as Anchoring Groups for the "Grafting-To" Approach. *Macromolecules* **2006**, 39, 2729-2731

Galeotti F., Bertini F., Scavia G. and Bolognesi A., A controlled approach to iron oxide nanoparticles functionalization for magnetic polymer brushes. *Journal of Colloid and Interface Science* **2011**, 360 ,540-547

Garcia I., Tercjak A., Gutierrez J., Rueda L. and Mondragon I., Nanostructuration via Solvent Vapor Exposure of Poly(2-vinyl pyridine-b-methyl methacrylate) Nanocomposites Using Modified Magnetic Nanoparticles. *J. Phys. Chem. C* **2008**, 112, 14343-14347

George K.M., Ruthenburg T., Smith J., Yu L., Zhang Q., Anastasio C. and Dillner A.M., FT-IR quantification of the carbonyl functional group in aqueous-phase secondary organic aerosol from phenols. *Atmospheric Environment* **2015**, 100, 230-237

Hailu S., Samant S., Grabowski C., Durstock M., Karim A. and Raghavan D., Synthesis of Highly Dispersed, Block Copolymer-Grafted TiO_2 Nanoparticles Within Neat Block Copolymer Films. *Journal of Polymer Science, Part A: Polymer Chemistry* **2015**, 53, 468-478

Jing Z., Preparation and magnetic properties of fibrous gamma iron oxide nanoparticles via nonaqueous medium. *Mater Lett* **2006**, 60, 2217-2221

Kim B. J., Bang J., Hawker C.J. and Kramer E.J., Effect of Areal Chain Density on the Locationof Polymer-Modified Gold Nanoparticles in a Block Copolymer Template. *Macromolecules* **2006**, 39, 4108-4114

Magonov S.N., Cleveland J., Elings V., Denley D. and Whangbo M.H., Tapping-mode atomic force microscopy study of the near-surface composition of a styrene butadiene-styrene triblock copolymer film. *Surface Science* **1997**, 389, 201-211

Mansfeldt T., Schuth S., Häusler W., Wagner F.E., Kaufhold S. and Overesch M., Iron oxide mineralogy and stable iron isotope composition in a Gleysol with petrogleyic properties. *Journal of Soils and Sediments* **2012,** 12, 97-114.

Marutani E., Yamamoto S., Ninjbadgar T., Tsujii Y., Fukuda T. and Takano M., Surface-initiated atom transfer radical polymerization of methyl methacrylate on magnetite nanoparticles. *Polymer* **2004**, 45, 2231-2235

Nakagawa S., Ishizone T., Nojima S., Kamimura K., Yamaguchi K., and Nakahama S., Effects of Chain-Ends Tethering on the Crystallization Behavior of Poly(ε-caprolactone) Confined in Lamellar Nanodomains. *Macromolecules* **2015**, 48, 7138-7145

Ohno K., Koh K., Tsuji Y. and Fukuda T., Synthesis of gold nanoparticles coated with well-defined, high density polymer brushes by surface initiated living radical polymerization. *Macromolecules* **2002**, 35, 8989-8993

Rana S., Yoo H.J., Cho J.W., Chun B.C. and Park J.S., Functionalization of Multi-Walled Carbon Nanotubes with Poly(ε-caprolactone) Using Click Chemistry. *Journal of Applied Polymer Science* **2011**, 119, 31-37

Sabuncu S. and Çulha M., Temperature-dependent breakdown of hydrogen peroxide-treated ZnO and TiO_2 nanoparticle agglomerates. *Beilstein J. Nanotechnol*. **2015**, 6, 1897-1903

Sawall D.D., Villahermosa R.M., Lipeles R.A. and Hopkins A.R., Interfacial Polymerization of Polyaniline Nanofibers Grafted to Au Surfaces. *Chem. Mater.* **2004**, 16, 1606-1608

Singho N.D., Lah N.A.C., Johan M.R. and Ahmad R., FTIR Studies on Silver-Poly(Methylmethacrylate) Nanocomposites via *In-Situ* Polymerization Technique. *Int. J. Electrochem. Sci.* **2012**, 7, 5596-5603

Veeco Manual **2005**, *A practical guide to SPM scanning probe microscopy*, Veeco Instruments Inc.

Wang S., Zhou Y., Guan W. and Ding B., One-step copolymerization modified magnetic nanoparticles via surface chain transfer free radical polymerization. *Applied Surface Science* **2008**, 254, 5170-5174

Wu J., Li H., Wu S., Huang G., Xing W., Tang M. and Fu Q., Influence of Magnetic Nanoparticle Size on the Particle Dispersion and Phase Separation in an ABA Triblock Copolymer. *J. Phys. Chem. B* **2014**, 118, 2186-2193

Xia Z., Li W., Ding J., Li A. and Gan W., Effect of PS-b-PCL Block Copolymer on Reaction-Induced Phase Separation in Epoxy/PEI Blend. *Journal of polymer science, part B: Polymer*

physics **2014**, 52, 1395-1402

Xu C., Ohno K., Ladmiral V. and Composto R.J., Dispersion of polymer grafted magnetic nanoparticles in homopolymers and block copolymers. *Polymer* **2008**, 49, 3568-3577

Yao Y., Metwalli E., Su B., Körstgens V., Moseguí Gonzalez D., Miasnikova A., Laschewsky A., Opel M., Santoro G., Roth S.V., and Müller-Buschbaum P., Arrangement of Maghemite Nanoparticles via Wet Chemical Self Assembly in PS-b-PNIPAM Diblock Copolymer. Films *ACS Appl. Mater. Interfaces* **2015**, 7, 13080-13091

Yu R., Zheng S., Li X. and Wang J., Reaction-Induced Microphase Separation in Epoxy Thermosets Containing Block Copolymers Composed of Polystyrene and Poly(ε-caprolactone): Influence of Copolymer Architectures on Formation of Nanophases. *Macromolecules* **2012**, 45, 9155-9168

Zhang F., Huang H., Hu Z., Chen Y. and He T., Crystallization of Weakly Segregated Poly(styrene-b-ε-caprolactone) Diblock Copolymer in Thin Films. *Langmuir* **2003**, 19, 10100-10108

Chapter 4

SYNTHESIS AND CHARACTERIZATION OF PS-*b*-P4VP/Fe_2O_3-PS NANOCOMPOSITES: *grafting through* method

4.1. INTRODUCTION

Polystyrene-*block*-poly(4-vinyl piridine) (PS-*b*-P4VP) has been widely used as matrix for preparing nanocomposites with different nanoparticles. Zhang et al. used PS-*b*-P4VP copolymer with quaternized P4VP block (PS-*b*-QP4VP) to prepare nanocomposites with montmorillonite, by cationic exchange reactions of quaternary ammonium ions of PS-*b*-QP4VP with those of montmorillonite, finding an enhancement in thermal stability of neat copolymer (Zhang et al. 2006). Sung et al. obtained transparent and low-electric-resistance nanocomposites with PS-*b*-P4VP and single-walled carbon nanotubes (SWCNT) (Sung et al. 2008). Gowd et al. developed a simple and efficient route to generate nanoscopic arrays of ordered inorganic nanodots with controlled feature sizes through the copolymer (Gowd et al. 2010). Zu et al. nanostructured the BCP by re-assembling with sequential vapor treatment using selected solvents, obtaining patterned polymeric or inorganic/polymer composite nano-islands and nano-ring arrays (Zu et al. 2011). Mendoza et al. modified PS-*b*-P4VP with a gold precursor to obtain an organic/inorganic hybrid in bulk with gold nanoparticles selectively incorporated in the P4VP block, and studied the viscoelastic rheology (Mendoza et al. 2011). Ye et al. used a fan-shaped small molecule to disperse and selectively place gold nanoparticles at PS domains of the copolymer (Ye et al. 2013). Lu and Kuo investigated the influence of functional groups present in polyhedral oligomeric silsesquioxane (POSS) nanoparticles on the self-assembled structures formed by PS-*b*-P4VP copolymer (Lu and Kuo 2014). Horechyy et al. prepared nanocomposites with asymmetric PS-*b*-P4VP loaded with iron oxide nanoparticles, analyzed the effect of nanoparticle addition in the morphology, and compared this effect with morphology changes produced in other BCPs (Horechyy et al. 2014). Chi et al. fabricated organic field-effect transistors (OFETs) and memory devices based on hybrid nanocomposites composed by PS-*b*-P4VP with two different block compositions and hydroxyl-functionalized ferrocene small

molecules (Chi et al. 2015). Our group has also used this BCP for the generation of nanocomposites. Etxeberria et al. studied the effect of the CdSe nanoparticle addition on the nanostructure development of this copolymer (Etxeberria et al. 2014a).

Grafting through is a promising method for the functionalization of surfaces. It is based on a surface polymerization through a covalently linked monomer. In this route the inorganic phase is incorporated inside the polymer chains. Different works can be found in the literature showing the success of this technique. Rozes et al. followed this method for copolymerizing oxo-alcoxo functional clusters with styrene leading to three dimensional networks in which the inorganic nano-fillers were covalently linked to the organic polymer (Rozes et al. 2005). Trabelsi et al. modified titanium-oxo-clusters via free radical polymerization of dimethacrylate oligomers and 2-hydroxyethyl methacrylate, for being incorporated into poly(2-hydroxyethyl methacrylate) (Trabelsi et al. 2005). Henze et al. investigated the influence of reaction parameters on the formation of surface-attached polymer monolayers, immobilizing methacrylic moieties on silica surfaces via silane linker by *grafting through* (Henze et al. 2014). Etxeberria et al. functionalized CdSe semiconductor nanoparticles by radical polymerization with PS brushes (Etxeberria et al. 2012) for being used to generate nanocomposites with SBS matrix, concluding that nanoparticles were successfully placed at the PS domains (Etxeberria et al. 2013) while nanocomposites maintained the conductive properties of CdSe nanoparticles (Etxeberria et al. 2014b).

The main objectives of the work described in this chapter are the following. Firstly, functionalization of the maghemite nanoparticle surface with PS brushes by *grafting through* technique together with their characterization; and then, the preparation and characterization of nanocomposites based on PS-*b*-P4VP block copolymer and functionalized magnetic nanoparticles. Functionalization of nanoparticles was analyzed by FTIR and TGA. Morphology of nanocomposites was

studied by AFM, while the magnetic properties were measured by vibrating sample magnetometer (VSM) and superconducting quantum interference device (SQUID).

4.2. MATERIALS AND METHODS

4.2.1. MATERIALS

Maghemite nanoparticles with a nominal size of 9 nm and a polydispersity of 1.08 were used as the inorganic filler. They were purchased from Integram Technologies. The silane used to attach the nanoparticle surface with the vinyl group required to grow polymer brushes was the 3-methacryloxypropyl trimethoxysilane (MPTS) one, with 98 % of purity, purchased from ABCR. The initiator for the polymerization reaction was the 2,2'-azobisisobutyronitrile (AIBN), used without further purification. Styrene monomer with a purity of 99 %, distilled under reduced pressure over CaH_2 to purify before use, was purchased from Aldrich. PS-*b*-P4VP was purchased from Polymer Source with M_n of 22,500 and 29,000 g/mol for PS and P4VP blocks, respectively, and a polydispersity index (M_w/M_n) of 1.2 for both blocks. Chemical structures of silane, styrene and PS-*b*-P4VP can be seen in Scheme 4.1. Solvents used were toluene, THF, dimethylformamide (DMF) and dioxane, purchased from Aldrich

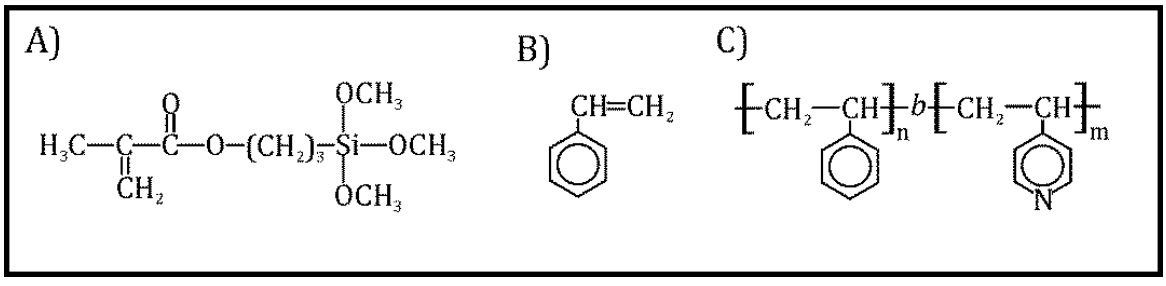

Scheme 4.1. Chemical structure of A) MPTS, B) styrene monomer and C) PS-*b*-P4VP copolymer

4.2.2. METHODS

4.2.2.1. Nanoparticle functionalization

Nanoparticle modification was carried out in two steps (Scheme 4.2): first the silanization process and then the growth of PS brushes by *grafting through* method.

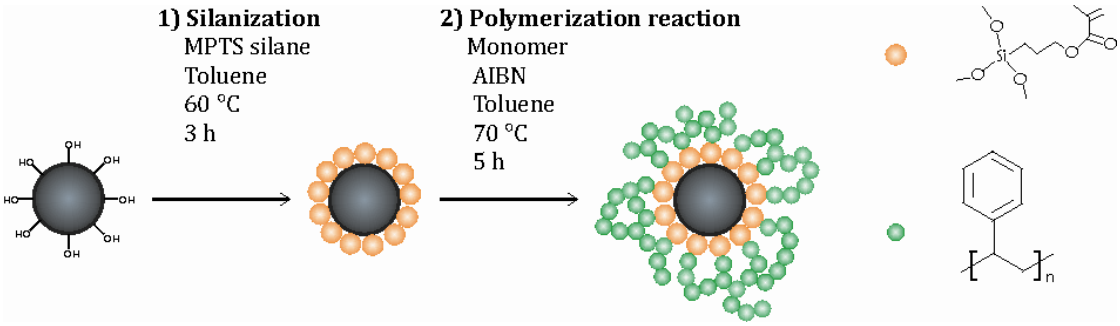

Scheme 4.2. Nanoparticle modification procedure

4.2.2.1.1. Silanization process

Silanization of nanoparticles with MPTS silane implies a nucleophilic attack of hydroxyl groups (-OH) at nanoparticle surface to the Si atoms of MPTS. The reaction was carried out by adding 0.05 g of nanoparticles and 10 µmol of silane to 40 mL of toluene under sonication. The reaction was carried out at inert atmosphere for 3 h at 60 °C. Nanoparticles were subsequently washed with THF, until any silane rest was eliminated (the presence of silane after washing was probed by FTIR), and dried in vacuum for 72 h at 40 °C.

4.2.2.1.2. Growth of PS brushes by *grafting through* method

After silanization the surface of nanoparticles was modified with PS brushes following the *grafting through* method. 0.02 g of silanized γ-Fe_2O_3 nanoparticles

and 0.1 g of AIBN were dispersed into 40 mL of toluene, and once they were well dispersed 2 mL of monomer were added. The reaction was carried out in inert N_2 atmosphere at 70 °C for 5 h. When reaction was ended, modified nanoparticles were subsequently washed with THF, until any monomer rest was eliminated (probed by FTIR), and dried in vacuum for 72 h at 40 °C.

4.2.2.2. Nanocomposite preparation

Nanocomposites were prepared by mixing PS-*b*-P4VP block copolymer with functionalized γ-Fe_2O_3 nanoparticles. Nanoparticles were first dispersed in DMF for 2 h by sonication, and then PS-*b*-P4VP block copolymer was added. Thin films of both neat block copolymer and organic/inorganic nanocomposites were prepared by spin-coating onto silicon wafers at 2000 rpm for 120 s, using a P6700 spin-coater from Specialty Coating Systems Inc.. For selective solvent annealing thin films were exposed to saturated dioxane vapors into a closed vessel for different exposure times at room temperature. After exposure samples were removed from the vessel and stored at room temperature for some days before characterization, for residual solvent removal. Nanocomposites were prepared with 1 to 5 wt% of nanoparticles.

4.2.2.3. Characterization techniques

Different characterization techniques have been used in order to characterize both the functionalization of nanoparticles and generated nanocomposites. Surface functionalization of nanoparticles has been confirmed by FTIR and TGA, while morphology of nanocomposites was followed by AFM. Magnetic properties of nanocomposites have been characterized by SQUID magnetometer and VSM measurements, in order to check the transference of magnetic properties from nanoparticles to nanocomposites.

4.2.2.3.1. FTIR

It was used to verify the functionalization of nanoparticles. Infrared spectra were carried out in a Nicolet Nexus 670 Spectrometer, as it was described in section 3.2.2.3.3 of Chapter 3.

4.2.2.3.2. TGA

It was used to determine the amount of hydroxyl groups of nanoparticle surface, the amount of the grafted silane and the weight loss related to the grafted PS brushes, which would probe the success of the polymerization reaction. TGA results were obtained using a TGA/SDTA-851e equipment running from 25 to 750 °C at a heating rate of 10 °C/min under nitrogen atmosphere.

4.2.2.3.3. AFM

It was used to study the morphology of neat block copolymers and nanocomposite thin film. Measurements were performed in tapping mode using a Dimension Icon Nanoscope V (Bruker) as it was described in section 3.2.2.3.6 of Chapter 3.

4.2.2.3.4. VSM

This technique allows the determination of the magnetic moment of a sample with high precision. It operates on Faraday's Law of Induction, based on the fact that a changing magnetic field will produce an electric field. This electric field can be measured, extracting information about the changing magnetic field. A VSM is used to measure the behavior of magnetic materials.

Magnetization was measured in a Quantum Design Physical Properties Measurement System (PPMS) with Vibrating Sample Magnetometer option, by measuring the hysteresis loops at 2, 200 and 300 K.

4.2.2.3.5. SQUID

The basic element of a SQUID magnetometer is a ring of superconducting metal containing one or two weak links, known as Josephson junctions. The SQUID magnetometer used in this work was radio frecuency (RF)-type SQUID, with only one Josephson junction. Variation of the flux in the ring results in a change of impedance. This change in impedance results in the retuning of a weakly coupled resonator circuit driven by a RF current source. Therefore, if a magnetic flux is applied to the ring, an induced current flows around it. In turn, this current induces a variation of the RF voltage across the circuit. This variation is detected with a lock-in amplifier. A feedback arrangement is used to minimize the current flowing in the ring, the size of the feedback current being a measure of applied magnetic flux. The operating mode of a SQUID magnetometer (Jiles 1998) can be seen in Scheme 4.3.

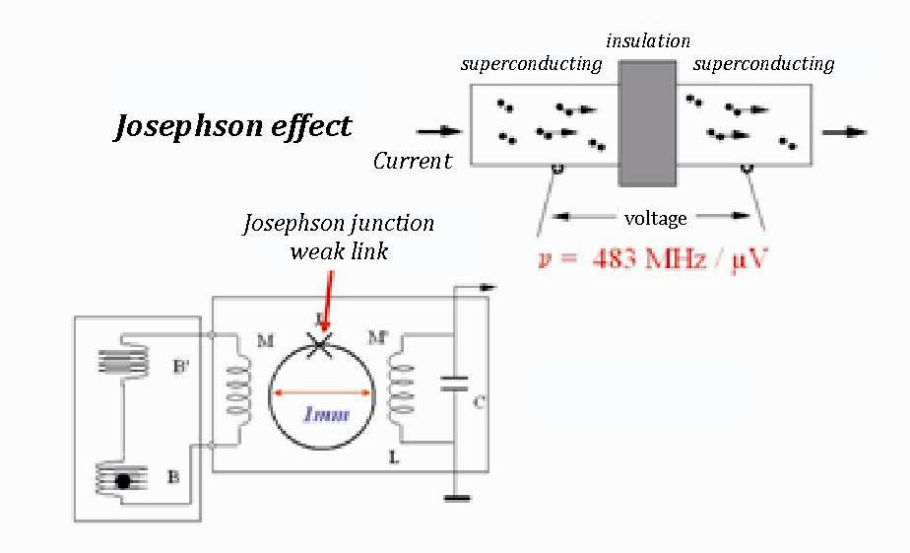

Scheme 4.3. Operating mode of a SQUID magnetometer

In this work SQUID magnetometer was used for ZFC/FC measurements. These measurements were carried out at 100 Oe, between 5 and 300 K. The equipment used for measurements was a SQUID magnetometer (MPMS-7T, Quantum Design), with a 7 T superconducting magnet.

4.3. RESULTS AND DISCUSSION

4.3.1. CHARACTERIZATION OF FUNCTIONALIZED NANOPARTICLES

Before the polymerization of PS brushes nanoparticles have been surface-modified with MPTS silane. The right attachment of the silane to the nanoparticle surface is of vital importance, as the MPTS contains the vinyl group that will be used for the polymerization of PS brushes (Kim et al. 2007). The success of silanization process has been probed by FTIR and TGA measurements.

From FTIR spectra of Figure 4.1, the appearance of bands related to the main bonds of MPTS can be seen: C=O stretching vibration at 1704 cm^{-1}, C-O-C stretching deformation vibration at 1329 and 1300 cm^{-1}, and Si-O-Fe stretching vibration at 1176 and 1011 cm^{-1}, indicating the presence of MPTS attached to the surface (Rodriguez et al. 1999). After silanization, nanoparticles have been modified with PS brushes by *grafting through* method. The presence of brushes into the surface has also been probed by FTIR. In the FTIR spectra of PS-modified iron oxide nanoparticles, main bands related to PS such as those corresponding to C-H aromatic stretching vibration (3023 cm^{-1}, inner part of the figure), C-C stretching frequency of the ring in plane (1600 cm^{-1}), C-C stretching vibration of the ring in plane (1494 cm^{-1}) and C-H out of plane bending vibration of the ring (700 cm^{-1}), can be seen (Sun et a. 2007, Etxeberria et al. 2013), thus probing the presence of PS in the surface of nanoparticles.

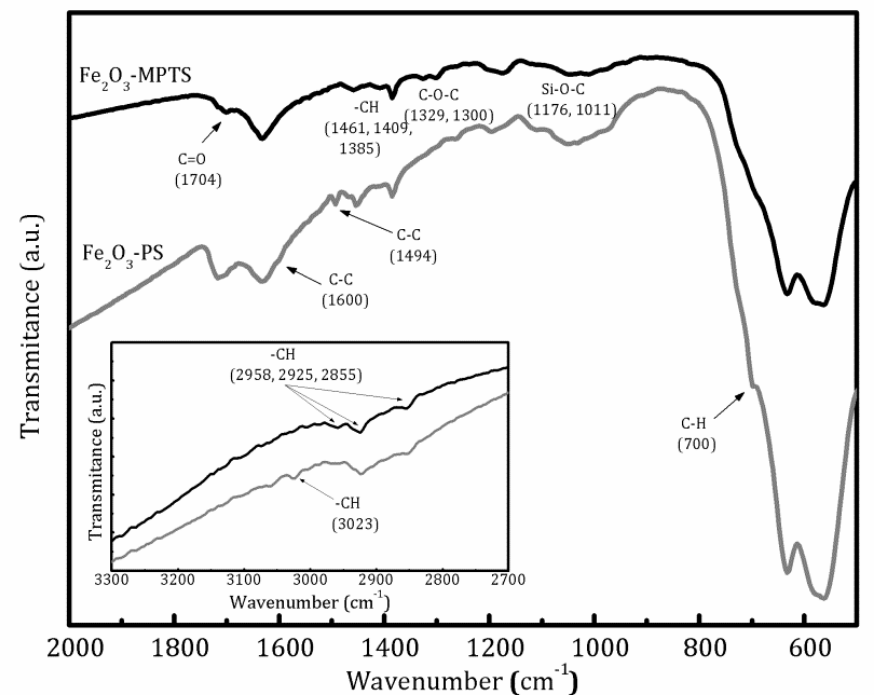

Figure 4.1 FTIR spectra of silanized and PS-modified nanoparticles

Figure 4.2 shows TGA thermograms of pristine, silanized and PS-modified nanoparticles. TGA measurements, besides for probing the modification of the nanoparticles with the organic compound, have been used to determine the amount of grafted organic part. The weight loss of unmodified nanoparticles is related to physisorbed water (until 120 °C) and surface -OH degradation (above 120 °C). For silanized nanoparticles, a significant weight loss starts at around 300 °C, which corresponds to the combustion of the silane molecules adsorbed on the surface and also to the elimination of hydroxyl groups (Rodriguez et al. 1999). The thermal degradation of the PS starts around 300 °C (Sun et al. 2007). The amount of grafted silane has been determined by using equation 4.1 (Bartholome et al. 2003). The calculated surface density of the silane is of 2.8 molecules/nm^2. A direct comparison of the surface density of hydroxyl groups (8.1 molecules/nm^2) and that of the silane on the surface yield a reaction efficiency of 34.5 %. Moreover, as the weight loss related to the degradation of PS can be clearly seen, the presence of the polymer in the sample has also been probed.

$$silane(mol/m^2) = \frac{\frac{\Delta m_{120-750}}{100-\Delta m_{120-750}} \cdot 100 - \Delta m_{OH120-750}}{PM_{MPTS} \cdot SSA \cdot 100} \quad (4.1)$$

Where $\Delta m_{120\text{-}750}$ is the weight loss of the silane-modified nanoparticle, $\Delta m_{OH120\text{-}750}$ the weight loss of pristine nanoparticles, PM_{MPTS} the molecular weight of the silane and SSA the specific surface area of the nanoparticle.

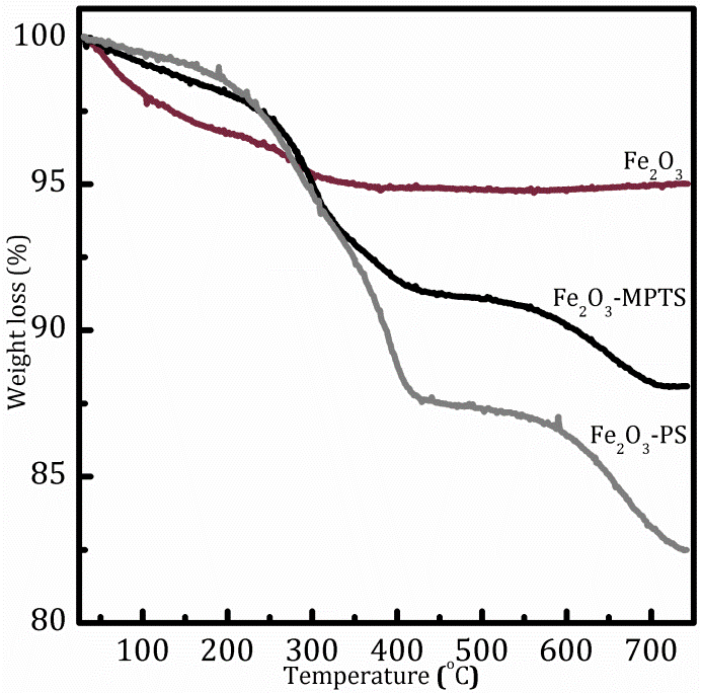

Figure 4.2. TGA thermograms of pristine, silanized and PS-modified nanoparticles

4.3.2. MORPHOLOGICAL CHARACTERIZATION OF NANOCOMPOSITES

PS-*b*-P4VP block copolymer thin films, as well as those of nanocomposites, have been exposed to dioxane vapors, which is a selective solvent for PS block (χ_{PS}= 0.35 and χ_{P4VP}= 2.61, as calculated from equations 2.1 and 2.2 from Chapter 2), in order to promote nanostructuring. In AFM images PS domains appear brighter than the P4VP ones (Wang et al 2014). For neat block copolymer films without any annealing treatment (Figure 4.3), although soft microphase separation is observed, no ordered microstructure is formed. Regarding films exposed to dioxane for 24 h (Figure 4.4), neat block copolymer presents a hexagonal

morphology, although some stripes can be appreciated, giving a clue about the evolution that will have the morphology with longer exposure times; with the addition of 1 wt% of functionalized nanoparticles the hexagonal morphology is maintained, while for higher nanoparticle amount a defined morphology is not obtained, nanoparticles disrupting hexagonal morphology of the copolymer. In any case, the absence of nanoparticle agglomerations shows the good dispersion of the nanofillers.

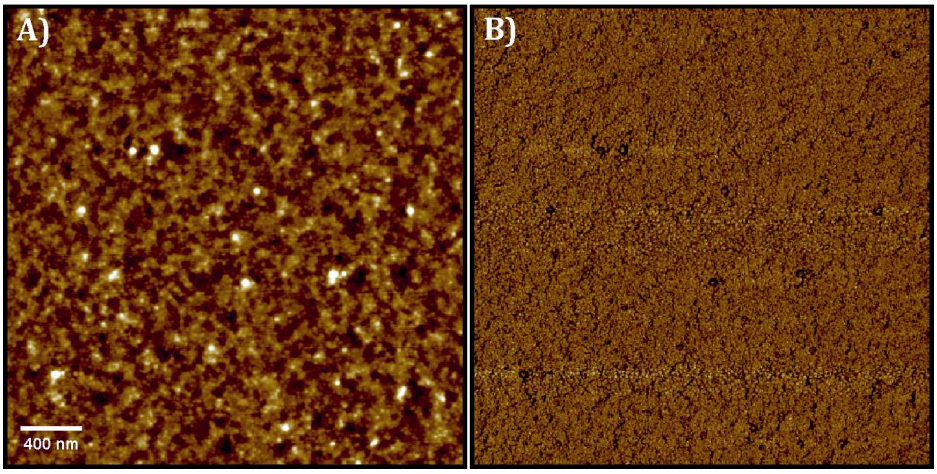

Figure 4.3. AFM height (A) and phase (B) images of spin coated PS-*b*-P4VP thin films

For longer exposure to dioxane vapors, the morphology of neat block copolymer evolves from hexagonal to stripped (Figure 4.5), presenting a totally stripped morphology after 48 h of exposure, with a lamellar structure normal to the substrate. When 1 wt% of functionalized nanoparticles is added the stripped morphology is maintained, despite the presence of some small areas with cylinders perpendicular to the surface. For higher nanoparticle amount, a morphology change promoted by nanoparticles can be seen. In this way, for 5 wt% nanocomposites, few lamellas can be seen, the main morphology consisting on cylinders perpendicular to the surface. The good dispersion of nanoparticles, the absence of remarkable agglomerations should be underlayed again.

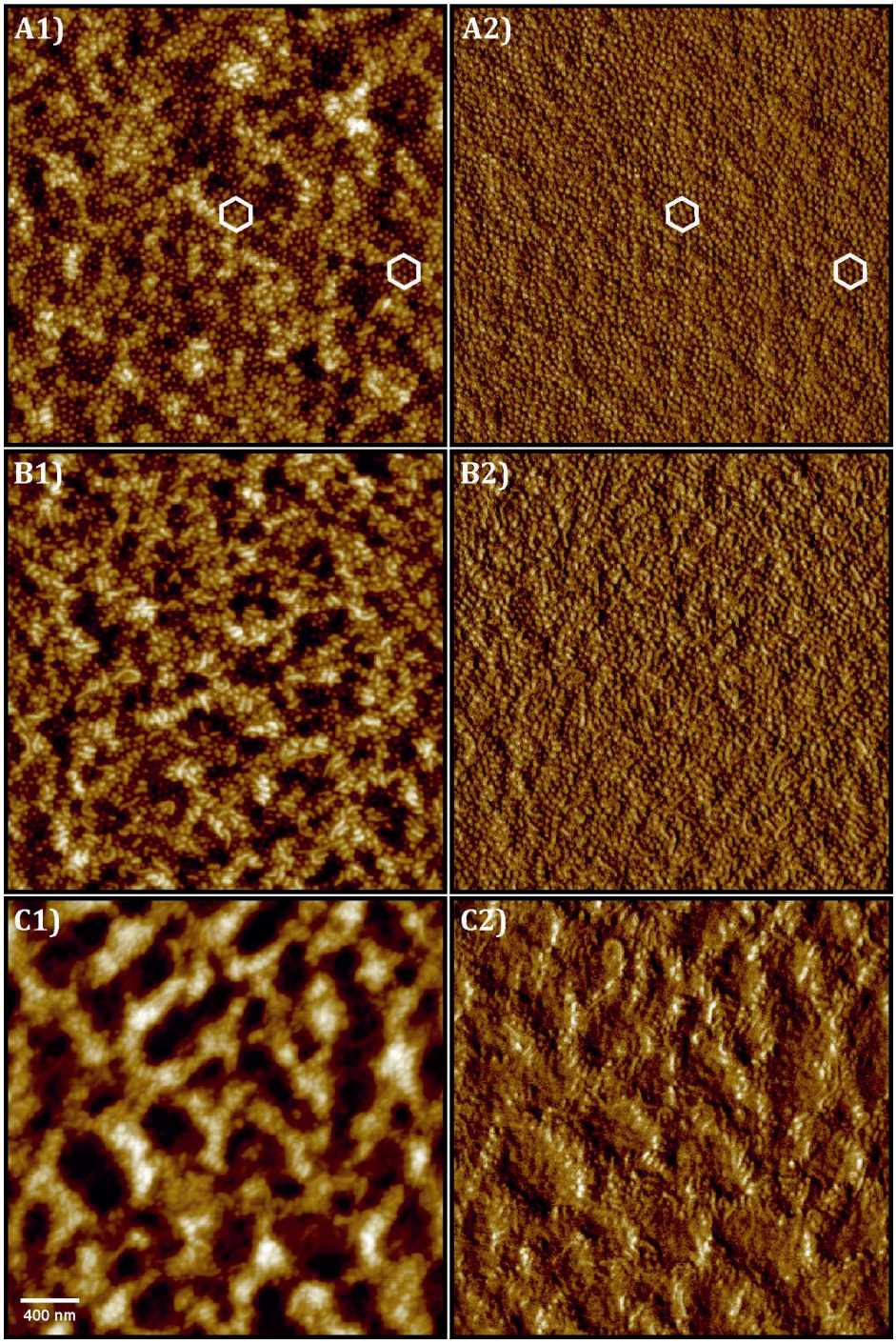

Figure 4.4. AFM height (1) and phase (2) images of thin films after 24 h of exposure to dioxane: A) neat block copolymer, nanocomposite with B) 1 wt% C) 5 wt% of nanoparticles

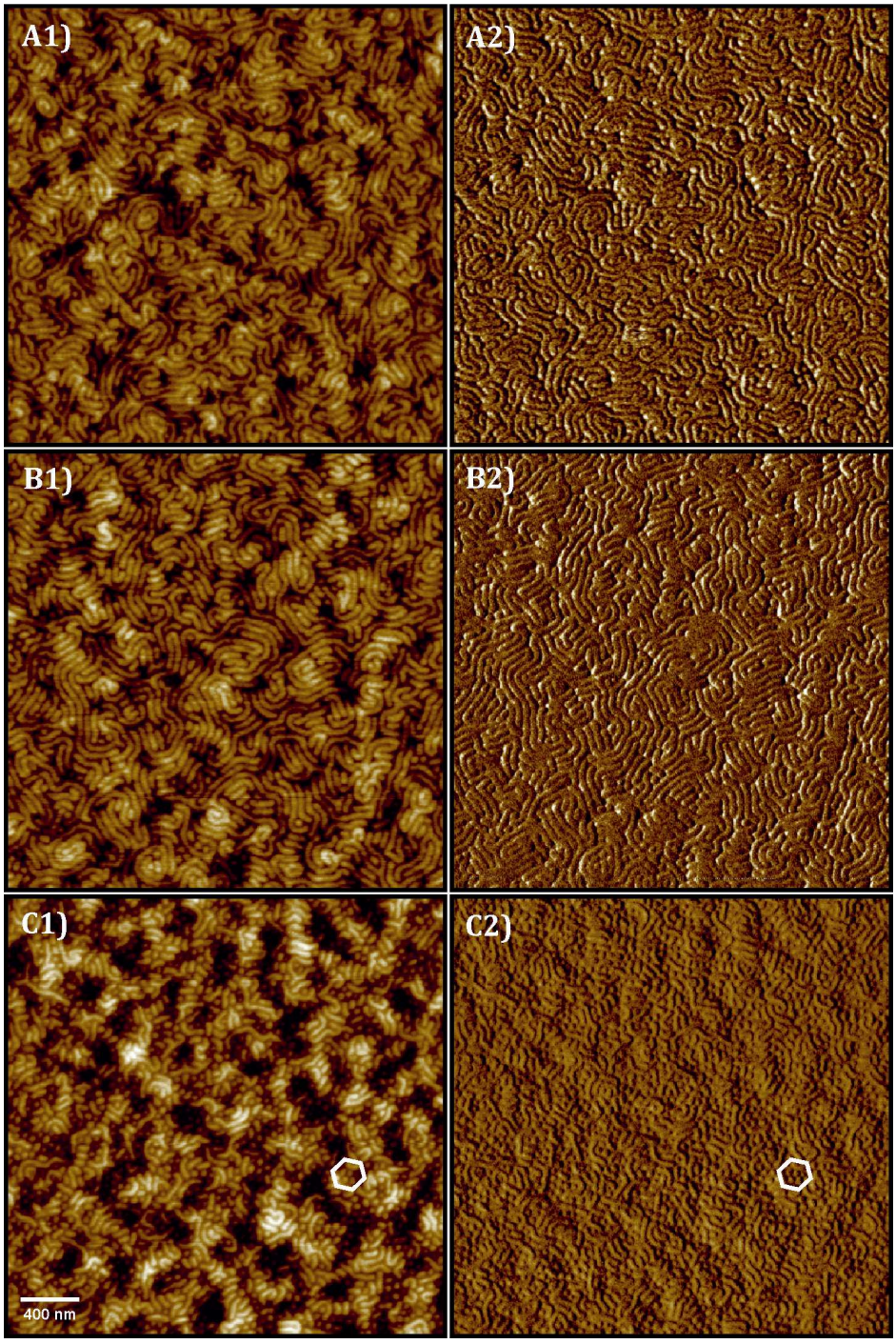

Figure 4.5. AFM height (1) and phase (2) images of nanocomposites after 48 h of exposure to dioxane, A) neat block copolymer, nanocomposites with B) 1 wt% and C) 5 wt% of nanoparticles

The morphological evolution of neat block copolymer with the exposure to dioxane vapors could be attributed to the migration of PS domains to the surface (Etxeberria et al. 2014), attracted by dioxane molecules. When nanoparticles are added to the block copolymer at low concentration there are no remarkable

effects, but for higher nanoparticle amounts morphology changed, probably because of the placement of nanoparticles at PS domains, which provoked a decrease in their mobility (Etxeberria et al. 2014). This fact could cause the morphology not to evolve enough to reach the same morphology as the neat block copolymer. However, a very good dispersion of nanoparticles has been obtained for all nanocomposites, showing the efficiency of nanoparticle modification for increasing the compatibility with the matrix.

4.3.3. DEGRADATION BY IRRADIATION WITH UV LIGHT

As nanoparticles are not placed at the surface of thin films, it is not possible to detect or visualize their location at PS domains by AFM; the removal of the organic part has been carried out for trying to observe the inner layers of the film. Different methods can be found in the literature with this purpose. Schulze et al. removed the organic part of organic/inorganic nanocomposites by exposing them to UV/O_3 oxidizing inorganic precursors and degrading the polymer scaffold (Schulze et al. 2015). Lu and Yi removed the PS-*b*-P2VP copolymer grafted to gold nanoparticles by O_2 plasma (Lu and Yi 2006). In this work the BCP removal has been carried out by exposing nanocomposites to UV light irradiation (Gutierrez et al. 2009). Figure 4.6 shows AFM images of neat block copolymer and nanocomposites with 1 wt% of nanoparticles before (A and B) and after (C and D) exposure to UV light irradiation for 6 h. While copolymer is removed by UV radiation (see Figures 4.6.A and C), by comparing Figures 4.6.B and 4.6.D it can be seen that nanoparticles have been mainly located at PS domains of block copolymer, detected by AFM as bright points rising from the partially degraded PS domains.

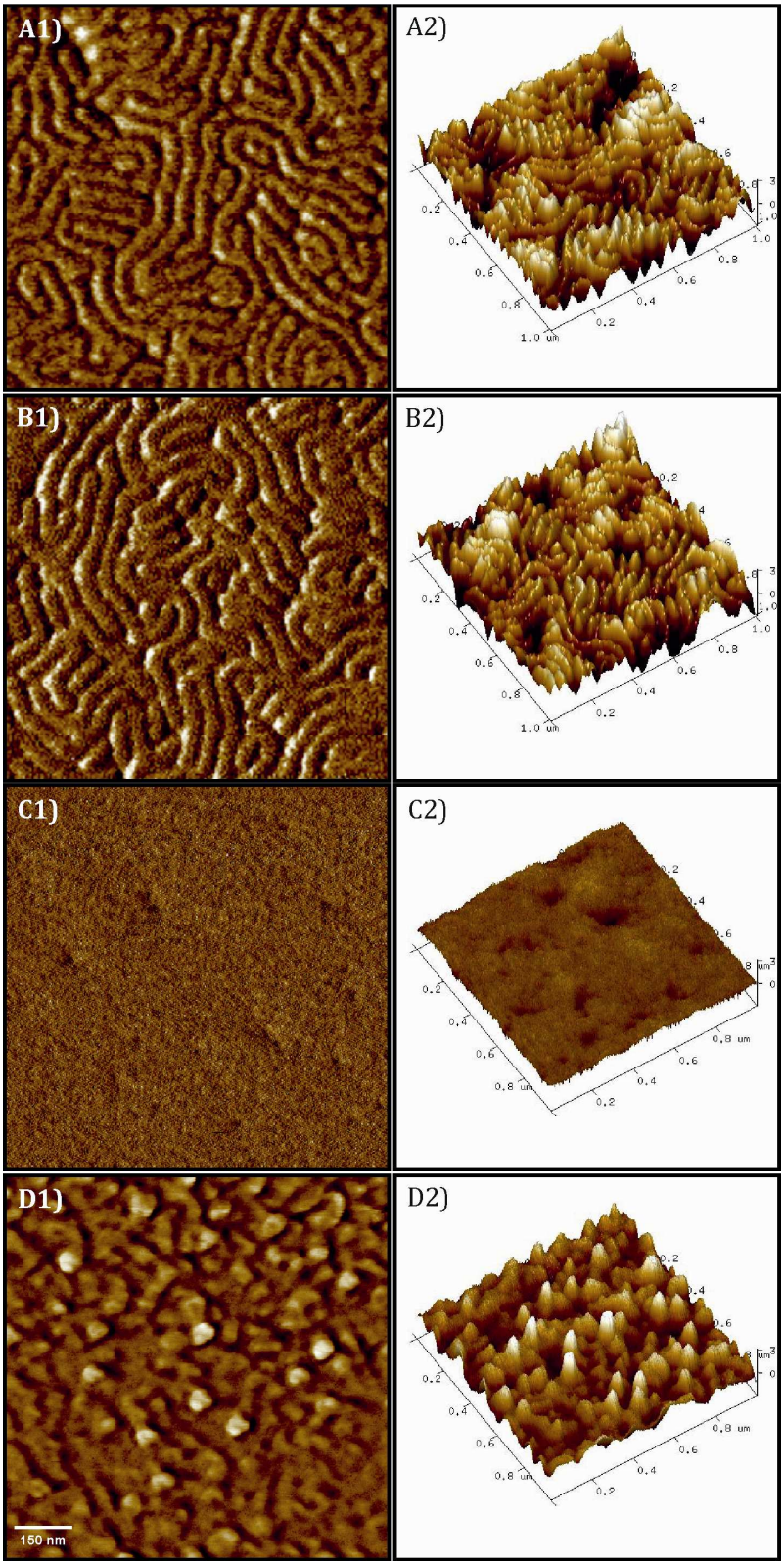

Figure 4.6. AFM phase (1) and 3D height (2) images of A) neat block copolymer, B) nanocomposite with 1 wt% of nanoparticles after 48 h of exposure to dioxane, and C) neat block copolymer and D) nanocomposite with 1 wt% of nanoparticles after 6 hours of exposure to UV light irradiation

4.3.4. MAGNETIC CHARACTERIZATION

Figure 4.7 shows the ZFC/FC curves of nanocomposites with 2 and 5 wt% of nanoparticles obtained from SQUID measurements. The organic/inorganic nanocomposites exhibit a typical superparamagnetic behavior at room temperature and a ferromagnetic one at low temperature (Zeng et al. 2006, Bean and Livingston 1959). Below the blocking temperature (T_B~250 K), the FC and ZFC magnetization curves diverge, magnetic moments are singledomain, spinned by anisotropy at low temperature. Above the blocking temperature, they are thermally disordered. Both samples show the same behavior, as for both measurements T_B coincides. This parameter is directly related to the size of nanoparticles (as it can be concluded from Néel-Brown expression, explained in the section 2.4 of Chapter 2), and, in this case, with the size of the aggregates that could be formed. The fact that both T_B values are equal could mean that probably aggregates have been created before thin film preparation during nanoparticle modification, and not during their dispersion and positioning on the block copolymer matrix. In the *grafting through* functionalization method, polymerization is carried out with silane-modified nanoparticles in the media and, distinctly from *grafting from* method, where the polymer chain grows only from the surface of the nanoparticle, the functional group located in the surface of the nanoparticle could join a growing PS chain in which there could be more nanoparticles previously joined. As the surface of the nanoparticles is multifunctional, with several double bonds, several chains could be bonded to different nanoparticles (Henze et al. 2014, Rahimidi-Razin et al. 2012). Due to these reasons it is supposed that nanoparticles, instead of being located individually, are bonded together with several polymer chains, creating a kind of network formed by nanoparticles and PS chains, as it is represented in Scheme 4.3. This fact was previously pointed out by our group (Etxeberria et al. 2013) for CdSe nanoparticles modified with PS brushes.

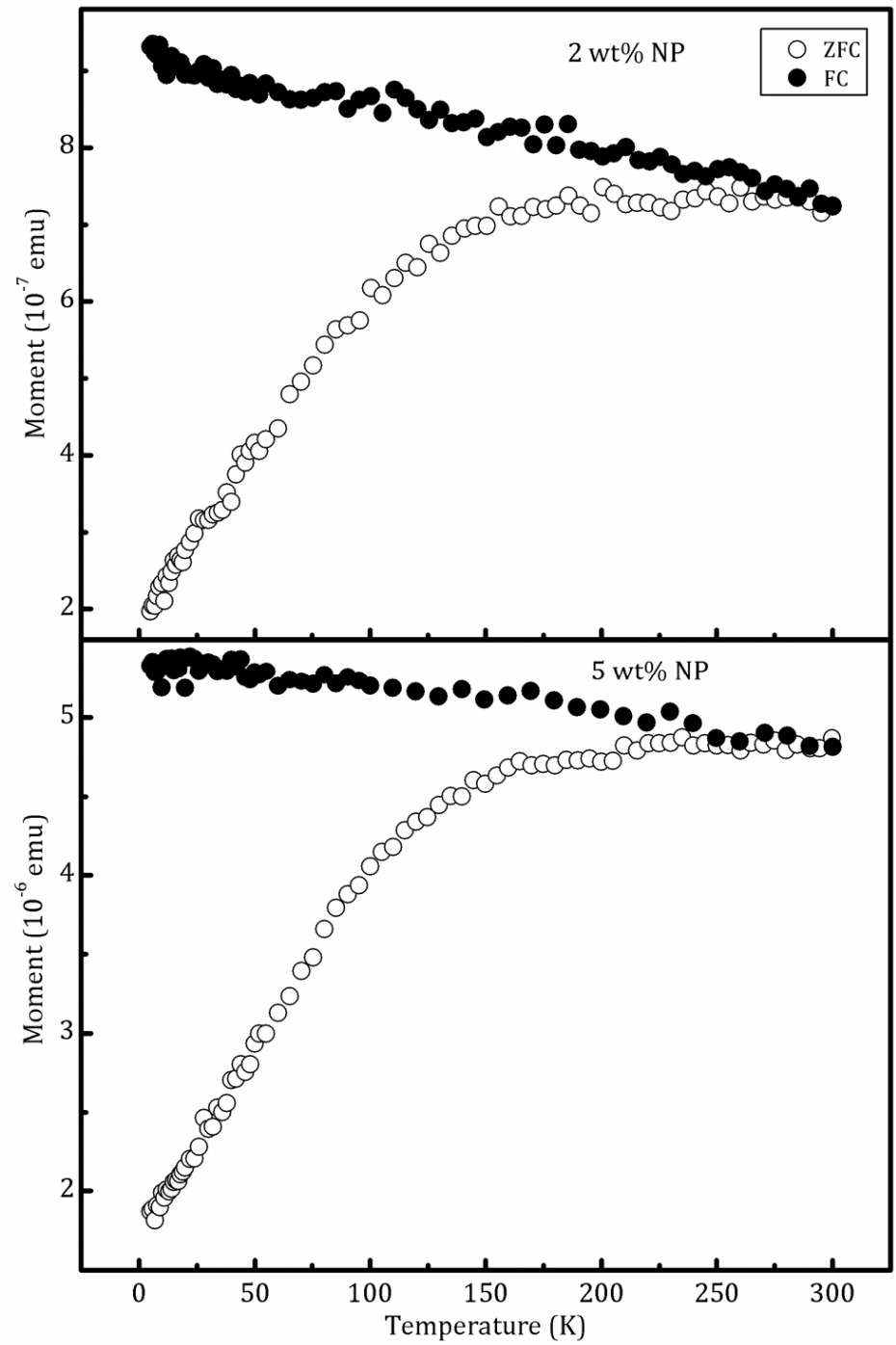

Figure 4.7. ZFC/FC curves at 100 Oe for nanocomposites with 2 and 5 wt% of nanoparticles

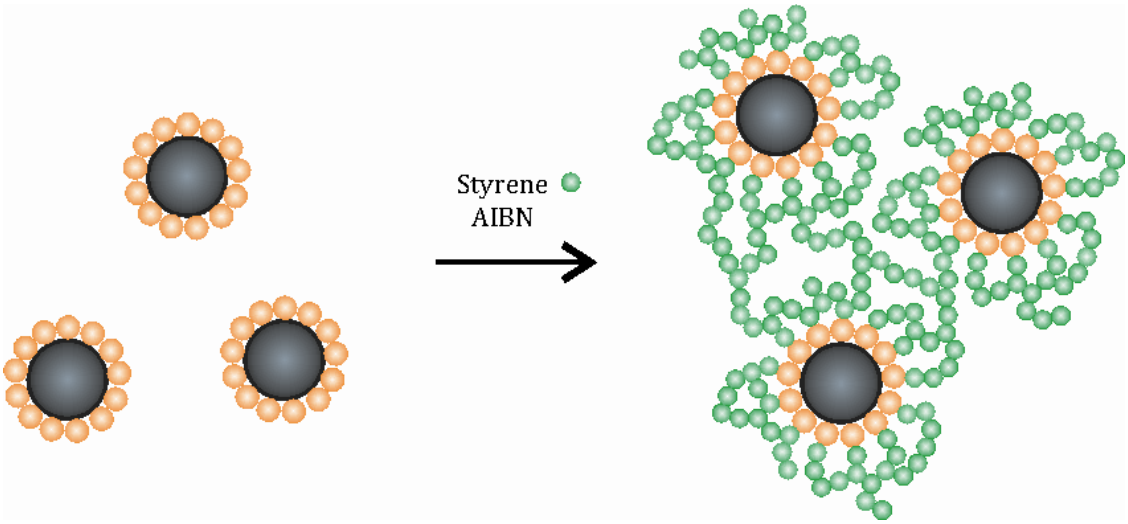

Scheme 4.4. Formation of nanoparticle aggregates by *grafting through* process

Apart from FC/ZFC curves the hysteresis loops have also been measured at different temperatures of 2, 100 and 300 K (Figure 4.8) for nanocomposites with 5 wt% of nanoparticles as an example. It should be taken into account that the diamagnetic contribution from the block copolymer matrix and sample holder is included, being these contributions big enough to produce a negative slope at high fields. Below T_B hysteresis loops are hysteretic while they are non-hysteretic above the T_B, with the appreciation of a smooth hysteresis at 100 K. In the M *vs* B magnetization curve at 2 K, the hysteresis is observed with a coercivity of approximately 175 Oe and a remanence of $5.6 \cdot 10^{-5}$ emu, whereas above the T_B both the coercivity and remanence are zero, demonstrating the superparamagnetic behavior of the final nanocomposites (Schulz et al. 2010, Xu et al. 2009).

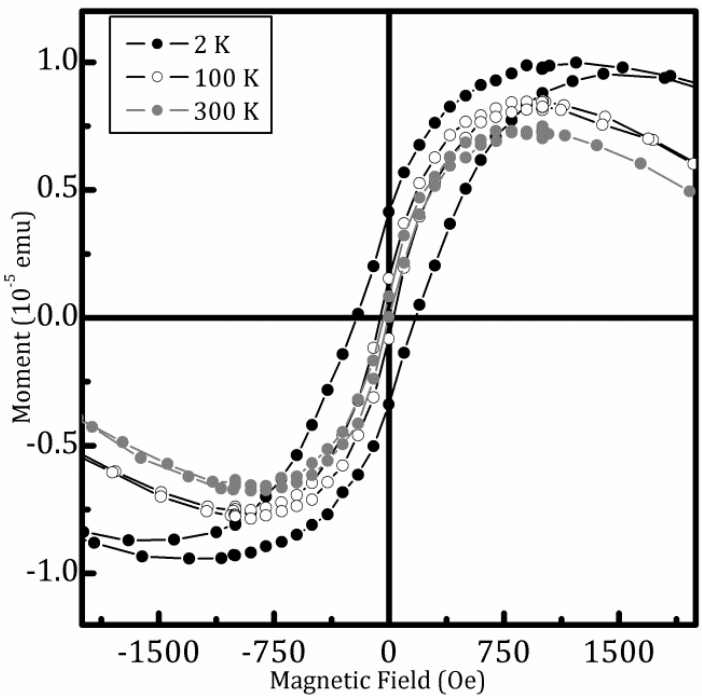

Figure 4.8. M *vs* B curves at 2, 100 and 300 K for nanocomposites with 5 wt% of nanoparticles

4.4. CONCLUSIONS

In this chapter maghemite nanoparticles were successfully modified by *grafting through* technique, as it was corroborated by FTIR and TGA. This functionalization with PS brushes was adequate to disperse the nanoparticles through the PS-*b*-P4VP block copolymer. Very good dispersions, without any remarkable agglomerates, were obtained. The addition of the nanoparticles affected the nanostructuring of the block copolymer. When neat block copolymer was exposed to dioxane vapors for 24 h, a hexagonal morphology was obtained, changing to a stripped one for a longer exposure time of 48 h. As the addition of nanoparticles seemed to reduce the mobility of PS domains, the formation of a totally stripped morphology after 48 h of exposure was not obtained. This fact seemed to indicate the presence of nanoparticles at PS domains, as it was confirmed after removing the organic part of nanocomposites by UV radiation. Moreover, the successful transference of magnetic properties to nanocomposites was demonstrated by magnetic characterization.

4.5. REFERENCES

Bartholome C., Beyou E., Bourgeat-Lami E., Chaumont P. and Zydowicz N., Nitroxide-Mediated Polymerizations from Silica Nanoparticle Surfaces: "Graft from" Polymerization of Styrene Using a Triethoxysilyl-Terminated Alkoxyamine Initiator. *Macromolecules* **2003**, 36, 7946-7952

Bean C.P. and Livingston J.D., Superparamagnetism. *J. Appl. Phys.* **1959**, 30, S120

Chi H.-Y., Hsu H.-W., Tung S.-H. and Liu C.-L., Nonvolatile Organic Field-Effect Transistors Memory Devices Using Supramolecular Block Copolymer/Functional Small Molecule Nanocomposite Electret. *ACS Appl. Mater. Interfaces* **2015**, 7, 5663-5673

Etxeberria H., Fernandez R., Zalakain I., Mondragon I., Eceiza A. and Kortaberria G,. Effect of CdSe nanoparticle addition on nanostructuring of PS-*b*-P4VP copolymer via solvent vapor exposure. *Journal of Colloid and Interface Science* **2014a**, 416, 25-29

Etxeberria H., Tercjak A., Mondragon I., Eceiza A. and Kortaberria G., Electrostatic force microscopy measurements of CdSe-PS nanoparticles and CdSe-PS/poly(styrene-b-butadiene-b-styrene) nanocomposites. *Colloid Polym Sci* **2014b**, 292, 229-234

Etxeberria H., Zalakain I., Fernandez R., Kortaberria G. and Mondragon I., Controlled placement of polystyrene-grafted CdSe nanoparticles in self-assembled block copolymers. *Colloid Polym Sci* **2013**, 291, 633-640

Etxeberria H., Zalakain I., Mondragon I., Eceiza A. and Kortaberria G., Generation of nanocomposites based on polystyrene-grafted CdSe nanoparticles by grafting through and block copolymer. *Colloid Polym Sci* **2013**, 291,1881-1886

Etxeberria H., Zalakain I., Tercjak A., Eceiza A., Kortaberria G. and Mondragon I., Functionalisation of CdSe Semiconductor Nanoparticles with Polystyrene Brushes by Radical Polimerization. *Journal of Nanoscience and Nanotechnology* **2012**, 12, 1-6

Gowd E.B., Nandan B., Bigall N.C., Eychmüller A., Formanek P. and Stamm M., Hexagonally ordered arrays of metallic nanodots from thin films of functional block copolymers. *Polymer* **2010**, 51, 2661-2667

Gutierrez J., Tercjak A., Garcia I. and Mondragon I., The effect of thermal and vapor annealing treatments on the self-assembly of TiO_2/PS-*b*-PMMA nanocomposites generated via the sol-gel process. *Nanotechnology* **2009**, 20, 225603 (9pp).

Henze M., Madge D., Prucker O. and Ruhe J., "Grafting through": mechanistic aspects of radical polymerization reactions with surface-attached polymers. *Macromolecules* **2014**, 47, 2929-2937

Henze M., Mädge D., Prucker O. and Rühe J., "Grafting Through": Mechanistic Aspects of Radical Polymerization Reactions with Surface-Attached Monomers. *Macromolecules* **2014**, 47, 2929-2937

Horechyy A., Nandan B., Zafeiropoulos N.E., Jehnichen D., Göbel M., Stamm M. and Pospiech D., Nanoparticle directed domain orientation in thin films of asymmetric block copolymers. *Colloid Polym Sci* **2014**, 292, 2249-2260

Jiles D., Intriduction to magnetism and magnetic materials. Taylor and Francis Group, Boca

Raton, **1998**

Kim M., Hong C.K., Choe S. and Shim S.E., Synthesis of polystyrene brush on multiwalled carbon nanotube treated with $KMnO_4$ in the presence of phase-transfer catalyst. *J Polym Sci Part A: Polym Chem* **2007**, 45, 4413-4420

Lu J. Q. and Yi S.S., Uniformly Sized Gold Nanoparticles Derived from PS-b-P2VP Block Copolymer Templates for the Controllable Synthesis of Si Nanowires. *Langmuir* **2006**, 22, 3951-3954

Lu Y.-S. and Kuo S.-W., Functional groups on POSS nanoparticles influence the self-assembled structures of diblock copolymer composites. *RSC Adv*. **2014**, 4, 34849-34859

Mendoza C.,·Gindy N., Wilhelm M.·and Fahmi A., Linear and non-linear viscoelastic rheology of hybrid nanostructured materials from block copolymers with gold nanoparticles. *Rheol Acta* **2011** 50, 257-275

Mueller R., Kammler H.K., Wegner K. and Pratsinis S.E., OH Surface Density of SiO_2 and TiO_2 by Thermogravimetric Analysis. *Langmuir* **2003**, 19, 160-165

Rahimi-Razin S., Haddadi-Asl V., Salami-Kalajahi M., Gehgoodi-Sadabad F. and Roghani-Mamaqani H., Matrix-grafted multiwalled carbon nanotubes/ poly(methyl methacrylate) nanocomposites synthesized by in situ RAFT polymerization: A kinetic study. *Int J Chem Kinet* **2012**, 44, 555-569

Rodriguez M.A., Liso M.J., Rubio F. Rubio J. and Oteo J.L., Study of the reaction of γ-methacryloxypropyltrimethoxysilane(γ-MPS) with slate surfaces. *Journal of Material Science* **1999,** 35, 3867–3873

Rozes L., Fornasieri G., Trabelsi S., Creton C., Zafeiropoulos N.E., Stamm M. and Sanchez C.,Reinforcement of polystyrene by covalently bonded oxo-titanium clusters. *Progress in Solid State Chemistry* **2005,** 33, 127-135

Schulz L., Schirmacher W, Omran A., Shah V.R., Böni P., Petry W. and Müller-Buschbaum P., Elastic torsion effects in magnetic nanoparticle diblock-copolymer structures. *J. Phys.: Condens. Matter* **2010**, 22, 346008 (6pp)

Schulze M.W., Sinturel C., and Hillmyer M.A., Poly(cyclohexylethylene)-block-poly(ethylene oxide) Block Polymers for Metal Oxide Templating. *ACS Macro Lett.* **2015**, 4, 1027-1032

Sun Y., Ding X., Zheng Z., Cheng X., Hu X. and Peng Y., Surface initiated ATRP in the synthesis of iron oxide/polystyrene core/shell nanoparticles. *Eur Polym J* **2007**, 43, 762-772

Sung J., Jo P.S., Shin H., Huh J., Min B.G., Kim D.H. and Park C., Transparent, Low-Electric-Resistance Nanocomposites of Self-Assembled Block Copolymers and SWNTs. *Adv. Mater.* **2008**, 20, 1505-1510

Trabelsi S., Janke A., Hassler R., Zafeiropoulos N.E., Fornasieri G., Bocchini S., Rozes L., Stamm M., Gerard J.-F. and Sanchez C., Novel Organo-Functional Titanium-oxo-cluster-Based Hybrid Materials with Enhanced Thermomechanical and Thermal Properties. *Macromolecules* **2005**, 38, 6068-6078

Wang J., de Jeu W.H., Müller P., Möller M. and Mourran A., Thin Film Structure of Block Copolymer−Surfactant Complexes: Strongly Ionic Bonding Polymer Systems. *Macromolecules* **2012**, 45, 974-985

Wu J., Li H., Wu S., Huang G., Xing W., Tang M. and Fu Q., Influence of Magnetic Nanoparticle

Size on the Particle Dispersion and Phase Separation in an ABA Triblock Copolymer. *J. Phys. Chem. B* **2014**, 118, 2186-2193

Xu C., Ohno K., Ladmiral V., Milkie D.E., Kikkawa J.M. and Composto R.J., Simultaneous Block Copolymer and Magnetic Nanoparticle Assembly in Nanocomposite Films. *Macromolecules* **2009,** 42, 1219-1228

Ye T., Chen X., Fan X. and Shen Z. Ordered gold nanoparticle arrays obtained with supramolecular block copolymers. *Soft Matter* **2013**, 9, 4715-4724

Zeng H., Black C.T., Sandstrom R.L., Rice P.M., Murray C.B. and Sun S., Magnetotransport of magnetite nanoparticle arrays. *Physical Reviw B* **2006**, 73, 020402(R)

Zhang B.-Q., Chen G.-D., Pan C.-Y., Luan B. and Hong C.-Y., Preparation, Characterization, and Thermal Properties of Polystyrene-*block*-Quaternized Poly(4-vinylpyridine)/ Montmorillonite Nanocomposites*. Journal of Applied Polymer Science* **2006**, 102, 1950-1958

Zu X., Gong J., Tu W. and Deng Y., Selective and Sequential Re-Assembly of Patterned Block Copolymer Thin Film for Fabricating Polymeric, Inorganic, and Their Composite Nanostructured Arrays. *Macromol. Rapid Commun.* **2011**, 32, 1526-1532

Chapter 5

SYNTHESIS AND CHARACTERIZATION OF PS-*b*-PMMA/Fe_2O_3-PMMA NANOCOMPOSITES: *grafting through* method

5.1. INTRODUCTION

PS-*b*-PMMA is one of the most used matrixes for preparing nanocomposites based on BCP and inorganic nanoparticles, as it can be seen in many works published in the literature. Among them, those based on silica nanoparticles or silicates have been the most studied. In this way, Limary et al. analyzed the stability of systems based on a symmetric diblock copolymer blended with layered silicates (Limary et al. 2000); Nyström et al. prepared organic/inorganic hybrid materials consisting of nanosized silica particles with surface-grafted PS or PS-*b*-PMMA (Nyström et al. 2005); and Chakkalakal et al. discussed the influence of rheological and morphological properties on the foaming behavior of PS-*b*-PMMA diblock copolymers and their composites with PMMA-modified silica nanoparticles (Chakkalakal et al. 2013). Apart from those with silica nanoparticles, many works on nanocomposites with other nanoparticles can be also found. Lopes and Jaeger demonstrated that this BCP could be a good platform for the generation of guided, large-scale assembly of laterally nanostructured systems. They prepared nanocomposites by thermal evaporation of metal onto copolymer films, allowing the diffusion of metal atoms. During the deposition of metal nanoparticles, the template morphology of BCP did not change, as long as the molecular mass was high enough to reach the order-disorder transition temperature (ODT). They studied the behavior of Au, Ag, In, Pb, Sn and Bi nanoparticles, Au and Ag nanoparticles were placed at PS domains, while the rest were placed at PMMA ones (Lopes and Jaeger 2001). Zhao et al. prepared nanocomposites by adding palladium nanoparticles to PS-*b*-PMMA, and studied how the ODT was altered (Zhao et al. 2013). Kim et al. fabricated nanocomposites based on PS-*b*-PMMA and shell-crosslinked, thermally stable gold nanoparticles functionalized with different compositions of PS and PMMA brushes for being selective to PS or PMMA or neutral, analyzing their effect on the morphology of BCP Pang et al. prepared nanocomposites with ferroelectric $BaTiO_3$ capped with PS chains, analyzing their

dielectric properties (Pang et al. 2013). Hailu et al. functionalized TiO_2 nanoparticles with PMMA-*b*-PS block copolymer and analyzed their dispersion in PS and PMMA homopolymers, and in PS-*b*-PMMA block copolymer. They obtained good dispersions for PMMA and PS-*b*-PMMA-based films, in contrast to the poor dispersion for PS-based ones. They explained this behavior on the basis of the outer PMMA corona of functionalized nanoparticles (Hailu et al. 2015).

PS-*b*-PMMA has also been used as a platform for preparing nanocomposites with magnetic nanoparticles. In this way, Xu et al. prepared nanocomposites with PMMA-functionalized Fe_3O_4 nanoparticles. Varying the length of PMMA brushes, they found that nanoparticles with short polymer brushes were better dispersed than those with long ones, which tend to form aggregates (Xu et al. 2009). Xia et al. prepared nanocomposites with γ-Fe_2O_3 nanoparticles, and analyzed the effect of their concentration on film morphology, both at the surface and across it (Xia et al. 2011). Yang et al. reported the effect of oleic acid-capped magnetic nanoparticles on the morphology and phase separation behavior of PS-*b*-PMMA thin films varying experimental parameters such as casting solvent, nanoparticle concentration, and annealing time (Yang et al. 2012). Schlage et al. obtained nanostructured magnetic antidot arrays by sputter deposition of Fe nanoparticles onto a highly ordered, nanostructured copolymer template by using a new kind of synchrotron radiation three-dimensional X-ray microscopy (Schlage et al. 2012). Yao et al. used this BCP as a platform for controlling the alignment of magnetic nanoparticles, obtaining hybrid films with superparamagnetic behavior and remarkable shape anisotropy that render them interesting for magnetic applications (Yao et al. 2014).

Hybrid systems based on PS-*b*-PMMA have also been prepared by our group. Gutierrez et al. used this BCP as structure-directing agent for generating TiO_2/PS-*b*-PMMA nanocomposites via the sol-gel process using a hydrophobic surfactant. They obtained arrays of TiO_2 nanoparticles on substrate surface. Cano et al.

incorporated as-synthesized organic-capped TiO_2 nanorods into PS-*b*-PMMA diblock copolymer to achieve TiO_2/PS-*b*-PMMA nanocomposites with enhanced optical and conductive properties.

The main objectives of the work described in this chapter are the following. Firstly, functionalization of maghemite nanoparticle surface with MPTS silane, in order to improve their compatibility with PS-*b*-PMMA copolymer. Second, functionalization and characterization of nanoparticle surface from previously attached silane with PMMA brushes by *grafting through* technique. Finally, the preparation and characterization of nanocomposites based on PS-*b*-PMMA block copolymer and both silanized and PMMA-modified magnetic nanoparticles. Functionalization of nanoparticles has been analyzed by FTIR and TGA while the morphology of nanocomposites was studied by AFM and TEM. In order to check if magnetic properties of nanoparticles have been transferred to the nanocomposites, their magnetic characterization has been carried out by VSM.

5.2. MATERIALS AND METHODS

5.2.1. MATERIALS

Maghemite nanoparticles with a nominal size of 9 nm and a polydispersity of 1.08 were used as inorganic fillers. They were purchased from Integram Technologies. In this chapter MPTS, purchased from ABCR with 98 % of purity, was used as the linking between nanoparticle surface and polymer brushes. AIBN was used as initiator without further purification. The monomer used for the synthesis of polymer brushes was the methyl methacrylate (MMA), purchased from Aldrich with a purity of 99 %, further purified by distilling under reduced pressure over CaH_2. PS-*b*-PMMA copolymer (f_{PS} = f_{PMMA} = 0.5) was purchased from Polymer Source, Inc., with a M_n of 80,000 g/mol for both PS and PMMA blocks, and a polydispersity index of 1.09. Toluene, THF and acetone, all purchased from

Aldrich, were used as solvents for nanocomposite preparation. Chemical structures of silane, monomer and copolymer are shown in Scheme 5.1.

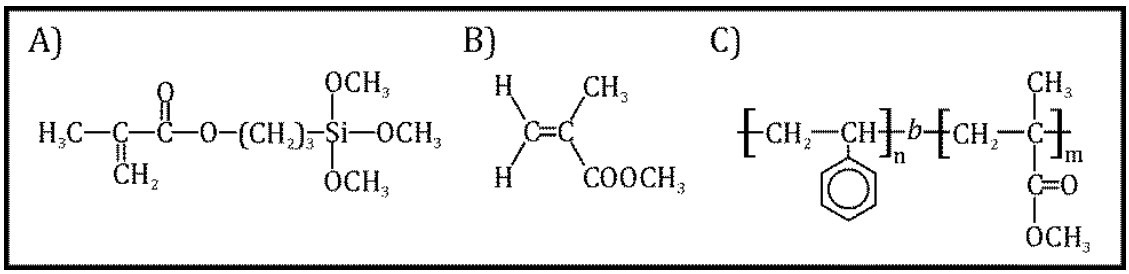

Scheme 5.1. Chemical structure of A) MPTS, B) MMA monomer and C) PS-*b*-PMMA copolymer

5.2.2. METHODS

5.2.2.1. Nanoparticle functionalization

Nanoparticle modification was carried out in two steps, as it is shown in Scheme 5.2: first the silanization process and then the synthesis of the PMMA polymer brushes onto the silanized nanoparticles by *grafting through* method.

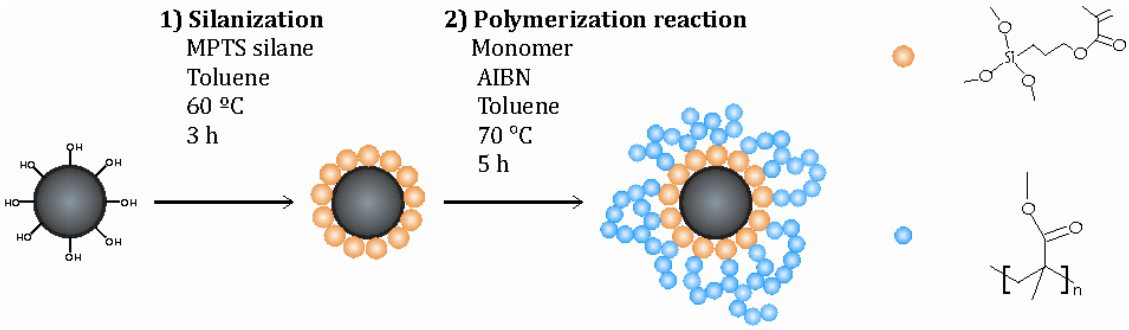

Scheme 5.2. Nanoparticle modification procedure

5.2.2.1.1. Silanization process

The silanization process was carried out following the procedure described in section 4.2.2.1.1 of Chapter 4.

5.2.2.1.2. Growth of PMMA brushes by *grafting through* method

After silanization, nanoparticles were modified with PMMA brushes by *grafting through* method. For this purpose, 0.02 g of silanized Fe_2O_3 nanoparticles and 0.1 g of AIBN were dispersed into 40 mL of toluene adding 2 mL of MMA monomer once nanoparticles were well dispersed. The reaction was carried out in inert N_2 atmosphere at 70 °C for 5 h. When reaction was ended, modified nanoparticles were subsequently washed with THF, until any monomer rest was eliminated (probed by FTIR), and dried in vacuum for 72 h at 40 °C.

5.2.2.2. Nanocomposite preparation

In order to analyze the effect of functionalization on nanoparticle dispersion nanocomposites were prepared by mixing PS-*b*-PMMA block copolymer with pristine, silanized and PMMA-modified Fe_2O_3 nanoparticles. First nanoparticles were dispersed in toluene for 2 h by sonication, then adding PS-*b*-PMMA block copolymer. Both neat block copolymer and organic/inorganic nanocomposite thin films were prepared by spin-coating onto silicon wafers (Si(100), from Si-Mat) at 2000 rpm for 120 s, using a P6700 spin-coater from Specialty Coating Systems Inc.. The nanostructuring of the copolymer was obtained by solvent vapor annealing, carried out by exposing thin films to acetone vapors for 16 h in a closed vessel at room temperature. Acetone is a selective solvent for PMMA, as it can be seen from its interaction parameters with both blocks: χ_{PMMA} = 0.18 and χ_{PS} = 1.1 (Xuan et al. 2004). After exposure samples were removed and stored at room temperature before characterization. This exposure time of 16 h was optimized in order to obtain a lamellar morphology for the neat copolymer. Nanocomposites with 1, 2, and 5 wt% of nanoparticles were prepared.

5.2.2.3. Characterization techniques

5.2.2.3.1. FTIR

It was used to verify the functionalization of iron oxide nanoparticles. Infrared spectra were carried out in a Nicolet Nexus 670 Spectrometer, as it was described in section 3.2.2.3.3 of Chapter 3.

5.2.2.3.2. TGA

It was used to determine the amount of hydroxyl groups at nanoparticle surface, the amount of grafted silane and the weight loss related to the grafted PMMA brushes, which would probe the success of the polymerization reaction. TGA results were obtained using a TGA/SDTA-851e equipment running from 25 to 750 °C at a heating rate of 10 °C/min under nitrogen atmosphere, as was shown in section 3.2.2.3.4 of Chapter 3.

5.2.2.3.3. AFM

It was used to study the surface morphologies of neat block copolymer films, and those of nanocomposites with silanized or PMMA-modified nanoparticles. AFM measurements were performed in tapping mode using a Dimension Icon Nanoscope V (Bruker) as it was described in section 3.2.2.3.6 of Chapter 3.

5.2.2.3.4. TEM

It was used to verify the morphology of neat block copolymer films, with a Philips Tecnai 20 transmission electron microscope operated at 200 kV with 2.5 Å resolution. This technique was described in section 3.2.2.3.5 of Chapter 3.

5.2.2.3.5. VSM

Magnetic characterization was carried out in a Quantum Design Physical Properties Measurement System (PPMS) with Vibrating Sample Magnetometer option, by measuring hysteresis loops at 2 and 150 K. This technique was described in section 4.2.2.3.4 of Chapter 4.

5.3. RESULTS AND DISCUSSION

5.3.1. NANOCOMPOSITES WITH SILANIZED NANOPARTICLES

MPTS presents a methacrylate group in its chemical structure (Scheme 5.1), that could increase the compatibility between nanoparticles and PMMA block of the BCP, improving their dispersion when compared with that of pristine nanoparticles. Moreover, MPTS silane gives the chance to synthesize PMMA brushes by *grafting through* procedure (Scheme 5.2). Both characteristics make it an interesting coupling agent to be investigated in this chapter.

5.3.1.1. Characterization of silanized nanoparticles

Characterization of MPTS-silanized nanoparticles has been shown in section 4.3.1 of Chapter 4. The success of silanization process has been probed by FTIR and TGA. In FTIR spectrum, the appearance of bands related to the main bonds of MPTS compound is observed: C=O stretching vibration, C-O-C stretching deformation vibration and Si-O-Fe stretching vibration. By TGA measurements surface density of grafted silane has been calculated to be around 2.8 molecules/nm^2.

5.3.1.2. Morphology of nanocomposites based on silanized nanoparticles

Surface morphologies of neat block copolymer and nanocomposite thin films have been analyzed by AFM and TEM. Figure 5.1 shows AFM images of neat PS-*b*-PMMA copolymer film. Brighter regions in the phase contrast AFM image correspond to PMMA block, as it presents a higher modulus than PS at room temperature (Xuan et al. 2004, Peng et al. 2005). For neat copolymer, surface-perpendicular lamellar microphase morphology can be seen, with an average interlamellar distance of 77 nm. This morphology is the typical equilibrium state phase structure in symmetric diblock copolymer thin films (Xuan et al. 2004). As it has been pointed out by several authors (Xuan et al. 2004, Gutierrez et al. 2009) this ordered microphase morphology can be obtained by exposing films to the vapors of a selective solvent for PMMA block. Previous works (Xuan et al. 2004, Gutierrez et al. 2009, Green et al. 1990, Green et al. 1991, Anastasiadis et al. 1989, Russel et al. 1989) have shown that when PS-*b*-PMMA is cast on a silicon wafer, PMMA segregates to the surface while PS segregates to the air interface. So after spin-coating it seems that PMMA dominates the substrate interface while PS is placed mainly at the free surface. Since acetone is a selective solvent for PMMA when compared with PS, when films are exposed to its vapors, there is a strong attraction between PMMA block and solvent, while the net interaction between polymer segments is repulsive. Polymer chains start to swell when they are in contact with the solvent. The diffusion of the solvent to the surface plays an important role in obtained morphology. In this way, for PS-*b*-PMMA, Xuan et al. proposed a mechanism of solvent vapor annealing for PMMA-selective solvents. Taking all this into account, several microphase-separated morphologies have been observed by different authors for PS-*b*-PMMA depending on exposure time and film thickness: hexagonally packed nanocylinders, striped or lamellar morphologies. In our case, as the aim was to obtain the typical equilibrium lamellar morphology, an exposure time of 16 h was performed in acetone vapors, achieving the desired morphology, as shown in the Figure 5.1.

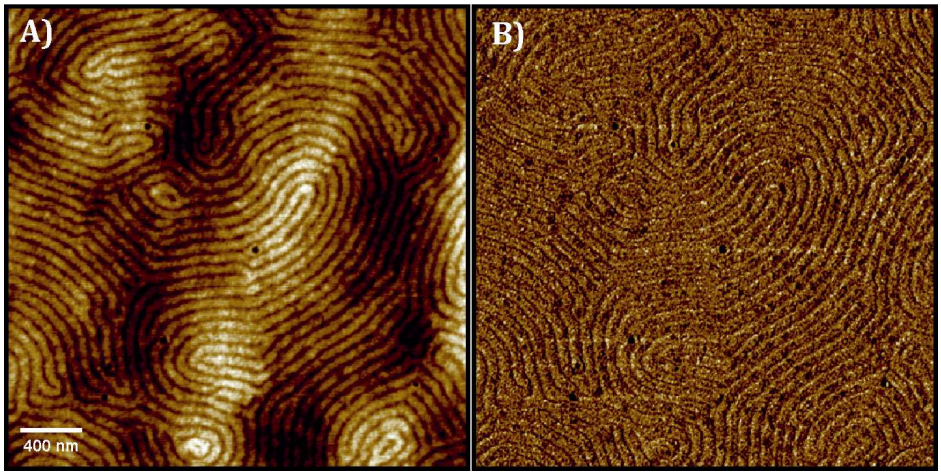

Figure 5.1. AFM height (A) and phase (B) images of neat PS-*b*-PMMA copolymer

Lamellar morphology of neat block copolymer films has also been confirmed by TEM, as it can be seen in Figure 5.2. PS domains are represented as dark areas, while PMMA ones correspond to bright areas, due to higher electron density of the former.

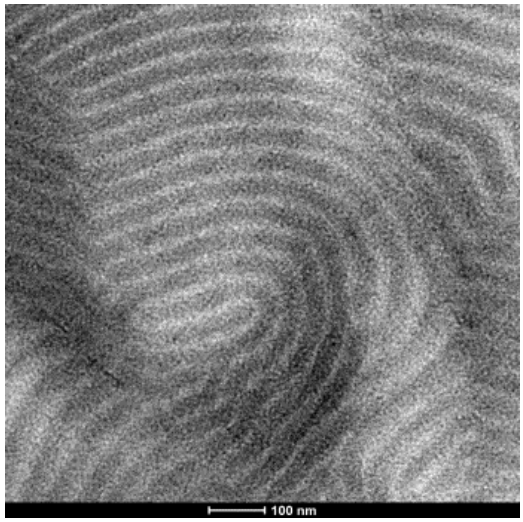

Figure 5.2. TEM micrograph of neat PS-*b*-PMMA copolymer

Figure 5.3 shows AFM images of nanocomposites thin film with 1, 2 and 5 wt% of silane-modified nanoparticles.

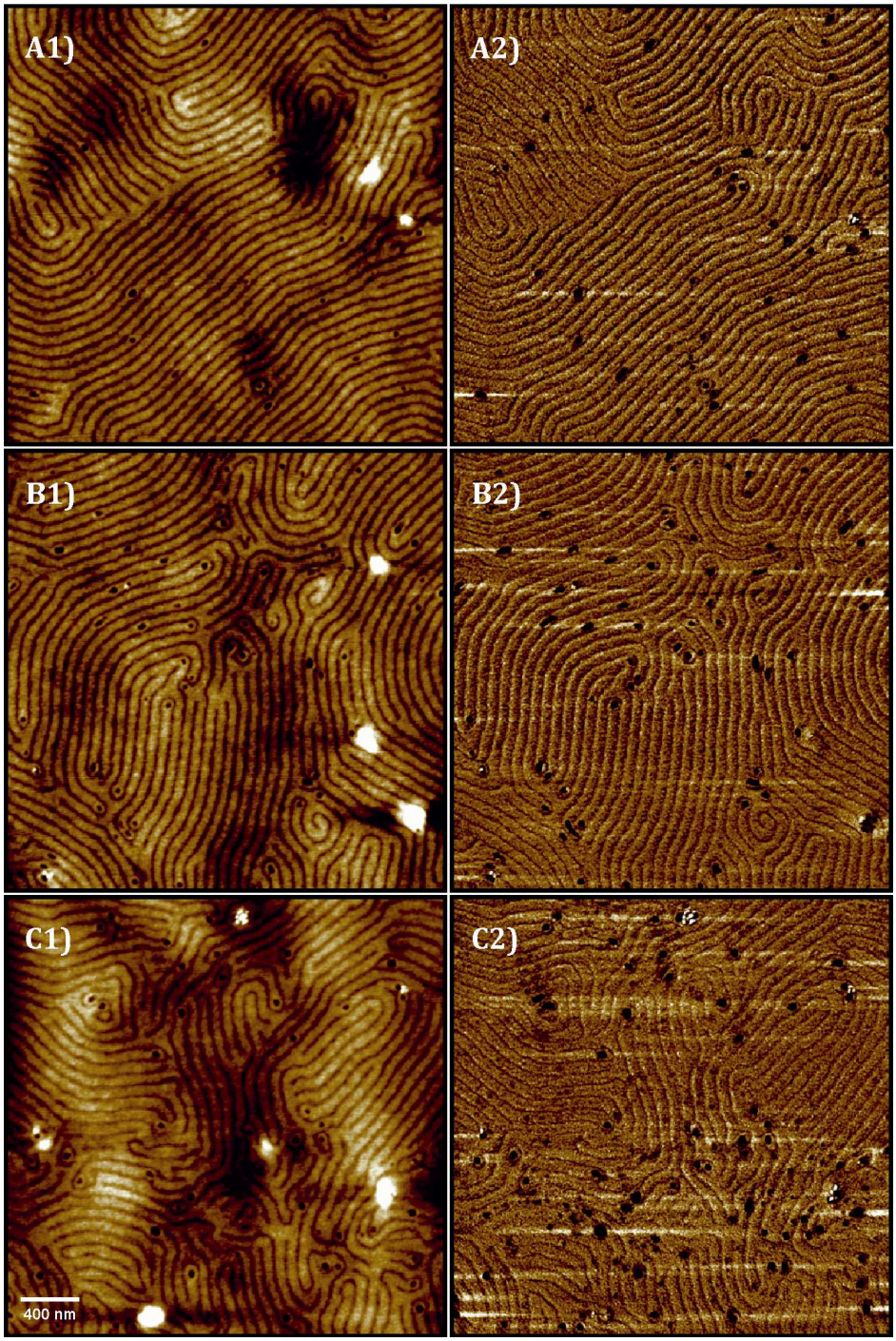

Figure 5.3. AFM height (1) and phase (2) images corresponding to thin films of nanocomposites with: A) 1 wt%, B) 2 wt%, and C) 5 wt% of silanized nanoparticles, after annealing with acetone vapors for 16 h

When silane-modified nanoparticles have been added lamellar morphology is maintained. Although big nanoparticle agglomerates appeared, they do not disturb the lamellar morphology of neat BCP. Those agglomerates tended to

PMMA domains but as their size is bigger than that of PMMA lamellae, they could not be selectively located at PMMA domains, as it was desired.

5.3.2. NANOCOMPOSITES WITH PMMA-MODIFIED NANOPARTICLES

5.3.2.1. Characterization of PMMA-modified nanoparticles

As the results obtained with silane-modified nanoparticle are not as good as expected and nanoparticles are not selectively placed at PMMA domains, they have been modified with PMMA brushes by *grafting through* method, in order to improve their dispersion through PMMA domains of nanostructured block copolymer. The presence of brushes in the surface has been probed by FTIR and TGA. In Figure 5.4 the FTIR spectra of pristine, silanized and PMMA-modified nanoparticles can be seen.

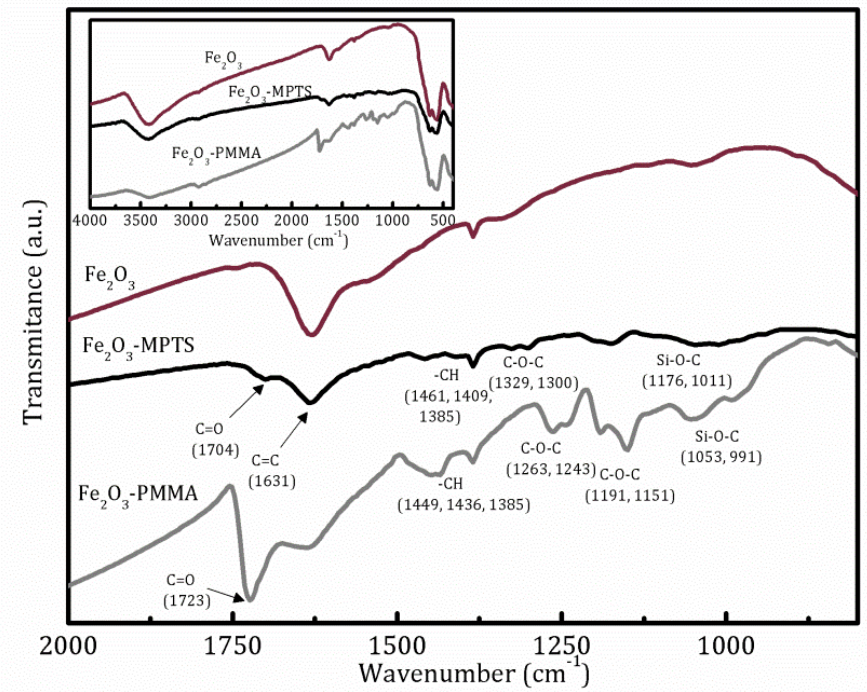

Figure 5.4. FTIR spectra of pristine, silanized and PMMA-modified nanoparticles. Main bands are indicated by arrows. Inner spectrum shows a magnification of the spectra

The presence of an intense band corresponding to the stretching vibration of carbonyl group of methacrylate at 1723 cm^{-1} demonstrates the presence of the PMMA brushes. Moreover, bands related to the stretching vibration of C-O-C bonds at 1263, 1243, 1191 and 1151 cm^{-1} corroborate the presence of the PMMA brushes (Yan et al. 2009).

TGA thermogram of pristine, silanized and PMMA-modified nanoparticles can be seen in Figure 5.5. The weight loss related to the degradation of PMMA brushes can be clearly seen, thus probing the presence of the polymer in the sample.

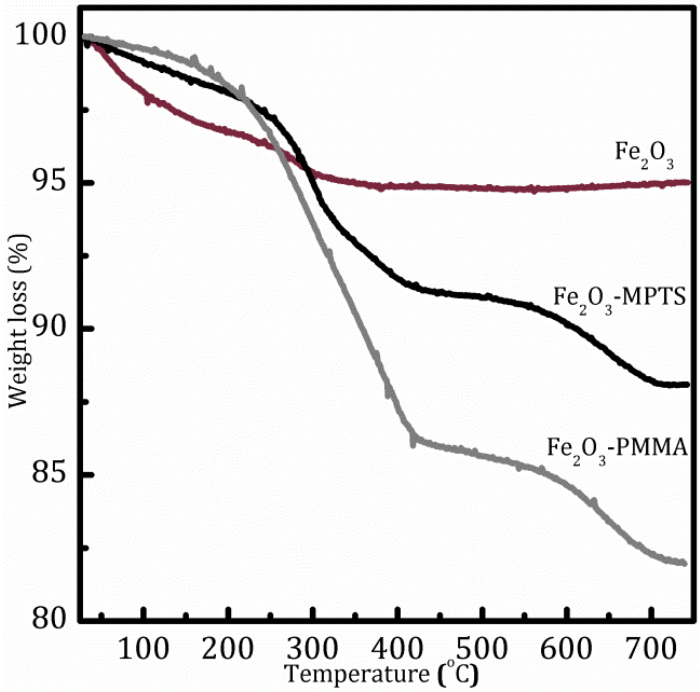

Figure 5.5. TGA thermograms of pristine, silanized and PMMA-modified nanoparticles

5.3.2.2. Morphology of nanocomposites with PMMA-modified nanoparticles

Surface morphology of nanocomposite films with PMMA-modified nanoparticles has also been analyzed by AFM. Figure 5.6 shows the AFM images of nanocomposites with 2 and 5 wt% of PMMA-modified nanoparticles.

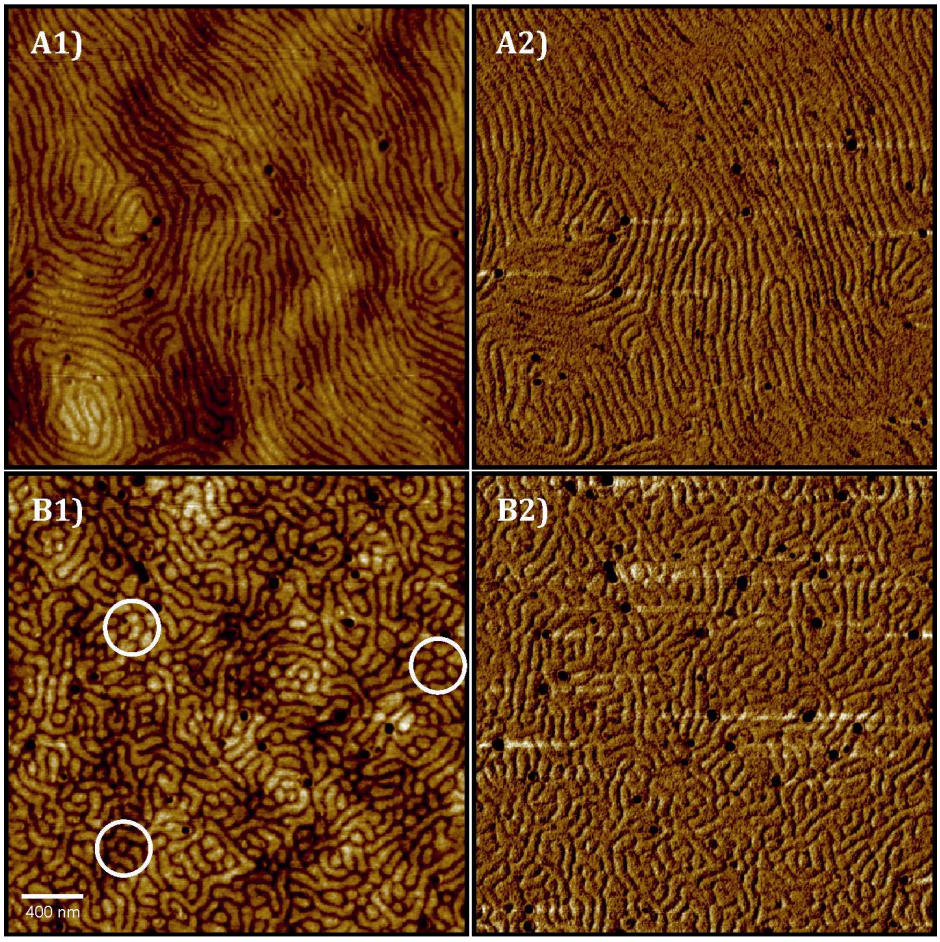

Figure 5.6. AFM height (1) and phase (2) images corresponding to nanocomposites thin films with: A) 2 wt% and B) 5 wt% of PMMA-grafted nanoparticles after annealing with acetone vapors for 16 h

As it can be seen, the lamellar morphology of neat copolymer is maintained for nanocomposites with 2 wt%, though lamellae are not as regular and parallel among them as has been for the neat block copolymer. In the same way, as the width of PMMA lamellae increases, it can be supposed that nanoparticles have been placed on them. There are no remarkable agglomerates in the nanocomposites, indicating that dispersion has been improved with PMMA brushes. Corroborating the reason for lamellae width increase, in height images the presence of nanoparticles at PMMA domains can be noticed. Moreover, as indicative of the presence of nanoparticles at PMMA domains, for nanocomposites with 5 wt% of nanoparticles, the morphology started to change and a mixture of lamellae and perpendicular hexagonally packed cylinders (circles in Figure 5.6.B1) can be seen. This could be due to the presence of nanoparticles, which,

located at PMMA domains, alter the volume fraction among blocks, altering the equilibrium morphology. As a higher amount of nanoparticles is present at PMMA domains when comparing with nanocomposites with 1 and 2 wt% of nanoparticles, the volume ratio among blocks is altered, promoting the morphology change. This change in morphology promoted by the specific location of nanoparticles in one block has also been found by other authors (Gutierrez et al. 2009, Xu et al. 2008). Gutierrez et al. found that PS-*b*-PMMA block copolymer thin films, annealed with acetone vapors for 48 h, changed their morphology from hexagonally packed cylinders to lamellar and striped structures with 5 and 10 w% of TiO_2 nanoparticles, respectively. Xu et al. dispersed magnetic nanoparticles with different molecular weight PMMA in thermally annealed PS-*b*-PMMA films. For around 4 wt% of nanoparticles with the lowest molecular weight brushes (2700 g/mol), the morphology changed from perpendicular lamellae to a mixture of perpendicular and parallel ones, frustrating the assembly of lamellar structure for contents higher than 10 wt%. Upon increasing molecular weight of brushes (35,700 g/mol), nanoparticles tended to aggregate, and the copolymer assembling into onion-like rings around them. In our case, morphology of nanocomposites started to change between 2 and 5 wt% of PMMA-modified nanoparticle concentration without remarkable agglomerates that could frustrate the assembly.

In order to clearly show the improvement of dispersion and the selective placement of nanoparticles by modifying them with PMMA brushes, Figure 5.7 shows the AFM images of nanocomposites prepared with 2 wt% of pristine, silanized and PMMA-modified nanoparticles. Pristine nanoparticles have frustrated the assembly of the copolymer, as it can be seen in Figure 5.7.A. Once they have been functionalized with MPTS, the lamellar morphology of the copolymer has been maintained but nanoparticles tended to aggregate, as it can be seen in Figure 5.7.B. Finally, when they have been surface-modified with PMMA

brushes, nanoparticles are well dispersed and selectively placed at PMMA domains maintaining lamellar morphology for 1 and 2 wt% nanocomposites.

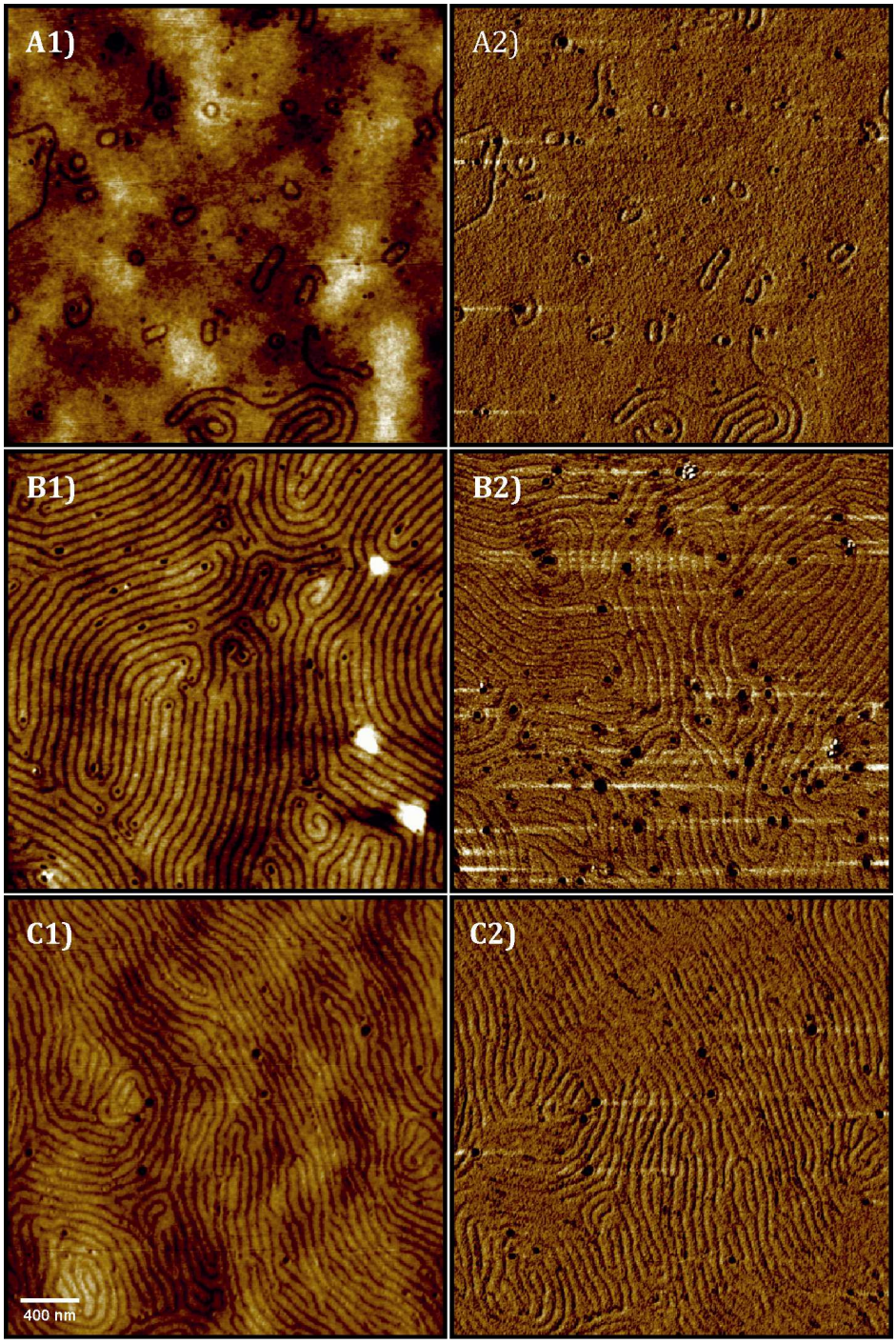

Figure 5.7. AFM height (1) and phase (2) images corresponding to thin films of nanocomposites with: A) 2 wt% of pristine, B) 2 wt% of silanized, and C) 2 wt% of PMMA-grafted nanoparticles, after annealing with acetone vapors for 16h

In three dimensional AFM images of thin film nanocomposites shown in Figure 5.8 the effect of nanoparticles on the morphology of BCP can be more clearly seen. As it is shown in Figure 5.8.A, corresponding to the neat block copolymer, the height of the lamellae is continuous, with no appreciable discontinuity. When silane-modified nanoparticles are added (Figure 5.8.B) the appearance of hills can be seen, located at PMMA domains. Apart from these hills, the height of PMMA lamellae can be considered continuous. These hills could represent small aggregates of Fe_2O_3 nanoparticles modified with MPTS silane, present at PMMA domains due to their improved affinity. However, a good dispersion has not been achieved, as their presence through the rest of the PMMA domains is negligible. Figures 5.8.C and D show 3D AFM images for nanocomposites with 2 and 5 wt% of PMMA-modified nanoparticles, respectively. The presence of the nanoparticles can be seen as small points standing out from PMMA domains. At 2 wt% of PMMA-modified nanoparticle concentration the surface of lamellae is no more continuous, in 3D height AFM images small discontinuities, as small points standing out, appear at PMMA domains, indicating that nanoparticles are well located through all PMMA domains, confirming the improvement of dispersion, respecting to nanocomposites with silane-modified nanoparticles. Also in 3D height AFM images of nanocomposites with 5 wt% of PMMA-modified nanoparticles, PMMA domains surface is not continuous, and nanoparticles can be identified as small points standing out. Comparing the images of nanocomposites with 2 and 5 wt%, previously shown morphology change is confirmed. With the lowest concentration lamellar morphology is maintained, while for higher amounts a mixture of lamellar and cylindrical morphology is obtained, as it has been previously pointed out.

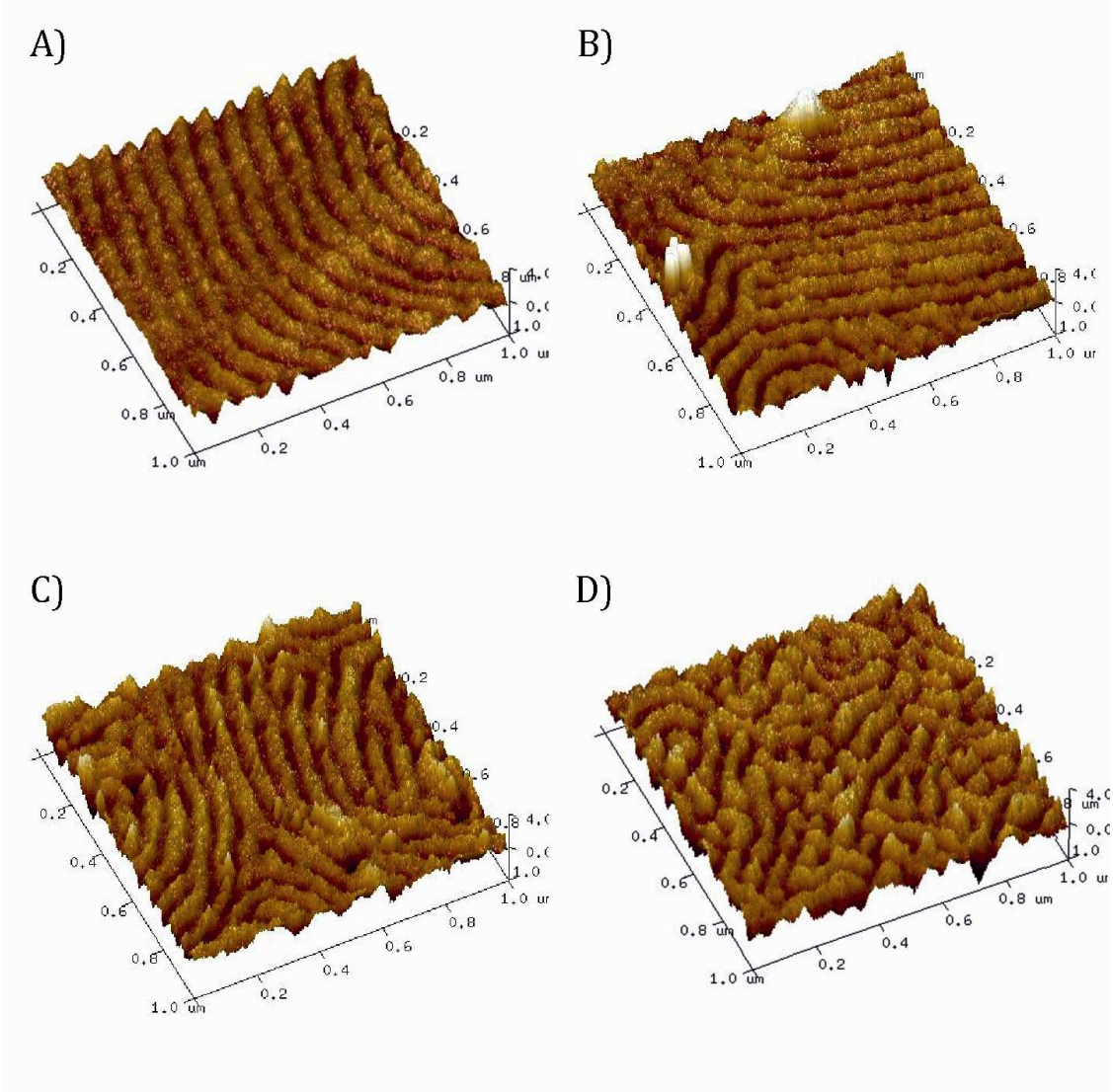

Figure 5.8. AFM 3D height images corresponding to thin films of: A) neat PS-*b*-PMMA copolymer, nanocomposites with B) 2 wt% of silanized, C) 2 wt% of PMMA-grafted, and D) 5 wt% of PMMA-grafted nanoparticles, after annealing with acetone vapors for 16 h

In Figure 5.9 AFM height and profile images of neat block copolymer and nanocomposite with 2 wt% of silanized nanoparticles and PMMA-modified nanoparticles can be seen. From the profiles, the effect of nanoparticles on PMMA domains can be clearly seen. For neat copolymer, PMMA domains are continuous while silanized nanoparticle addition creates some hills on the lamellae. The good dispersion of PMMA-modified nanoparticles on PMMA domains can be also seen from the corresponding profile.

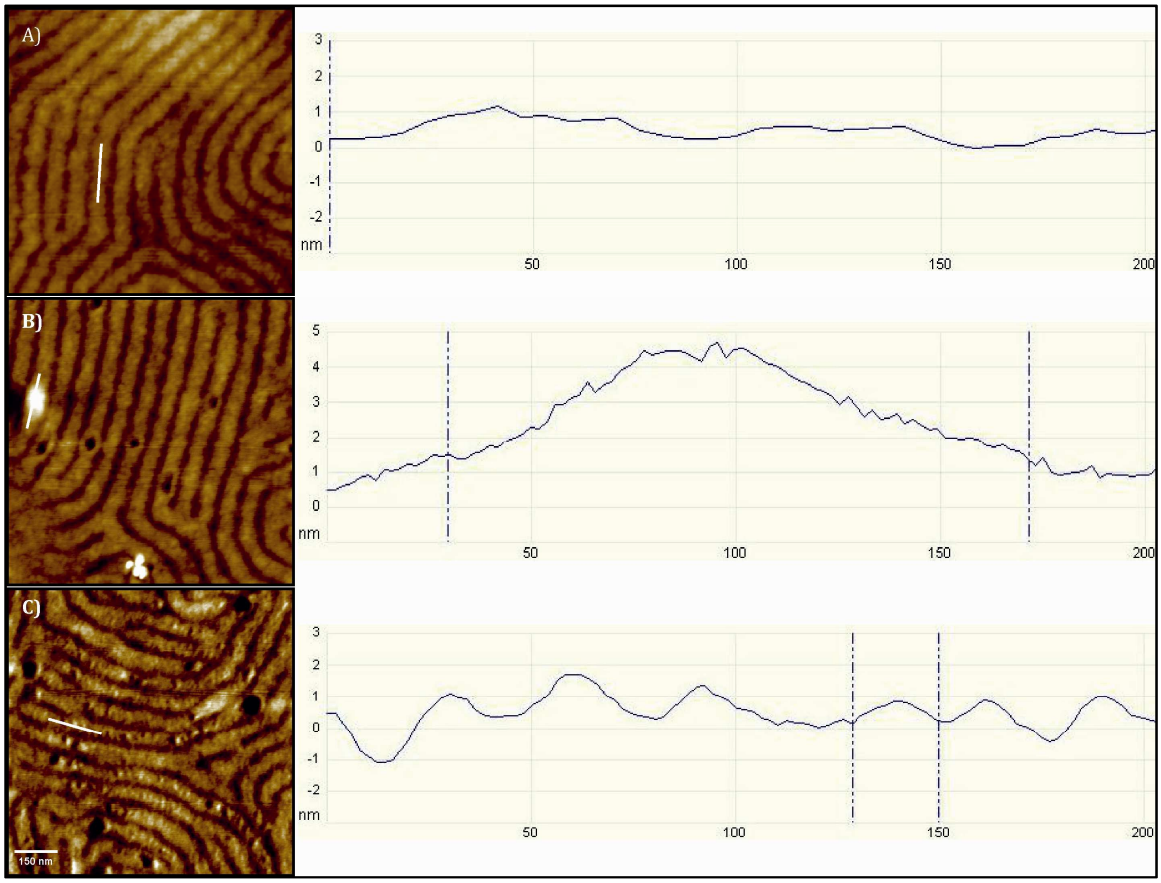

Figure 5.9. AFM height and the profile images of: A) neat PS-*b*-PMMA copolymer, and nanocomposites with B) 2 wt% of silanized, C) 2 wt% of PMMA-grafted nanoparticles

In order to better visualize nanoparticles and have an approximate idea of their average size, films of nanocomposites containing PMMA-grafted nanoparticles have been thermally degraded removing the organic part. As an example, Figure 5.10 shows the AFM image of charred nanocomposite film containing 5 wt% of nanoparticles. Nanoparticle size varies from around 20 to 45 nm for all the nanocomposites studied, smaller than the size of PMMA domains in which they are located. It is clear that some nanoparticles appear together since their nominal diameter is around 9 nm. Obtained nanoparticle sizes agree with those obtained from the profile images of Figure 5.9.C. Those small aggregates probably have been formed during functionalization by *grafting through* and not during nanocomposite preparation or during annealing, as it was pointed out in Chapter 4.

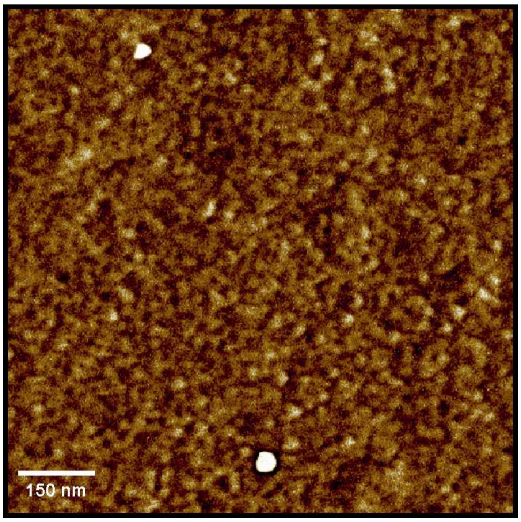

Figure 5.10. AFM phase image corresponding to a thin film of the nanocomposite with 5 wt% of PMMA-grafted nanoparticles after thermal degradation of the polymeric matrix

5.3.3. MAGNETIC CHARACTERIZATION

Figure 5.11 shows the ZFC/FC curves of nanocomposites with 2 and 5 wt% of nanoparticles, as obtained with VSM. Usually, organic/inorganic nanocomposites exhibit a typical superparamagnetic behavior at room temperature and a ferromagnetic one at low temperatures (Zeng et al. 2006, Bean and Livingston 1959). Below the blocking temperature (T_B~175 K) FC and ZFC magnetization curves diverge, magnetic moments are singledomain and spinned by anisotropy, while they appear thermally disordered above the T_B. Both samples show the same behavior, as T_B coincides for both measurements. This parameter is directly related to the size of nanoparticles (as it can be concluded from Néel-Brown expression, explained in the section 2.4 of Chapter 2), or to the size of aggregates that could be formed. As it was mentioned in Chapter 4, aggregates could be formed when nanoparticles were in solution during their modification, before thin film preparation. This fact would reinforce the hypothesis about the formation of small aggregates of nanoparticles during the polymerization reaction in the *grafting through* process, as it has been pointed out in Chapter 4.

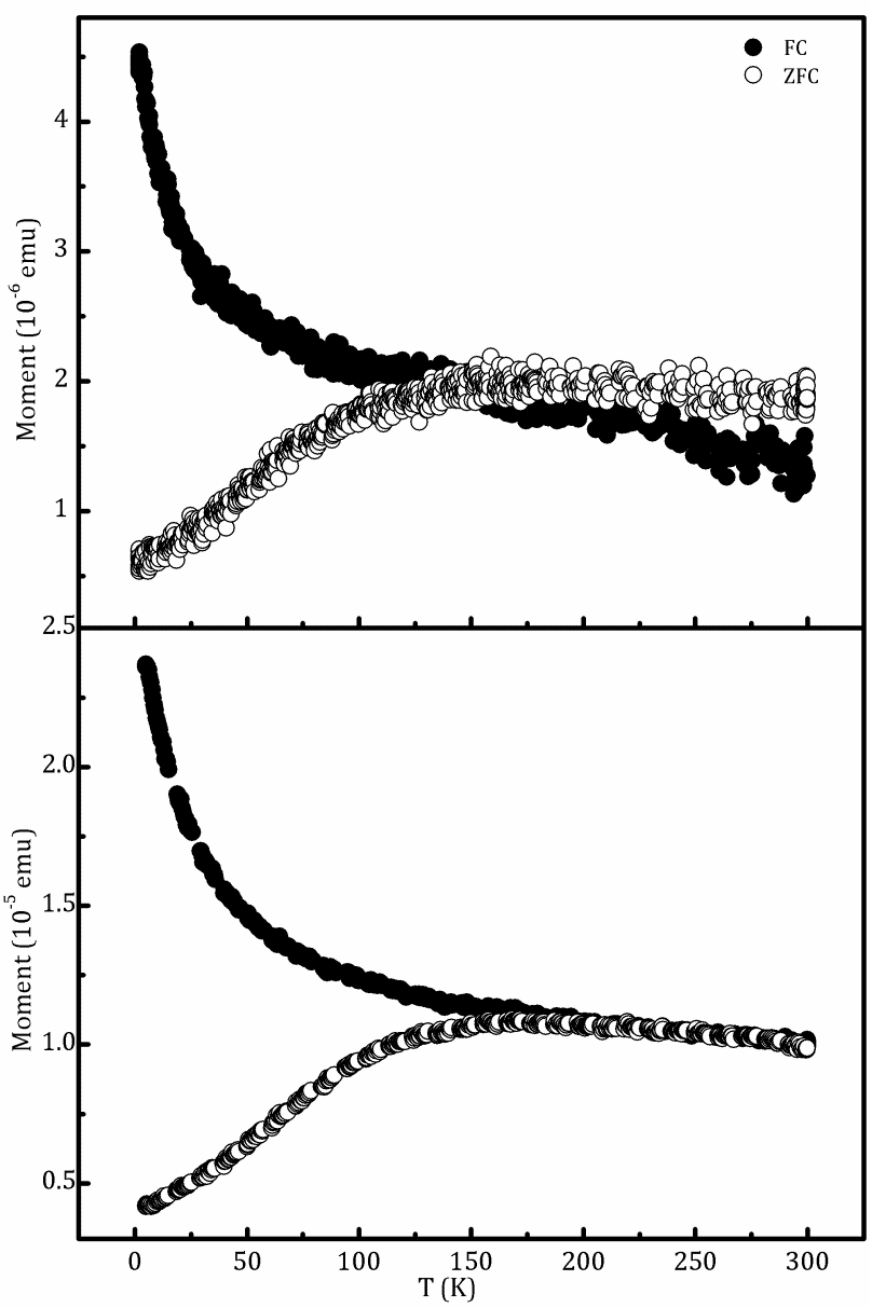

Figure 5.11. ZFC/FC curves at 100 Oe for nanocomposites with 2 and 5 wt% of nanoparticles

In addition, hysteresis loops of nanocomposites have also been measured at 2 and 150 K. Figure 5.12 shows M *vs* B curves for nanocomposites with 5 wt% of PMMA-modified nanoparticles as an example. Below the blocking temperature, at 2 K, M *vs* B curve is hysteretic, with a coercivity of approximately 270 Oe and a remanence of $1.8 \cdot 10^{-5}$ emu. The hysteresis disappears at 150 K and both coercivity

and remanence become zero, demonstrating the superparamagnetic behavior of nanocomposites (Schulz et al. 2010, Xu et al. 2009).

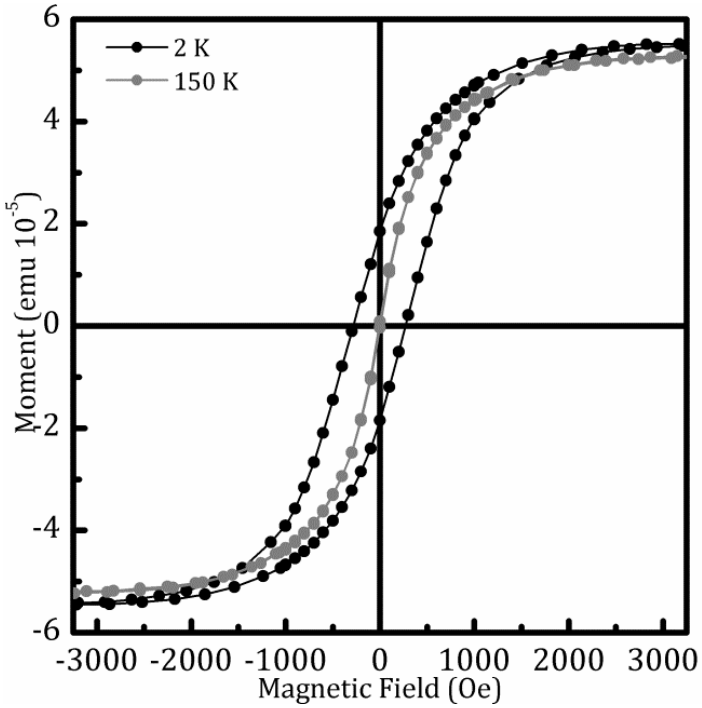

Figure 5.2. M *vs* B curves at 2 and 150 K for nanocomposites with 5 wt% of nanoparticles

5.4. CONCLUSIONS

From this chapter the following conclusions can be extracted about the synthesis and characterization of nanocomposite thin films based on PS-*b*-PMMA copolymer and γ-Fe_2O_3 nanoparticles. Copolymer films were annealed by exposure to acetone (selective for PMMA) vapors for 16 h in order to obtain the classical lamellar morphology. For nanocomposites with pristine nanoparticles lamellar morphology was disrupted due to the low compatibility among matrix and fillers. Nanoparticles were then successfully surface-modified with MPTS silane in order to increase their compatibility with PMMA domains. Lamellar morphology of films was maintained with nanoparticle adding, dispersion was improved, but they tended to agglomerate. In order to better disperse and selectively place, nanoparticles were surface modified with PMMA brushes by *grafting through*

technique. Once modified, they were well dispersed into PMMA domains of the copolymer films maintaining the lamellar morphology for nanocomposites with 1 and 2 wt% of nanoparticles. For higher nanoparticle amount (5 wt%) morphology started to change to a mixture of lamellas and hexagonally packed cylinders. This fact seemed to confirm the presence of nanoparticles at PMMA domains, increasing their volume and altering the volume fraction of the copolymer and consequently, the equilibrium morphology. As the size of nanoparticles in PMMA domains has been found to be bigger than that of single nanoparticles, it seems that more than one single nanoparticle was present at PMMA domains. This slight agglomeration could occur during *grafting through* process, in which nanoparticles, instead of being located individually, could be bonded together with several polymer chains, creating a kind of network. In any case, these agglomerates were smaller than PMMA domains, not big enough to disrupt copolymer morphology. Finally, the superparamagnetic behavior of the nanocomposites was demonstrated by magnetic measurements, showing that magnetic properties of nanoparticles have been transferred to the nanocomposites.

5.5. REFERENCES

Anastasiadis S.H., Russell T.P., Satij, S.K. and Makjarzak C.F., Neutron reflectivity studies of the surface-induced ordering of diblock copolymer films. *Phys Rev Lett* **1989**, 62, 1852-1855

Bean C.P. and Livingston J.D., Superparamagnetism. *J. Appl. Phys.* **1959**, 30, S120

Cano L., Di Mauro A.E., Striccoli M., Curri M.L. and Tercjak A., Optical and Conductive Properties of As-Synthesized Organic Capped TiO2 Nanorods Highly Dispersible in Polystyrene-blockpoly(methyl methacrylate) Diblock Copolymer. *ACS Appl. Mater. Interfaces* **2014**, 6, 11805-11814

Chakkalakal G.L., Abetz C., Vainio U., Handge U.A. and Abetz V., Influence of rheology and morphology on foaming of PS-b-PMMA diblock copolymers and their composites with modified silica nanoparticles. *Polymer* **2013**, 54, 3860-3873

Green P.F., Christenson T.M. and Russell T.P., Ordering at diblock copolymer surfaces. *Macromolecules* **1991**, 24, 252-255

Green P.F., Christenson T.M., Russell T.P. and Jerome R., Equilibrium surface composition of diblock copolymers. *J Chem Phys* **1990**, 92, 1478-1482

Gutierrez J., Garcia I., Tercjak A. and Mondragon I., The effect of termal and vapor annealing treatments on the self-assembly of TiO2/PS-b-PMMA nanocomposites generated via the sol-gel process. *Nanotechnology* **2009**, 20, 225603 (9 pp)

Hailu S., Samant S., Grabowski C., Durstock M., Karim A. and Raghavan D., Synthesis of Highly Dispersed, Block Copolymer-Grafted TiO_2 Nanoparticles Within Neat Block Copolymer Films. *Journal of Polymer Science, Part A: Polymer Chemistry* **2015**, 53, 468-478

Kim S., Yoo M., Kang N., Moon B., Kim B.J., Choi S.-H., Kim J.U. and Ban J., Nanoporous Bicontinuous Structures via Addition of ThermallyStable Amphiphilic Nanoparticles within Block Copolymer Templates. *ACS Appl. Mater. Interfaces* **2013**, 5, 5659-5666

Limary R., Swinnea S. and Green P.F., Stability of Diblock Copolymer/Layered Silicate Nanocomposite Thin Films. *Macromolecules* **2000**, 33, 5227-5234

Lopes W.A. and Jaeger H.M., Hierarchical self-assembly of metal nanostructures on diblock copolymer scaffolds. *Nature* **2001**, 414, 735-738

Nyström D., Antoni P., Malmström E., Johansson M., Whittaker M. and Hult A., Highly-Ordered Hybrid Organic/inorganic Isoporous Membranes from Polymer Modified Nanoparticles. *Macromol. Rapid Commun.* **2005**, 26, 524-528

Pang X., He Y., Jiang B., Iocozzia J., Zhao L.Z., Guo H., Liu J., Akinc M., Bowler N., Tanb X. and Lin Z., Block copolymer/ferroelectric nanoparticle nanocomposites. *Nanoscale*, **2013**, 5, 8695-8702

Peng J., Wei Y., Wang H., Li Y. and Han Y., Solvent induced sphere development in symmetric diblock copolymer thin films. *Macromol Rapid Commun* **2005**, 26, 738-742

Rodriguez M.A., Liso M.J., Rubio F. Rubio J. and Oteo J.L., Study of the reaction of γ-methacryloxypropyltrimethoxysilane(γ-MPS) with slate surfaces. *Journal of Material*

Science 1999, 35, 3867–3873

Russell T.P., Coulon G., Deline V.R. and Miller D.C., Characteristics of the surface-induced orientation for symmetric PS-b-PMMA diblock copolymer. *Macromolecules* **1989**, 22, 4600-4606

Schlage K., Couet S., Roth S.V., Vainio U., Rüffer R., Abul Kashem M.M., Müller-Buschbaum P. and Röhlsberger R., The formation and magnetism of iron nanostructures on ordered polymer templates. *New Journal of Physics* **2012**, 14, 043007

Schulz L., Schirmacher W, Omran A., Shah V.R., Böni P., Petry W. and Müller-Buschbaum P., Elastic torsion effects in magnetic nanoparticle diblock-copolymer structures. *J. Phys.: Condens. Matter* **2010**, 22, 346008 (6pp)

Xia X., Metwalli E., Ruderer M.A., Körstgen V., Busch P., Böni P. and Müller-Buschbaum P., Nanostructured diblock copolymer films with embedded magnetic nanoparticles. *J. Phys.: Condens. Matter* **2011**, 23, 254203 (9pp)d

Xu C., Ohno K., Ladmiral V. and Composto R.J. Dispersion of polymer-grafted magnetic nanoparticles in homopolymers and block copolymers. *Polymer* **2008**, 49, 3568-3577

Xu C., Ohno K., Ladmiral V., Milkie D.E., Kikkawa J.M. and Composto R.J., Simultaneous Block Copolymer and Magnetic Nanoparticle Assembly in Nanocomposite Films. *Macromolecules* **2009**, 42, 1219-1228

Xuan Y., Peng J., Cui L., Wang H., Li B. and Han Y., Morphology development of ultrathin symmetric diblock copolymer film via solvent vapor treatment. *Macromolecules* **2004**, 37, 7301-7307

Yan H., Zhang X.-h., Wei L.-q., Liu X.-g. and Xu B.-s., Hydrophobic magnesium hydroxide nanoparticles via oleica cid and poly(methyl methacrylate)-grafting surface modification. *Powder Technology* **2009**, 193, 125-129

Yang P., Wang S., Teng X., Wei W., Dravid V.P. and Huang L., Effect of Magnetic Nanoparticles on the Morphology of Polystyrene-b-Poly(methyl methacrylate) Diblock Copolymer Thin Film. *J. Phys. Chem. C* **2012**, 116, 23036-23040

Yao Y., Metwalli E., Niedermeier M.A., Opel M., Lin C., Ning J., Perlich J., Roth S.V. and Müller-Buschbaum P., Nano- and Microstructures of Magnetic Field-Guided Maghemite Nanoparticles in Diblock Copolymer Films. *ACS Appl. Mater. Interfaces* **2014**, 6, 5244−5254

Zeng H., Black C.T., Sandstrom R.L., Rice P.M., Murray C.B. and Sun S., Magnetotransport of magnetite nanoparticle arrays. *Physical Reviw B* **2006**, 73, 020402(R)

Zhao Y., Saijo K. and Hashimoto T., Order−Disorder Transition of Nanocomposites: Polystyrene-block-Poly(methyl methacrylate) with Palladium Nanoparticles. *Macromolecules* **2013**, 46, 957−970

Chapter 6

SYNTHESIS AND CHARACTERIZATION OF NANOCOMPOSITES BASED ON SBM TRIBLOCK COPOLYMER AND PS- OR PMMA-MODIFIED NANOPARTICLES

6.1. INTRODUCTION

Due to the ability of ABC-type copolymers for the generation of many different nanostructures, many authors have studied their morphological behavior. Löbling et al. analyzed the self-assembly of polystyrene-*block*-polybutadiene-*block*-poly(*tert*-butyl methacrylate) (SBT) copolymer in bulk, obtaining unusually broad stability regions. They focused on χ parameter, concluding that a proper combination of this parameter can control the phase behavior, implying a minor influence of block volume fraction (Löbling et al. 2015). Hückstädt et al. investigated the influence of block sequence on the morphological behavior of polystyrene-*block*-polybutadiene-*block*-poly(2-vinyl pyridine) (SBV) and polybutadiene-*block*-polystyrene-*block*-poly(2-vinyl pyridine) (BSV) copolymers, concluding that block sequence is decisive (Hückstädt et al. 2000). Nagpal et al. predicted by simulation different morphologies obtained with linear triblock copolymers as a function of composition and interaction strength, and also the differences between bulk and thin film morphologies (Nagpal et al. 2011). Morphologies generated for ABC-type copolymer thin films have also been investigated. Fukunaga et al. analyzed the effect of substrates on the generated morphology, using two types of substrates, polyimide and oxide silicon, finding significant differences (Fukunaga et al. 2003). Elbs et al. studied the differences in the resulting structure depending on the solvent used for vapor annealing of polystyrene-*block*-poly(2-vinyl pyridine)-*block*-poly(*tert*-butyl methacrylate) (SVT) triblock copolymer (Elbs et al. 2002).

Regarding to polystyrene-*block*-polybutadiene-*block*-poly(methyl methacrylate) (SBM) triblock copolymers, similar to that used in the present work, some works can also be found in the literature. Kirschich et al. used SBM copolymer to compatibilize polymer blends based on poly(2,6-dimethyl-1,4-phenylene ether) (PPE) and polystyrene-*co*-polyacrylonitrile (SAN) (Kirschich et al. 2004). Kabir et

al. studied the morphological changes caused by the deformation and orientation of different domains, analyzing the influence of polybutadiene (PB) isomers (1,2 or 1,4). In the case of 1,2 isomer containing SBM copolymer, a co-existing lamellar and cylindrical morphology of PB block was observed, while 1,4 isomer containing-SBM copolymer, only well segregated lamellar patterns were found (Kabir et al. 2012). Higuchi et al. observed the different helical structures formed with SBM copolymers self-assembled into a helical structure of PB domains around hexagonally packed core of PS cylinders in a PMMA matrix (Higuchi et al. 2013). Ritzenthaler et al. prepared nanostructured thermosetting systems by modifying an epoxy matrix with SBM copolymer (Ritzenthaler et al. 2003), showing the ability of ABC-type copolymers for nanostructuring epoxy-based systems.

Although ABC-type triblock copolymers present high versatility due to the higher amount of possible nanostructures that can be formed respecting to AB or ABA-type copolymers, this type of copolymers have barely been used for organic/inorganic nanocomposite generation. Choi et al. analyzed the effect of ABA or ABC-type triblock copolymers and that of hydroxylation degree on organoclay dispersion, concluding that a proper functionalization improves considerably their dispersion (Choi et al. 2004). Toombes et al. prepared poly(ethylene-*alt*-propylene-*block*-ethylene oxide-*block*-*n*-hexyl methacrylate) (PEP-*b*-PEO-*b*-PHMA) triblock copolymer/aluminosilicate hybrid materials with aluminosilicates confined at PEO domains, obtaining hexagonally patterned lamellar morphology in which lamellae were aligned parallel to the surface (Toombes et al. 2008). Stefik et al. used different polyisoprene-*block*-polystyrene-*block*-poly(ethylene oxide) (ISO) copolymers for synthesizing highly ordered nanocomposites with alumino silicate and niobia sols, underlaying that copolymer removal enabled simple and direct synthesis of mesoporous oxide materials (Stefik et al. 2009).

The main objectives of the work described in this chapter are the preparation and characterization of nanocomposites based on SBM triblock copolymer and maghemite nanoparticles functionalized with PS or PMMA brushes. The effect of adding pristine, PS- or PMMA-modified nanoparticles has been analyzed. Morphology of nanocomposites has been studied by AFM, thermal characterization by DSC and the transference of magnetic properties from nanoparticles to nanocomposites has been analyzed by magnetic characterization in terms of VSM. To the best of our knowledge, this is the first report describing the use of ABC triblock copolymers for preparing nanocomposites with metal oxide nanoparticles as inorganic nanofillers.

6.2. MATERIALS AND METHODS

6.2.1. MATERIALS

Maghemite nanoparticles purchased from Integram Technologies with a nominal size of 9 nm and a polydispersity of 1.08 were used as inorganic fillers. MPTS purchased from ABCR with 98 % of purity, was used as link between nanoparticle surface and polymer brushes. AIBN was used as initiator without further purification. The monomers used for the synthesis of polymer brushes were styrene and MMA, both purchased from Aldrich with a purity of 99 % and purified by distilling under reduced pressure over CaH_2. SBM triblock copolymer, with a M_n of 96.142 g/mol was kindly supplied by Repsol, with the following volumetric composition: f_{PS}=0.3, f_{PB}=0.4 and f_{PMMA}=0.3. Its chemical structure is shown in Scheme 6.1. Toluene and THF, both purchased from Aldrich, were used as solvents for nanocomposite preparation.

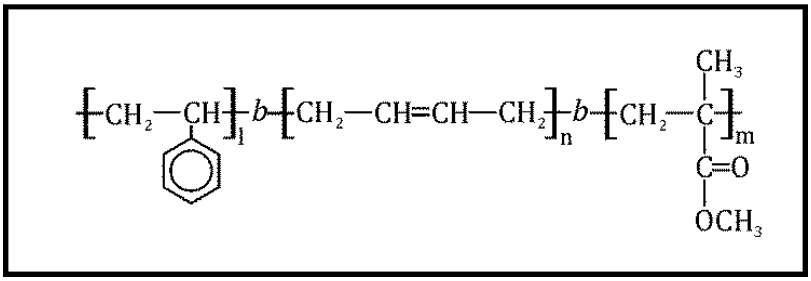

Scheme 6.1. Chemical structure of SBM copolymer

6.2.2. METHODS

6.2.2.1. Nanoparticle functionalization

Nanoparticle functionalization was carried out following the procedures described in sections 4.2.2.1 and 5.2.2.1 of Chapters 4 and 5.

6.2.2.1.1. Silanization process

It was carried out following the procedure described in section 4.2.2.1.1 of Chapter 4.

6.2.2.1.2. Growth of PS and PMMA brushes by *grafting through* method

Modification of nanoparticles with PS brushes was carried out following the procedure described in section 4.2.2.1.2 of Chapter 4, while that of PMMA brushes was carried out by following the procedure described in section 5.2.2.1.2 of Chapter 5.

6.2.2.2. Nanocomposite preparation

In order to analyze the effect of functionalization on the dispersion and selective placement of nanoparticles into the desired domains, nanocomposites were

prepared by mixing SBM copolymer with pristine, PS- and PMMA-modified nanoparticles. Nanoparticles were first dispersed in toluene for 2 h by sonication, and then SBM block copolymer was added. Thin films of neat block copolymer and nanocomposites were then prepared by casting SBM solutions in toluene with a concentration of 5 wt% onto Si(100) wafers. Nanocomposites with 1, 2, and 5 wt% of nanoparticles were prepared.

6.2.2.3. Characterization techniques

6.2.2.3.1. FTIR

It was used to verify the functionalization of iron oxide nanoparticles. Infrared spectra were carried out in a Nicolet Nexus 670 Spectrometer, as it was described in section 3.2.2.3.3 of Chapter 3.

6.2.2.3.2. TGA

It was used to determine the amount of hydroxyl groups at nanoparticle surface, the amount of grafted silane and the weight loss related to the grafted PS and PMMA brushes, which would probe the success of the polymerization reaction. TGA results were obtained using a TGA/SDTA-851e equipment running from 25 to 750 °C at a heating rate of 10 °C/min under nitrogen atmosphere, as was shown in 3.2.2.3.4 section of Chapter 3.

6.2.2.3.3. AFM

It was used to analyze surface morphologies of neat BCP films, and those of nanocomposites with pristine and PS- or PMMA-modified nanoparticles. AFM

measurements were performed in tapping mode using a Dimension Icon Nanoscope V (Bruker), as it was described in section 3.2.2.3.6 of Chapter 3.

6.2.2.3.4. DSC

By DSC measurements glass transition temperatures (T_g) of PS and PMMA blocks of SBM triblock copolymer were analyzed, both for neat BCP and for nanocomposites, in order to analyze the effect of nanoparticle addition on them. Measurements were performed in a Mettler Toledo DSC-822 differential scanning calorimeter equipped with a Sample Robot TSO 801 RO. Measurements were performed from 25 to 160 °C at a heating rate of 10 °C/min in sealed aluminum pans, with N_2 as a purge (10 mL/min).

6.2.2.3.5. VSM

Magnetic characterization was carried out in a Quantum Design PPMS with Vibrating Sample Magnetometer option, this equipment was used for ZFC/FC measurements and also for measuring hysteresis loops at 2, 225 and 300 K. This technique was described in section 4.2.2.3.4 of Chapter 4.

6.3. RESULTS AND DISCUSSION

6.3.1. CHARACTERIZATION OF FUNCTIONALIZED NANOPARTICLES

Characterization of MPTS-silanized nanoparticles has been shown in 4.3.1 section of Chapter 4. The success of silanization process has been probed by FTIR with the appearance of bands related to the main bonds of MPTS compound, and by TGA measurements. By TGA measurements also the surface density of grafted silane has been calculated (2.8 molecules/nm^2), as it has been previously shown.

Characterization of PS-modified nanoparticles has been shown in section 4.3.1 of Chapter 4, and characterization of PMMA-modified nanoparticles in section 5.3.2.1 of Chapter 5. By FTIR, the functionalization of nanoparticles with PS or PMMA brushes has been corroborated by the appearance of bands related to their main bonds. TGA measurements have also corroborated the presence of polymer brushes in both cases, showing the corresponding weight loss.

6.3.2. CHARACTERIZATION OF NANOCOMPOSITES

The first step has been to characterize surface morphologies obtained for neat triblock copolymer films. Figure 6.1 shows AFM images of neat copolymer films, showing a lamellar morphology. This lamellar morphology is one of the morphologies that can be obtained for ABC-type triblock copolymer thin films (Nagpal et al. 2011). Stadler et al. investigated the morphologies formed for SBM and their hydrogenated polystyrene-*block*-poly(ethylene-*co*-butylene)-*block*-poly(methyl methacrylate) (SEBM) analogues. They highlighted the importance of interaction parameters in order to determine the morphologies of ABC copolymers, respecting to AB diblock or ABA triblock copolymers, for which the composition is main factor determining the morphology. However, they indicated that interaction parameters made the difference mainly when the amount of the middle block was low, of around 6 wt%. For copolymers with block ratios similar to those analyzed in this work (30/40/30 in volume) they pointed out that a lamellar morphology could be expected (Stadler et al 1995). In AFM images of Figure 6.1, PB domains can be clearly identified as the dark ones due to the lower modulus. However, PS and PMMA domains cannot be clearly differentiated.

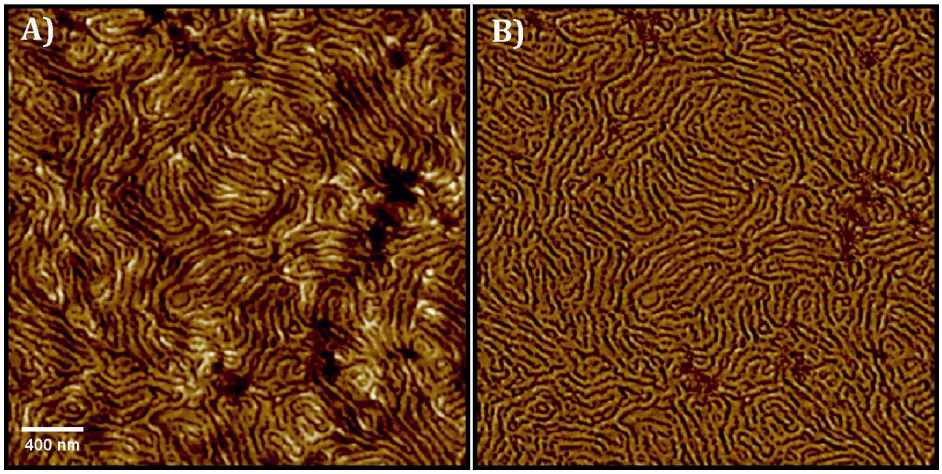

Figure 6.1. AFM height (A) and phase (B) images of SBM thin film

In order to better visualize the morphology and differentiate PS and PMMA domains, amplified height and phase AFM images of neat triblock copolymer thin film are shown in Figure 6.2. As it can be seen, PS and PMMA domains can be better distinguished as PMMA domains appear brighter than PS ones due to its higher modulus (Xu et al. 2009). Profiles obtained for height and phase images, also shown in Figure 6.2, help in distinguishing between SBM domains. In those profile images, four domains stand up from PB ones, placed at the bottom as they are the softener; they correspond to PS and PMMA domains, which can be separated into two pairs depending on their height, placed alternatively. The highest one represents PMMA domains, as it presents the highest modulus.

From these images it can be concluded that SBM triblock copolymer assembles into a lamellar morphology with S-B-M-B sequence and an average interlamellar distance of ~71 nm, although some interruptions of the sequence can be appreciated (marked with a circle in Figure 6.2), as PS and PMMA domains appear joined. Scheme 6.2 shows a representation of this lamellar structure.

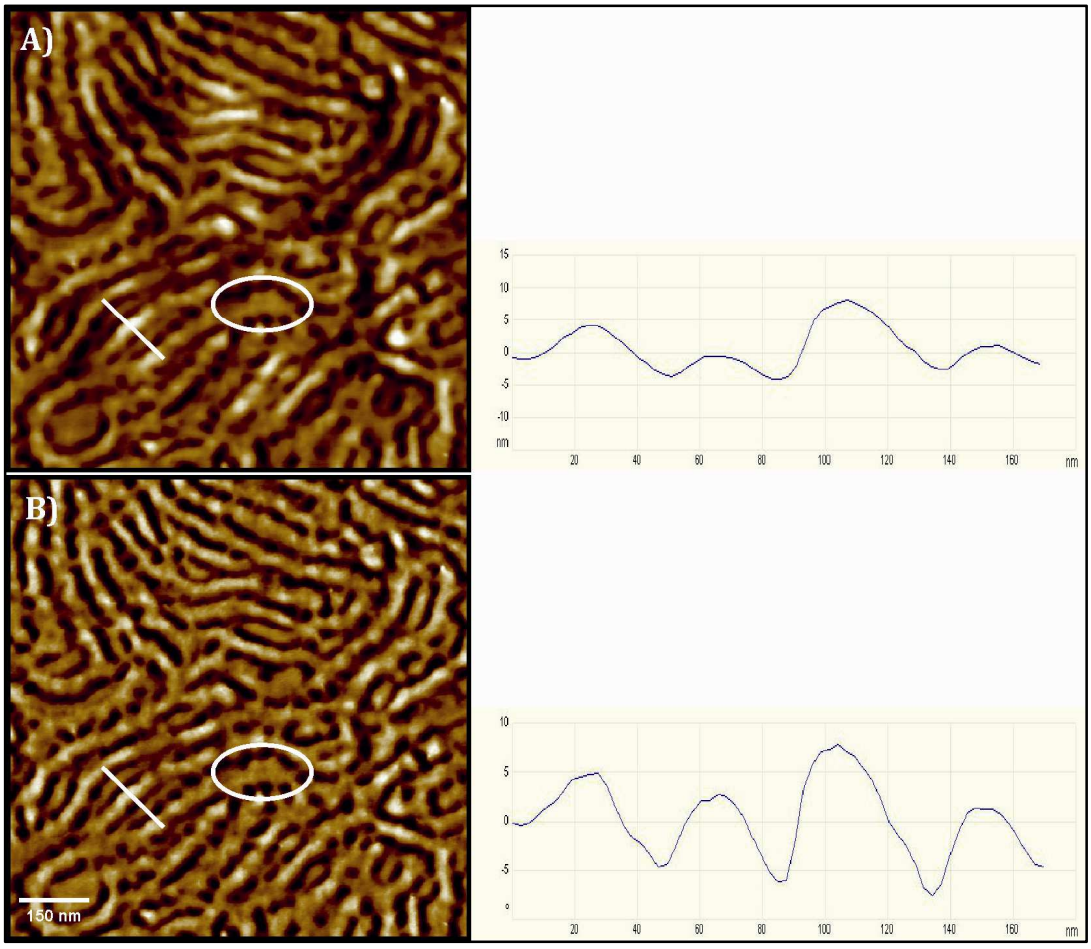

Figure 6.2. AFM height (A) and phase (B) images of SBM thin film with the corresponding profile images

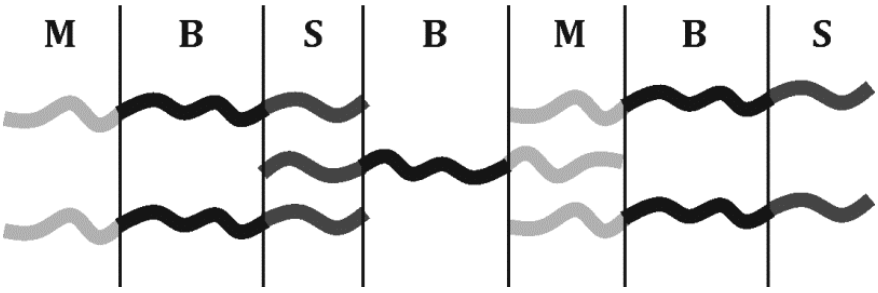

Scheme 6.2. Schematic representation of the lamellar nanostructure formed

Nanocomposites have been prepared by adding magnetic nanoparticles to SBM matrix. In Figures 6.3 and 6.4 AFM images for nanocomposites with 1, 2 and 5 wt% of PS- and PMMA-modified nanoparticles, respectively, can be seen.

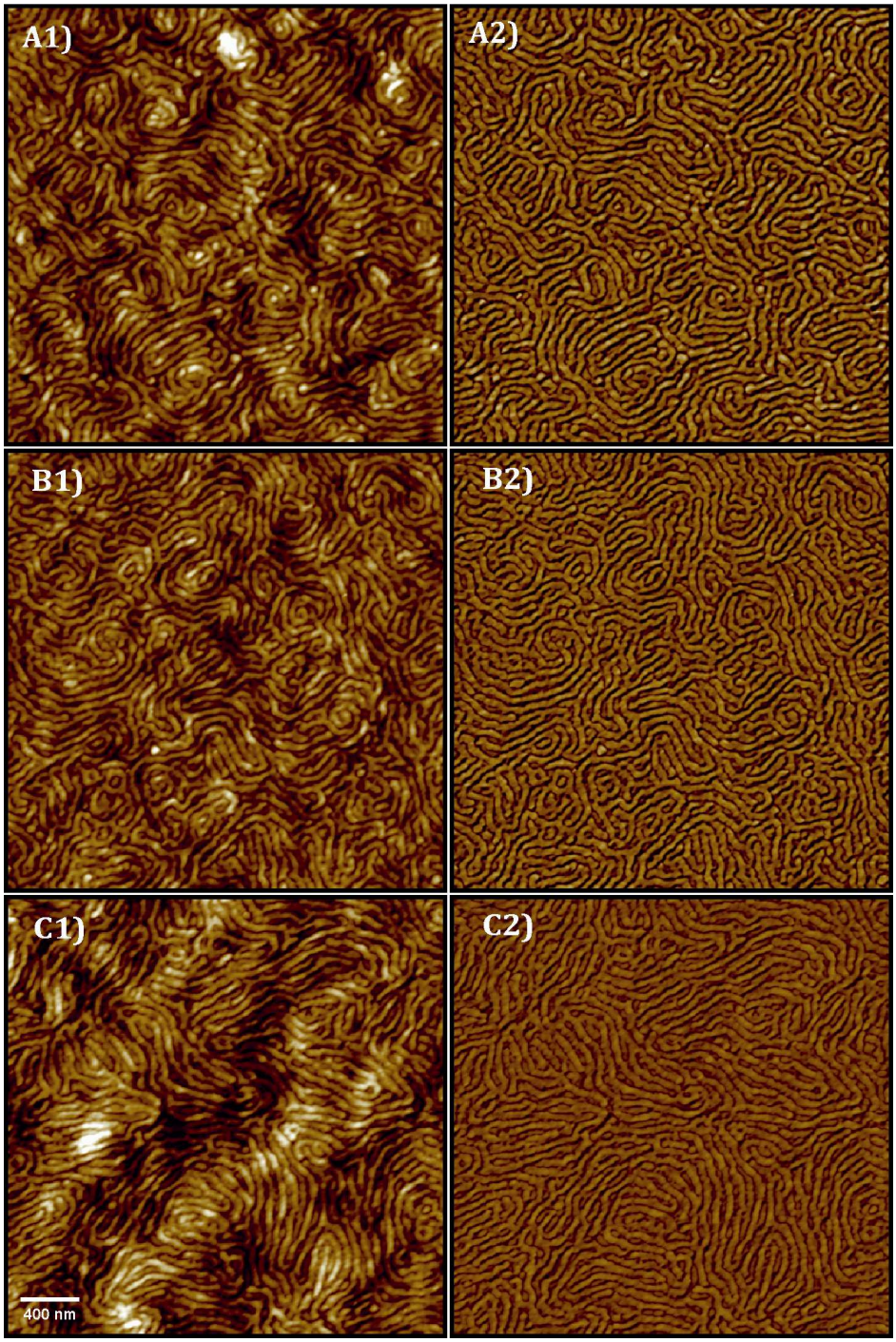

Figure 6.3. AFM height (1) and phase (2) images of nanocomposites with A) 1, B) 2 and C) 5 wt% of PS-modified nanoparticles

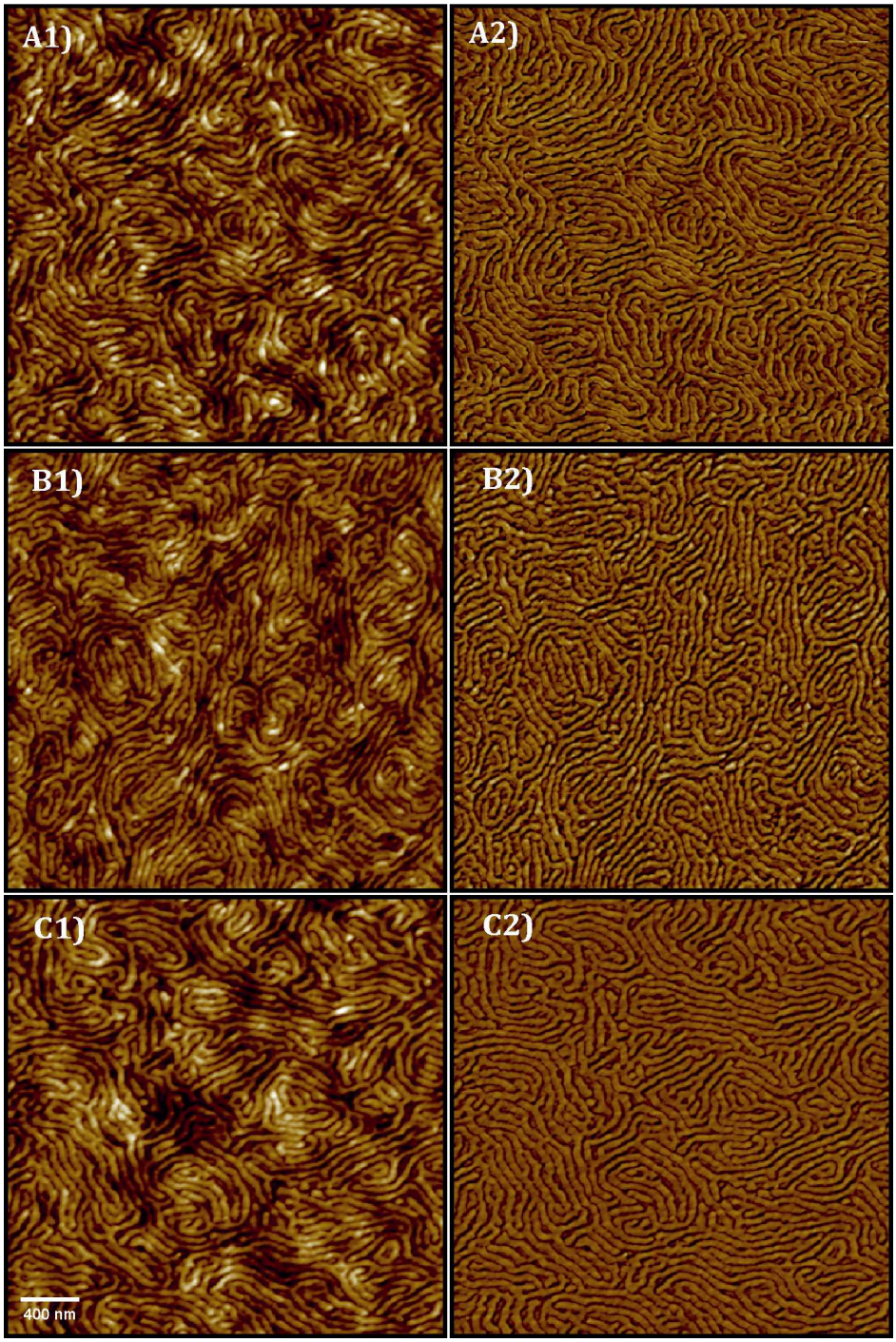

Figure 6.4. AFM height (1) and phase (2) images of nanocomposites with A) 1, B) 2 and C) 5 wt% of PMMA-modified nanoparticles

As it can be seen, lamellar morphology of neat triblock copolymer is maintained with nanoparticle addition, independently of the modification. Moreover, nanoparticles are well dispersed through the triblock copolymer matrix, without

the presence of remarkable aggregates. For a better visualization of the effect of nanoparticles on film morphology, amplified height and phase images of nanocomposite thin films with 5 wt% of nanoparticles are shown in Figure 6.5, together with the corresponding height profile.

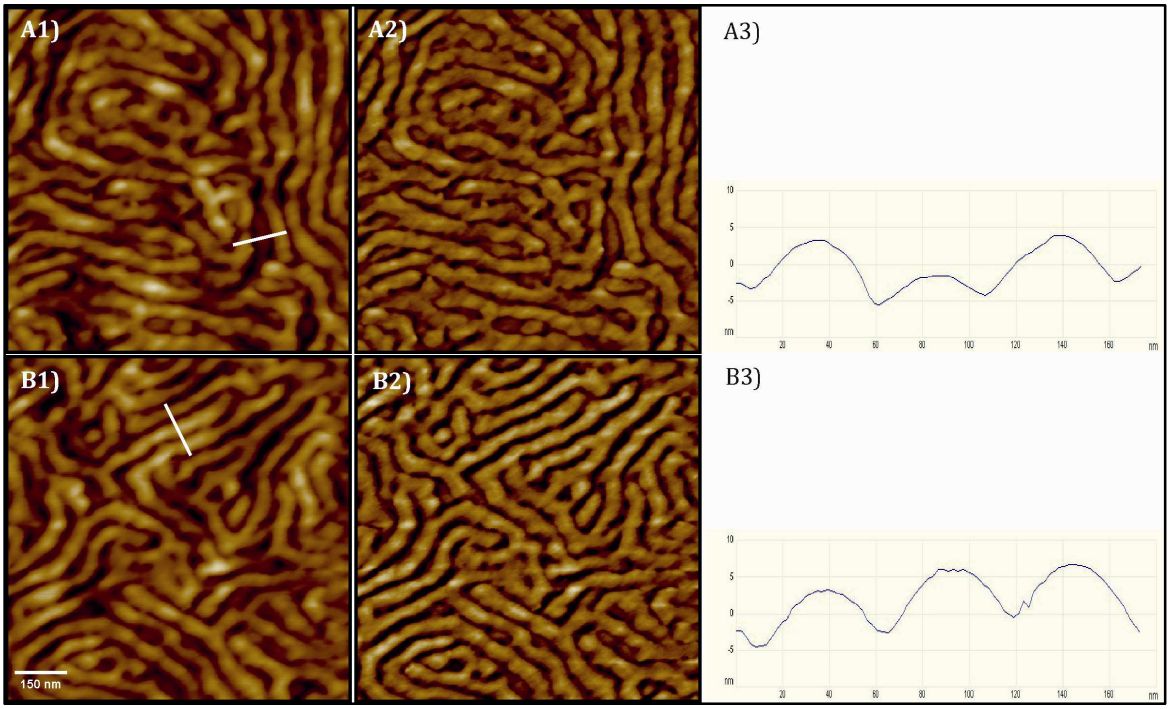

Figure 6.5. AFM height (1), phase (2) and profile (3) images of nanocomposites with 5 wt% of A) PS- and B) PMMA-modified nanoparticles

In both cases, although lamellar morphology is maintained after nanoparticle addition, it appears more disrupted. When PS-modified nanoparticles are added, PS domains can be better distinguished in AFM images, comparing to the images corresponding to nanocomposites with PMMA-modified nanoparticles. When PMMA-modified nanoparticles are added, it seems that PS and PMMA domains tend to join. If the profile images are compared with those of Figure 6.2, it can be clearly seen that PS and PMMA domains tend to swollen with nanoparticle addition. All profiles are around 170 nm length. In these profiles, for neat BCP four domains can be separated, identified as PMMA (higher ones) and PS (lower ones), when nanoparticles are added, only 3 domains can be observed. This fact could indicate that nanoparticles are located at PS and PMMA domains, as nanoparticles

placement at the PS or PMMA domains would increase the respective domain volume (Gutierrez et al. 2009).

Differences found between neat BCP and nanocomposite thin film nanostructures could be due to the effect of nanoparticles on system thermodynamics, as they can affect the interaction forces between blocks. Lo et al. concluded that nanoparticle addition weakened the phase segregation between blocks, while Lin et al. induced the self-assembly of BCP by adding inorganic nanoparticles, due to a strengthening of interaction forces between blocks (Lo et al. 2007, Lin et al. 2011). Those examples show the complexity of understanding nanostructures based on BCP and inorganic nanoparticles. As it has been mentioned before, if PS- or PMMA-modified nanoparticles are added, more notoriously with PMMA-modified ones, PS and PMMA domains of the triblock tend to join. This could be due to the low repulsive forces between PS and PMMA blocks. Standler et al. calculated that $\chi_{PMMA/PS}$= 0.0044 is much lower than $\chi_{PS/PB}$= 0.045 and $\chi_{PMMA/PB}$= 0.071 (Stadler et al. 1995). Hückstädt et al. analyzed the effect of block sequence on obtained nanostructure, analyzing first SBV and BSV copolymer nanostructures in which three components are strongly incompatibles, finding that they were affected by the block sequence. Then they compared obtained results with those for SBM and polybutadiene-*block*-polystyrene-*block*-poly(methyl methacrylate) (BSM) copolymers, in which the incompatibility between PS and PMMA blocks is low. Due to this low incompatibility, PS/PMMA mixtures were obtained (Hückstädt et al. 2000). On the other hand, the incompatibility between PMMA and PB blocks, higher than that among PS and PB ones, could explain the reason for PS and PMMA domains to be better distinguished when PS-modified nanoparticles are added than when PMMA-modified ones are added. Larger incompatibilities between blocks lead to the generation of larger interfaces (Löbling et al. 2015).

In order to reinforce the importance of nanoparticle surface functionalization when preparing organic/inorganic nanocomposites based on BCP,

nanocomposites with pristine nanoparticles have also been prepared. In Figure 6.6 AFM images of the nanocomposite with 1 and 5 wt% of pristine nanoparticles can be seen. In these images big nanoparticle aggregates are detected. Different areas of the thin film have been analyzed, and the presence of aggregates is repetitive. With pristine nanoparticle addition the lamellar nanostructure of the triblock copolymer is maintained, but their dispersion is not as good as for modified ones.

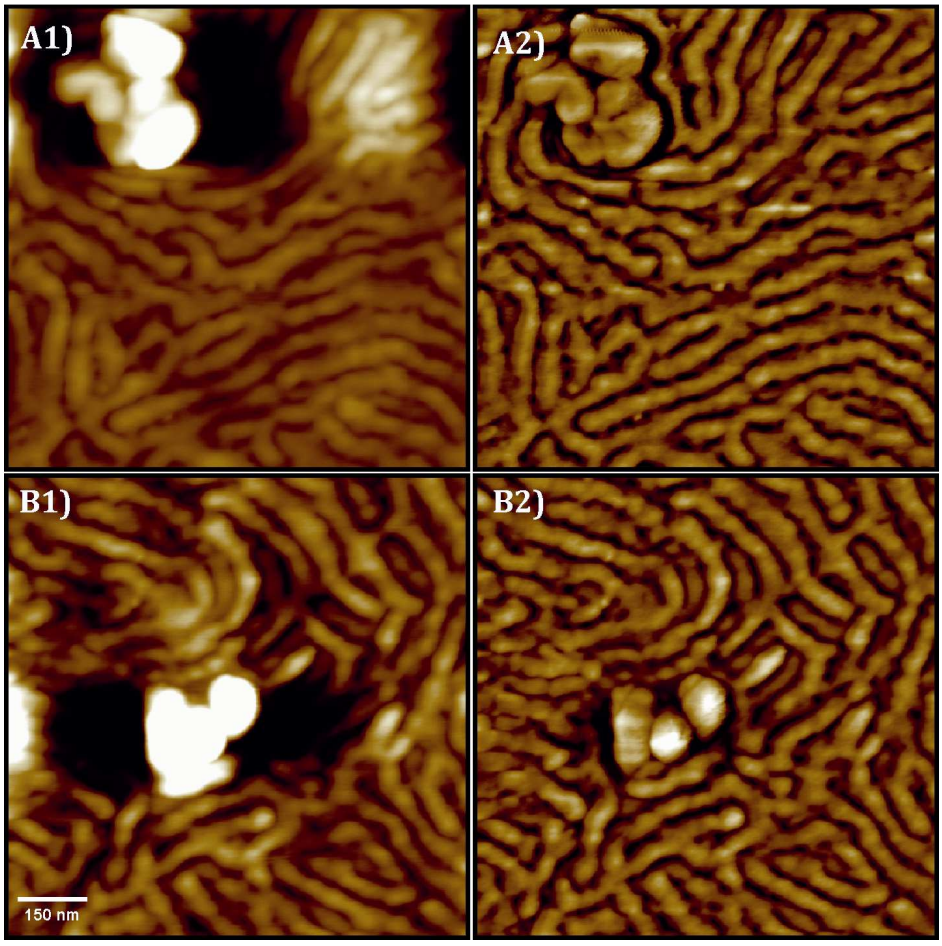

Figure 6.6. AFM height (1) and phase (2) images of nanocomposite thin film with A) 1 and B) 5 wt% of pristine nanoparticles

DSC thermograms for neat SBM and nanocomposites with PMMA- and PS-modified nanoparticles (1, 2 and 5 wt%) are shown in Figure 6.7, in order to check the effect of nanoparticle addition on the T_g values of blocks.

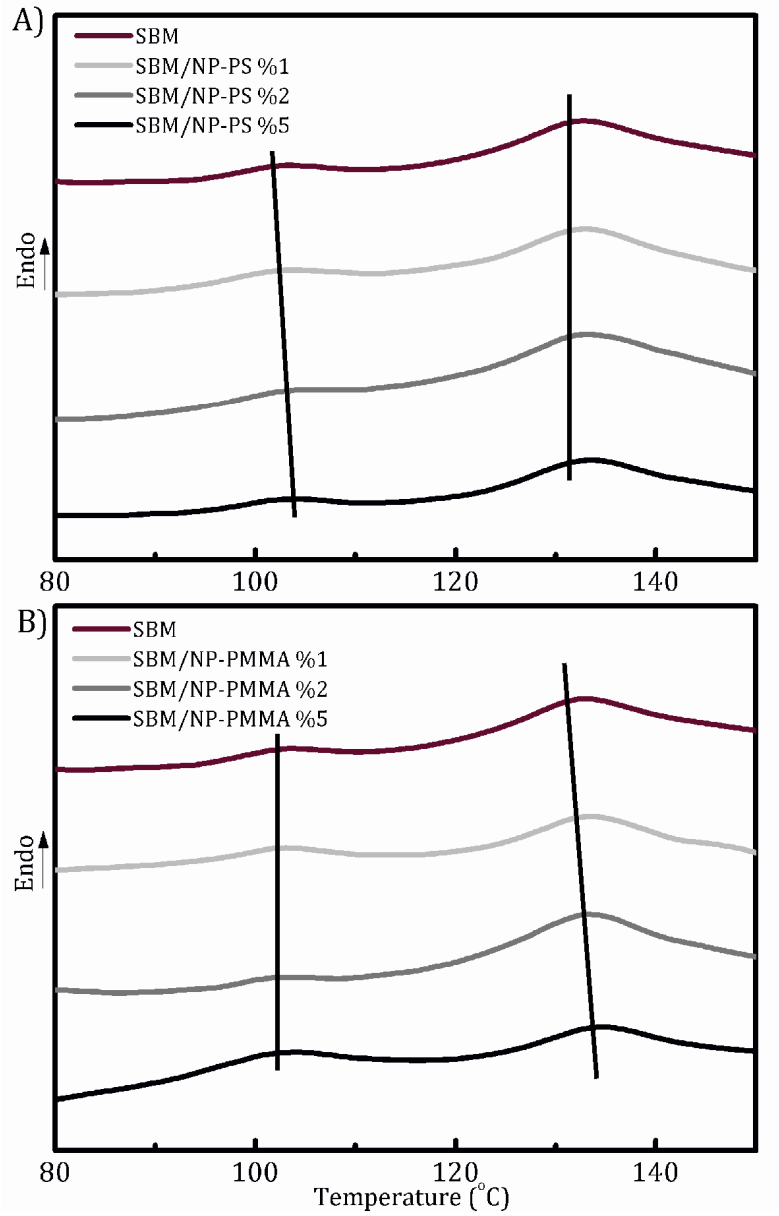

Figure 6.7. DSC thermograms of neat SBM and nanocomposites

In the analyzed temperature range two T_g can be distinguished. For the neat copolymer, they appear at 102 and 131 °C, corresponding to PS and PMMA blocks, respectively. With nanoparticle addition, T_g values of the blocks corresponding to the brushes anchored to nanoparticles show a slight increase, reaching up to 105 °C and 134 °C for 5 wt% of PS- and PMMA-modified nanoparticles, respectively. As the T_g of PS increases when PS-modified nanoparticles are added and that of PMMA increases with PMMA-modified nanoparticle addition, it seems that PS-

modified nanoparticles could be mainly located at PS domains and PMMA-modified ones at PMMA domains, as the presence of the nanoparticles would hinder chain mobility, resulting in a higher T_g for the corresponding block (Cano et al. 2013).

6.3.3. MAGNETIC CHARACTERIZATION

Figures 6.8 and 6.9 show the ZFC/FC curves of nanocomposites with 1 and 5 wt% of PS- and PMMA-modified nanoparticles obtained from VSM measurements. As other nanocomposites presented at previous chapters, nanocomposites present superparamagnetic behavior at room temperature and ferromagnetic at lower temperature; magnetic properties of nanoparticles have been transferred to nanocomposites successfully, despite surface functionalization. T_B do not vary with nanoparticle concentration, probably indicating, as it has been mentioned in Chapter 4 and 5, that nanoparticle do not aggregate during nanocomposite thin film formation but during nanoparticle modification following the *grafting through* method. If results of both nanocomposites are compared it can be seen that in both cases behavior of nanocomposites in ZFC/FC measurements is very similar, although T_B is slightly higher in nanocomposites with PS-modified nanoparticles than in those with PMMA-modified ones. This tendency is in accordance with the results obtained in Chapter 4 and 5.

M *vs* B curves have also been measured for nanocomposites with 5 wt% of PS- and PMMA-modified nanoparticles, as it can be seen in Figure 6.10. In both cases nanocomposites have a hysteretic loop at 2 K, with a coercivity of approximately 315 Oe, and remanence between $1.6 \cdot 10^{-4}$ and $2.1 \cdot 10^{-4}$ emu. Near to T_B (225 K) both nanocomposites become un-hysteretic, and coercivity and remanence become zero. At room temperature, both coercivity and remanence also become zero, proving the superparamagnetic behavior of the nanocomposites. Again, it has been demonstrated that the magnetic properties of the nanoparticles have

been successfully transferred to the nanocomposite, despite the modification of nanoparticle surface with polymeric brushes.

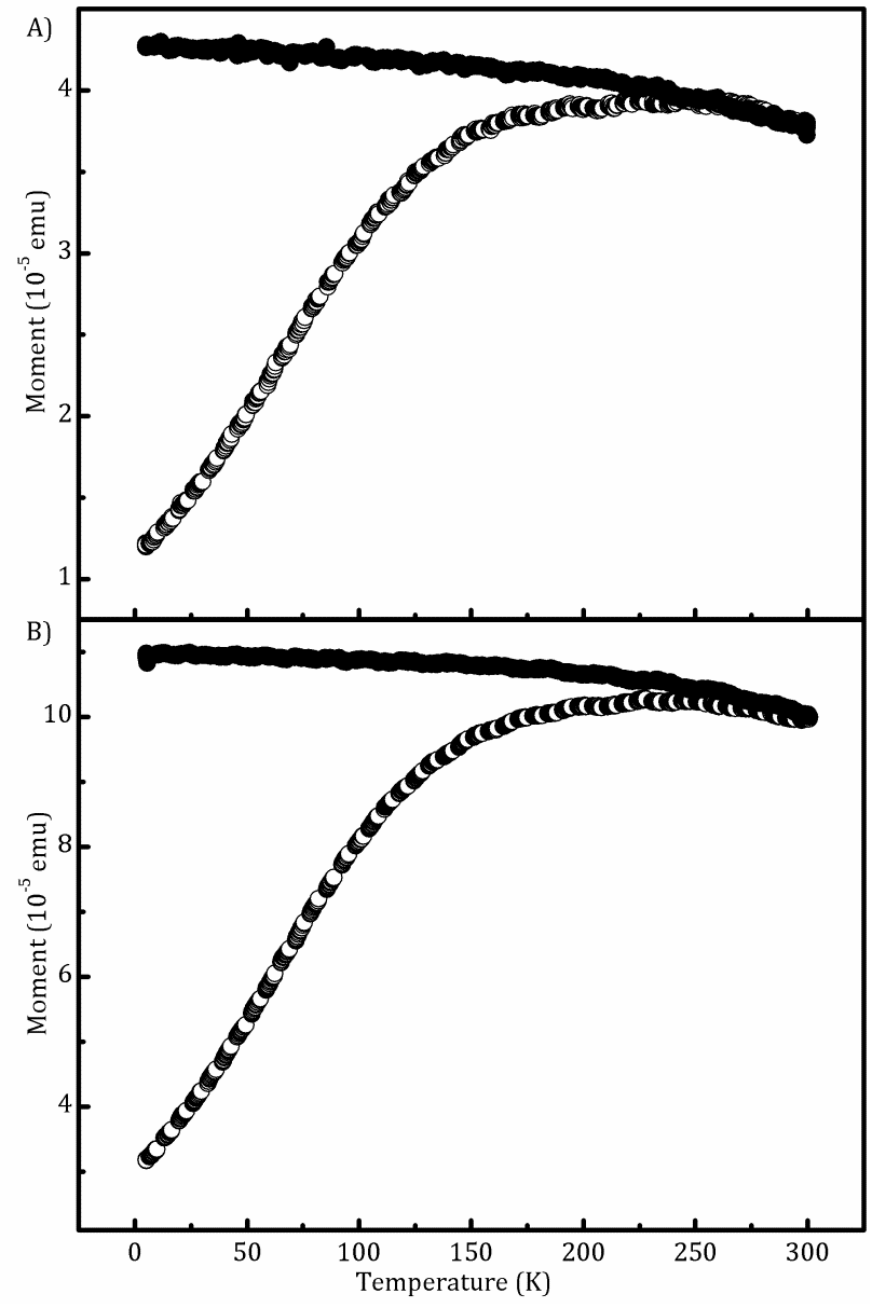

Figure 6.8. ZFC/FC curves at 100 Oe for nanocomposites with A) 1 and B) 5 wt% of PS-modified nanoparticles

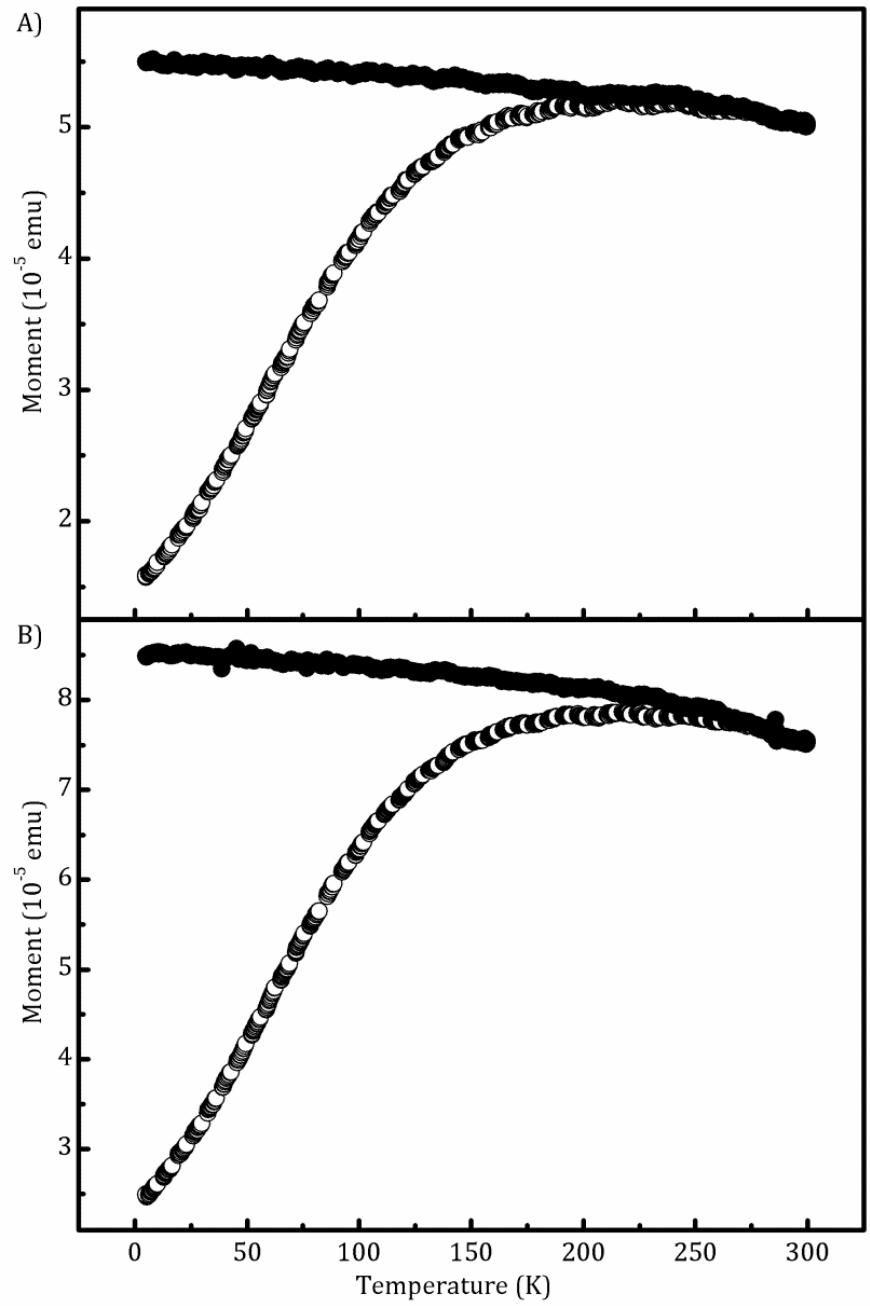

Figure 6.9. ZFC/FC curves at 100 Oe for nanocomposites with A) 1 and B) 5 wt% of PMMA-modified nanoparticles

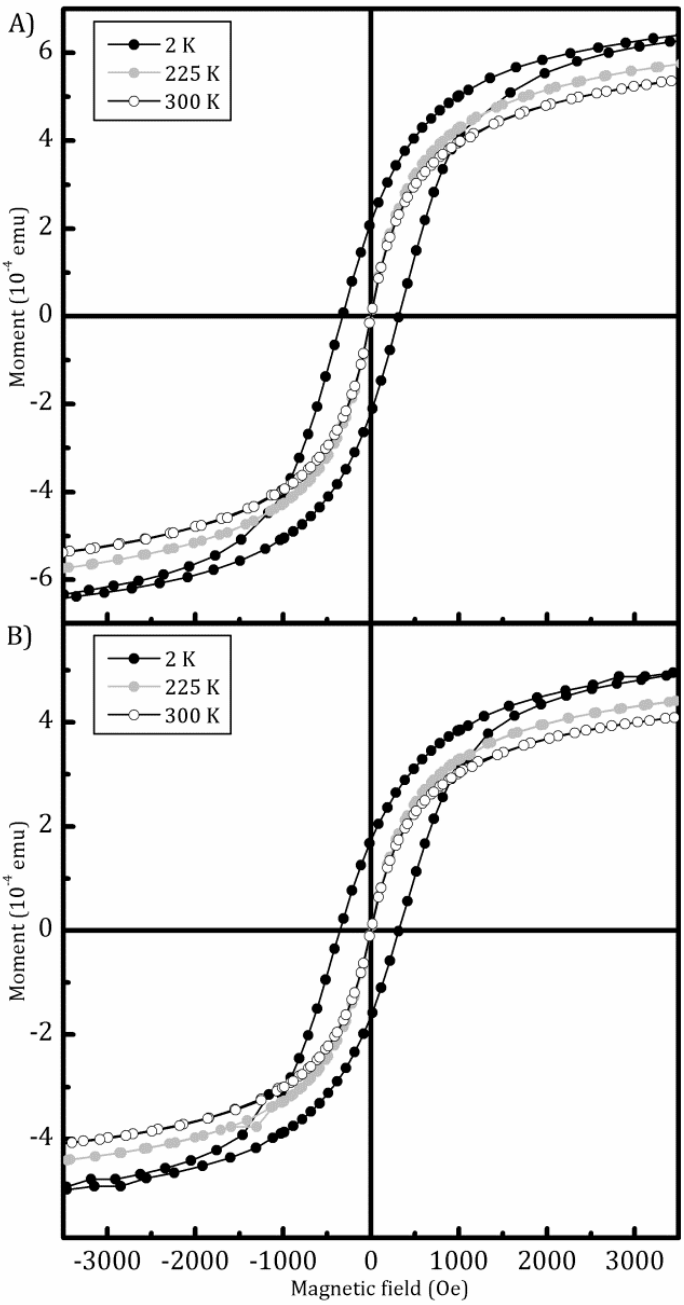

Figure 6.10. M *vs* B curves at 2, 225 and 300 K for nanocomposites with 5 wt% of A) PS- and B) PMMA-modified nanoparticles

6.4. CONCLUSIONS

In this chapter nanocomposites based on SBM triblock copolymer and maghemite nanoparticles have been prepared. Results seem to indicate that modification of

nanoparticles by *grafting through* method enables their placement at the desired domains: at PS domains for PS-modified nanoparticles and at PMMA domains for PMMA-modified ones, as it was shown by AFM and DSC measurements. This fact would reinforce the conclusions of Chapter 4 and 5, in which it was shown that modified nanoparticles were also successfully placed at the desired domains. In this chapter the complexity of ABC-type copolymers have been explored too. As their self-assembling is affected by more parameters the interpretation of nanostructures is more complicated. Their versatility related with the high amount of nanostructures that can generate, and their ability to host nanoparticles, makes them very interesting materials for nanocomposite fabrication, and, as only a few works can be found about them, it constitutes an interesting topic for further research. To finish with this chapter, superparamagnetic behavior of the nanocomposites was also demonstrated by magnetic measurements, magnetic properties of nanoparticles have been transferred to the nanocomposites.

6.5. REFERENCES

Bai J., Shi Z., Yina J. and Tian M., A simple approach to preparation of polyhedral oligomeric silsesquioxane crosslinked poly(styrene-b-butadiene-b-styrene) elastomers with a unique micro-morphology via UV-induced thiol–ene reaction. *Polym. Chem.* **2014**, 5, 6761-6769

Cano L., Gutierrez J., and Tercjak A., Rutile TiO_2 Nanoparticles Dispersed in a Self-Assembled Polystyrene-block-polymethyl Methacrylate Diblock Copolymer Template. *J. Phys. Chem. C* **2013**, 117, 1151-1156

Choi S., Lee K.M. and Han C.D., Effects of Triblock Copolymer Architecture and the Degree of Functionalization on the Organoclay Dispersion and Rheology of Nanocomposites. *Macromolecules* **2004,** *37,* 7649-7662

Elbs H., Drummer C., Abetz V. and Krausch G., Thin Film Morphologies of ABC Triblock Copolymers Prepared from Solution. *Macromolecules* **2002,** 35, 5570-5577

Fukunaga K., Hashimoto T., Elbs H. and Krausch G., Self-Assembly of a Lamellar ABC Triblock Terpolymer Thin Film. Effect of Substrates. *Macromolecules* **2003,** *36,* 2852-2861

Gutierrez J., Garcia I., Tercjak A. and Mondragon I., The effect of thermal and vapor annealing treatments on the self-assembly of TiO2/PS-b-PMMA nanocomposites generated via the sol-gel process. *Nanotechnology* **2009**, 20, 225603 (9 pp)

Higuchi T., Sugimori H., Jiang X., Hong S., Matsunaga K., Kaneko T., Abetz V., Takahara A. and Jinnai H., Morphological Control of Helical Structures of an ABC-Type Triblock Terpolymer by Distribution Control of a Blending Homopolymer in a Block Copolymer Microdomain. *Macromolecules* **2013**, 46, 6991-6997

Hückstädt H., Göpfert A. and Abetz V., Influence of the block sequence on the morphological behavior of ABC triblock copolymers. *Polymer* **2000**, 41, 9089-9094

Kabir R., Albuerne J., Simon P.F.W., Filiz V., Abetz C., Böttcher H., Perlich J. and Abetz V., Deformation and orientation behavior of polystyrene-*b*-polybutadiene-*b*-poly(methyl methacrylate) triblock terpolymers: Influence of polybutadiene microstructures and the molar masses. *Polymer* **2013**, 54, 673-684

Kirschnick T., Gottschalk A., Ott H., Abetz V., Puskas J. and Altstädt V., Melt processed blends of poly(styrene-*co*-acrylonitrile) and poly(phenylene ether) compatibilized with polystyrene-*b*-polybutadiene-*b*-poly(methyl methacrylate) triblock terpolymers. *Polymer* **2004**, 45, 5653-5660

Lin Y., Daga V.K., Anderson E.R., Gido S.P. and Watkins J.J., Nanoparticle-Driven Assembly of Block Copolymers: A Simple Route to Ordered Hybrid Materials. *J. Am. Chem. Soc.* **2011**, 133, 6513-6516

Lo C.-T., Lee B., Pol V.G., Dietz Rago N.L., Seifert S., Winans R.E. and Thiyagarajan P., Effect of Molecular Properties of Block Copolymers and Nanoparticles on the Morphology of Self-Assembled Bulk Nanocomposites. *Macromolecules* **2007**, 40, 8302-8310

Löbling T.I., Hiekkataipale P., Hanisch A., Bennet F., Schmalz H., Ikkala O., Gröschel A.H. and Müller A.H.E., Bulk morphologies of polystyrene-*block*-polybutadiene-*block*-(*tert*-butyl

methacrylate) triblock terpolymers. *Polymer* **2015**, 479-489

Nagpal U., Detcheverry F.A., Nealey P.F. and de Pablo J.J., Morphologies of Linear Triblock Copolymers from Monte Carlo Simulations. *Macromolecules* **2011**, 44, 5490-5497

Ritzenthaler S., Court F., Girard-Reydet E., Leibler L. and Pascault J.P., ABC Triblock Copolymers/Epoxy-Diamine Blends. 2. Parameters Controlling the Morphologies and Properties. *Macromolecules* **2003,** *36,* 118-126

Stadler R., Auschra C., Beckmann J., Krappe U., Voigt-Martin I. and Leibler L., Morphology and thermodynamics of symmetric poly(A-block-B-block-C) triblock copolymers. *Macromolecules* **1995**, 28, 3080-3097

Stefik M., Mahajan S., Sai H., Epps T.H., Bates F.S., Gruner S.M., DiSalvo F.J. and Wiesner U., Ordered Three- and Five-ply Nanocomposites from ABC Block Terpolymer Microphase Separation with Niobia and Aluminosilicate Sols. *Chem. Mater*. **2009**, 21, 5466-5473

Toombes G.E.S., Mahajan S., Thomas M., Du P., Tate M.W., Gruner S.M. and Wiesner U., Hexagonally Patterned Lamellar Morphology in ABC Triblock Copolymer/Aluminosilicate Nanocomposites. *Chem. Mater.* **2008,** *20,* 3278-3287

Xu C., Ohno K., Ladmiral V., Milkie D.E., Kikkawa J.M. and Composto R.J., Simultaneous block copolymer and magnetic nanoparticle assembly in nanocomposite films. *Macromolecules* **2009,** 42, 1219-1228

Chapter 7

SYNTHESIS AND CHARACTERIZATION OF PI-*b*-PMMA/Fe_2O_3-PMMA NANOCOMPOSITES: *grafting from* method

7.1. INTRODUCTION

Grafting from is a widely used technique for the functionalization of surfaces with polymer brushes. In this method polymer chains grow *in situ* from initiator molecules that have been pre-grafted onto the surface of nanoparticles or from a surfactant. As it was mentioned in section 2.5 of Chapter 2, different polymerization methods such as RAFT or NMP can be found for the functionalization of surfaces by *grafting from* technique. Among them ATRP was chosen for the functionalization of nanoparticles shown in the present chapter. Many works can be found in the literature regarding this functionalization by ATRP. On one hand, this technique has been used for growing polymer brushes onto planar substrates. Liu et al. synthesized PMMA and PEGMA polymer bushes by surface-initiated ATRP, onto poly(vinylidene fluoride) films, by previous surface hydroxylation and attachment of 2-bromoisobutyrate bromide initiator (Liu et al. 2006). Jain et al. combined a highly reactive monomer, 2-(methacryloyloxy)ethyl succinate, and active catalyst systems for the rapid growing of poly(carboxylic acid) (PCA) brushes on Au-coated Si wafers, obtaining films with an ellipsometric thickness of 120 nm in less than 15 min (Jain et al. 2008). Due to the difficulty of preparing binary brushes using normal ATRP, Ye et al. introduced a new method to prepare binary polymer brushes using surface-initiated two-step reverse ATRP, and synthesized poly(*n*-butyl acrylate) (PnBA) and poly(acrylic acid) (PAA) binary polymer brushes onto silicon wafers (Ye et al. 2010). On the other hand, by this method carbon nanotubes and different inorganic nanoparticles have also been functionalized. Sun et al. synthesized poly(2-methacryloyloxyethyl phosphorylcholine) from magnetic nanoparticles by ATRP. Functionalized nanoparticles showed a good biocompatibility in cytotoxicity tests, making these nanoparticles as potential contrast agents for magnetic resonance imagining (MRI) (Sun et al. 2012). Qin et al. synthesized polymer brushes with SWCNTs as backbones by grafting *n*-butyl methacrylate on

them via ATRP, concluding that functionalization and polymerization converted original SWCNT bundles into individual tubes (Qin et al. 2004). Ohno et al. modified the surface of silica particles with (2-bromo-2-methyl)propionyloxy hexyl triethoxysilane as ATRP initiating site, successfully obtaining PMMA brushes (Ohno et al. 2005). Shanmugharaj et al. synthesized well defined PMMA brushes by ATRP using 6-(2-bromo-2-methyl) propionyloxy hexyl triethoxysilane as initiator attached to the surface of zinc antimonate nanoparticles (Shanmugharaj et al.2010). Marutani et al. synthesized PMMA brushes by previous attachment of 2-(4-chlorosulfonylphenyl) ethyl trichlorosilane (CTCS) onto magnetic nanoparticle surface; CTCS was the initiator for MMA polymerization (Marutani et al. 2004). Our group also functionalized magnetic nanoparticles following the method proposed by Marutani et al., obtaining a good dispersion of nanoparticles through P2VP-*b*-PMMA copolymer (García et al. 2007, García et al. 2008).

Although polyisoprene-*block*-poly(methyl methacrylate) (PI-*b*-PMMA) copolymers have not been very used as matrix for organic/inorganic nanocomposites generation, some works about them can be found in literature. Tcherkasskaya et al. studied the validity of this BCP as non-reactive energy transferee (Tcherkasskaya et al. 1997). Schillén et al. prepared PI-*b*-PMMA copolymer-based micelles, with a dense core of insoluble polyisoprene (PI) block and a soft solvent-swollen corona of soluble PMMA block (Schillén et al. 1999). Lopes et al. studied the interfacial behavior of this BCP at the air-interface characterized different PI-*b*-PMMA copolymers by size exclusion chromatography-nuclear magnetic resonance (SEC-NMR) to elucidate their average chemical compositions and molar masses, analyzing also the microstructure distributions of both blocks (Hehn et al. 2012). PI-*b*-PMMA has also been used in our group for preparing nanostructured thermosetting systems by modifying an epoxy matrix with it. Multi-walled carbon nanotubes (MWCNT), modified with PI brushes to improve compatibility with the segregated PI block, were added as the third phase of nanocomposites (Espósito et al. 2013).

The main objectives of the work described in this chapter are the following. Firstly, the functionalization of maghemite nanoparticles with PMMA brushes by *grafting from* technique together with their characterization; second, morphological characterization of PI-*b*-PMMA copolymers with different block ratios; and third, preparation and characterization of nanocomposites based on selected PI-*b*-PMMA block copolymer and functionalized magnetic nanoparticles. Functionalization of nanoparticles was analyzed by FTIR and TGA. Morphological characterization of PI-*b*-PMMA and nanocomposite thin films was carried out by AFM, TEM and small-angle X-ray scattering (SAXS). Finally, nanocomposites were magnetically characterized by means of VSM and SQUID measurements. To the best of our knowledge, it is the first time that PI-*b*-PMMA copolymer is used for preparing nanocomposites with nanoparticles.

7.2. MATERIALS AND METHODS

7.2.1. MATERIALS

Two PI-*b*-PMMA copolymers with different block weight ratios have been used, synthesized in the department of Materials Science and Engineering of the University of Ioannina by Avgeropoulos and co-workers. Synthesis was carried out by anionic polymerization using high-vacuum techniques in evacuated, *n*-butyllithium-washed glass vessels (Litina et al. 2006). Isoprene (Fluka), MMA (Merck), benzene and THF (Merk) were first purified to the standards required for anionic polymerization. Additions were made through break seals while removals were accomplished through heat sealing of constrictions. The initiator was *sec*-butyllithium (*sec*-BuLi), prepared in vacuum from *sec*-butylchloride and lithium dispersion. Initially, isoprene reacted with *sec*-BuLi in benzene at room temperature in order to give the first living chain and subsequent polymerization of PI block. Then a small amount of 1,1-diphenylethylene was added in order to

end-cap living PI ends, together with THF (THF/Benzene = 3/1). Finally, MMA monomer was added for the polymerization of PMMA block in THF. The mixture was stirred for 1 h at -78 °C and then terminated by adding methanol. Small amounts of PI homopolymer were successfully removed by fractionation using THF and methanol as solvent and non-solvent, respectively. Main characteristics of PI-*b*-PMMA copolymers used in this work are summarized in Table 7.1.

Table 7.1. Characteristics of PI-*b*-PMMA copolymers

	M_{nPI}	M_{nPMMA}	M_{ntot}	M_w	f_{PI}	I
52/48	41,800	48,000	89,800	97,000	0.52	1.08
22/78	17,000	60,500	77,500	93,000	0.22	1.2

Maghemite nanoparticles with a nominal size of 9 nm were purchased from Integram Technologies, Inc. MMA monomer used for the functionalization of nanoparticles with PMMA brushes was purchased from Aldrich, with a purity of 99 %, and was distilled under reduced pressure over CaH_2 before use. CTCS was purchased from ABCR and used in 50 wt% solution in dichloromethane (DCM), containing 30 wt% of free sulfonic acid and small amounts of silylsulfonic acid, without any further purification. Catalysts used were copper (I) bromide (CuBr; 98.0 %), copper (II) bromide ($CuBr_2$; 99.9 %), and bipyridine (Bip; 99.0 %), all of them purchased from Aldrich and used as received. Hydrofluoric acid (48-51 %), used for brush cleavage, was purchased from Probus. Extra-dry toluene, THF and DCM from Aldrich were used as solvents without any further purification. Chemical structures of the silane containing initiator for the polymerization, MMA monomer and PI-*b*-PMMA block copolymer can be seen in Scheme 7.1.

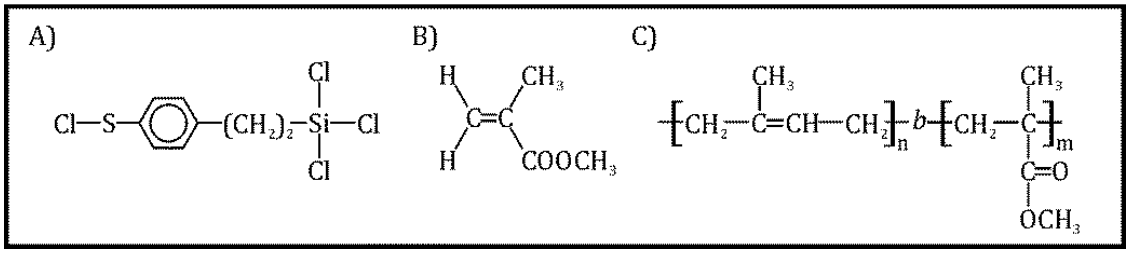

Scheme 7.1. Chemical structure of A) CTCS, B) MMA monomer and C) PI-*b*-PMMA copolymer

7.2.2. METHODS

7.2.2.1. Nanoparticle functionalization

Nanoparticle modification was carried out in two steps. First the silanization process and then the synthesis of PMMA brushes from the surface of silanized nanoparticles by *grafting from* method, as it is described in Scheme 7.2.

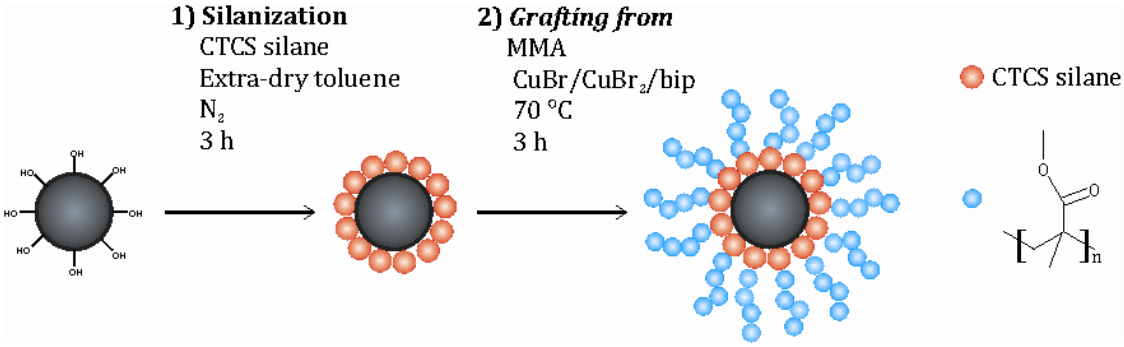

Scheme 7.2. Nanoparticle modification procedure

7.2.2.1.1. Silanization process

CTCS initiator was immobilized on nanoparticle surface following the method proposed by Marutani et al. (Marutani et al. 2004). 0.1 g of iron oxide nanoparticles, 1 µL of CTCS and extra-dry toluene were mixed in an ultrasonic bath at room temperature for 3 h at inert N_2 atmosphere. Nanoparticles were subsequently washed with THF, until any silane rest was eliminated (the presence

of silane after washing was probed by FTIR) and then were dried in vacuum at 40 °C for a period of 2 days.

7.2.2.1.2. Growth of PMMA brushes by *grafting from* method

Polymerization of MMA was performed with CuBr/bip as catalyst (Wang et al. 1995, García et al. 2007) and CTCS on the surface of nanoparticles as initiator. First, CuBr (16.06 mg), $CuBr_2$ (2.35 mg), bip (78.55 mg), and 0.25 g of CTCS-modified nanoparticles were placed in a flask under N_2 atmosphere and deoxygenated MMA (30 mL) was added. The flask was then sealed under N_2 atmosphere, leaving the mixture to react under stirring at 70 °C for 3 h. Nanoparticles were subsequently washed with THF, until any monomer rest was eliminated (probed by FTIR), and then were vacuum dried at 40 °C for a period of 2 days. Polymerization conditions were optimized in order to obtain polymer brushes with the desired molar mass, big enough for compatibilizing and low enough for the placement of nanoparticles at PMMA domains (if brush chains are smaller than those of PMMA block, their wetting is expected to be better) (Xu et al. 2009).

7.2.2.1.3. *Cleavage* of PMMA brushes from nanoparticle surface

In order to characterize the molar mass of PMMA brushes, they were cleavaged from the nanoparticle surface with the following procedure. In a polyethylene flask, 0.1 g of nanoparticles were inserted together with 3.5 mL of toluene and 3.5 mL of aqueous hydrogen fluoride (HF) (5 %), and were left to react for 2 h. Then organic and aqueous phases were separated, repeating the process at least twice (Lan et al. 2007). Molar mass of separated brushes was measured by gel permeation chromatography (GPC).

7.2.2.2. Neat BCP and nanocomposite thin film preparation

In order to choose the most adequate BCP for preparing nanocomposite thin films, thin films of both 52/48 and 22/78 neat BCP were prepared. Solutions with 1 wt% of BCP in DCM were prepared, as this solvent is adequate for both blocks BCP (χ_{PI}= 0.35 and χ_{PMMA}= 0.49, as calculated from equations 2.1 and 2.2 shown in Chapter 2). Thin films were prepared by solvent casting onto precleaned silicon wafers. In order to get nanostructured BCP, both thermal and solvent vapor annealing were carried out.

Once the most adequate copolymer was selected nanocomposites were prepared. First, nanoparticles were dissolved in DCM by sonication, and then PI-*b*-PMMA was added. Solution droplets were placed on silicon wafers and maintained at room temperature until complete solvent removal. Nanocomposites with nanoparticle amounts from 0.1 to 5 wt% were prepared.

7.2.2.3. Characterization techniques

7.2.2.3.1. FTIR

It was used to verify the functionalization of iron oxide nanoparticles. Infrared spectra were carried out in a Nicolet Nexus 670 Spectrometer, as it was described in section 3.2.2.3.3 of Chapter 3.

7.2.2.3.2. TGA

It was used to determine the amount of hydroxyl groups at nanoparticle surface, the amount of grafted initiator and the amount of grafted PMMA brushes. TGA results were obtained using a TGA/SDTA-851e equipment running from 25 to 750

°C at a heating rate of 10 °C/min under N_2 atmosphere, as it was shown in section 3.2.2.3.4 of Chapter 3.

7.2.2.3.3. AFM

It was used to study the surface morphologies of neat block copolymer and nanocomposite films. AFM measurements were performed in tapping mode using a Dimension Icon Nanoscope V (Bruker), as it was described in section 3.2.2.3.6 of Chapter 3.

7.2.2.3.4. TEM

It was used to verify the morphology of neat block copolymer films, with a Philips Tecnai 20 transmission electron microscope operated at 200 kV with a resolution of 2.5 Å. This technique was described in section 3.2.2.3.5 of Chapter 3.

7.2.2.3.5. SAXS

SAXS is a non-destructive and highly versatile standard method to study the nanoscale structure of any type of material ranging from new composite nanosystems to biological macromolecules. Parameters as averaged particle sizes, shapes and distributions, porosity and degree of crystallinity, as well as electron density maps with nanometer precision can be obtained. Materials can be solid, liquid or even exhibit gaseous-like properties. In this work SAXS measurements were carried out to analyze the nanostructure of block copolymer thin film. SAXS measurements of a self-assembled block copolymer allow distinguishing between different nanostructures formed, like lamellar or hexagonally packed cylinders among others (Li et al. 2013, Porto et al. 2011).

SAXS measurements were performed on a Ganesha 300XL SAXS-WAXS system (SAXSLAB ApS, Copenhagen/ Denmark) equipped with a GENIX 3D microfocus X-ray source and optic, a three-(scatterless)-slit collimation system, a fully evacuated sample chamber and beam path, and a movable two-dimensional Pilatus 300 K detector. Samples on mica were measured at room temperature.

7.2.2.3.6. SQUID

SQUID magnetometer was used for ZFC/FC measurements. These measurements were carried out at 100 Oe, between 5 and 300 K. The equipment used for the measurements was a SQUID magnetometer (MPMS-7T, Quantum Design), with a 7 T superconducting magnet. This technique was described in section 4.2.2.3.5 of Chapter 4.

7.2.2.3.7. VSM

Magnetization was measured in a Quantum Design Physical Properties Measurement System (PPMS) with Vibrating Sample Magnetometer option. This equipment was used to measure the hysteresis loops at 2, 50 and 150 K, as it was described in section 4.2.2.3.4 of Chapter 4.

7.3. RESULTS AND DISCUSSION

7.3.1. CHARACTERIZATION OF FUNCTIONALIZED NANOPARTICLES

The first step of this work has been the functionalization of nanoparticle surfaces with CTCS silane, since its sulfonyl chloride groups will allow the growth of PMMA chains from the surface following the *grafting from* technique (García et al. 2007). Due to this fact, the proper attachment of the silane to the surface is of vital

importance. The success of silanization process and the subsequent functionalization of nanoparticle surface by PMMA brushes have been studied by FTIR and TGA measurements.

Figure 7.1 shows the FTIR spectra of silanized and PMMA-modified nanoparticles, demonstrating the success of both steps. In CTCS-modified nanoparticle FTIR spectrum characteristic bands related to CTCS such as those corresponding to the stretching vibration of sulfonyl group at 1406 and 1174 cm^{-1} and the stretching vibration of Fe-O-Si bond at 1121 cm^{-1} can be seen, proving the grafting of CTCS to nanoparticle surface from the –OH groups present on it. FTIR spectrum of PMMA-modified nanoparticles suggests that polymerization of PMMA brushes has been carried out successfully, as the presence of bands related to the methacrylate group (C=O stretching vibration at 1703 cm^{-1} and C-O-C stretching deformation vibration at 1237 cm^{-1}) are detected.

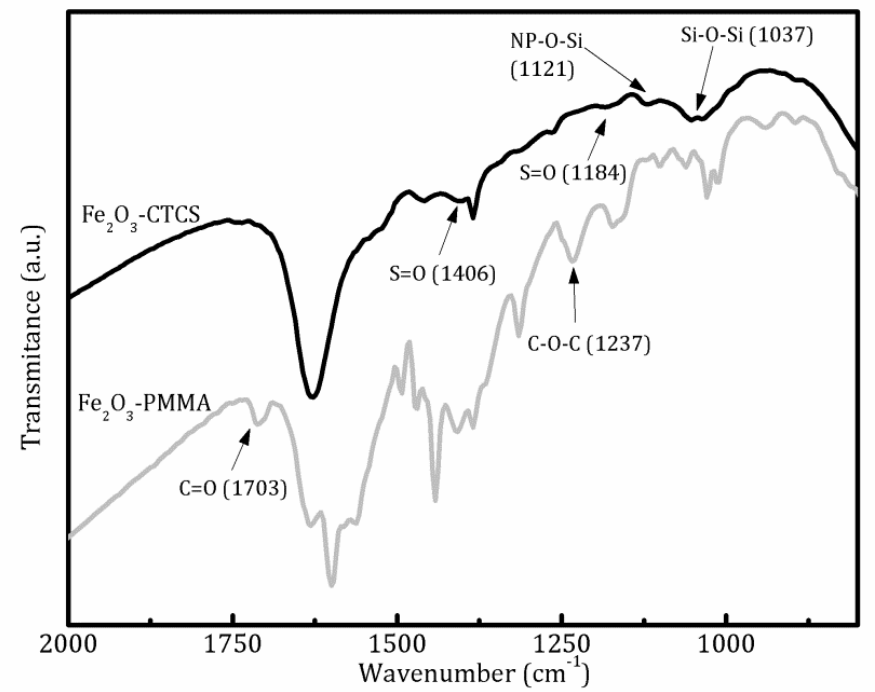

Figure 7.1. FTIR spectra of silanized and PMMA-modified nanoparticles

TGA thermograms in Figure 7.2 also show the presence of CTCS silane and PMMA brushes at the surface.

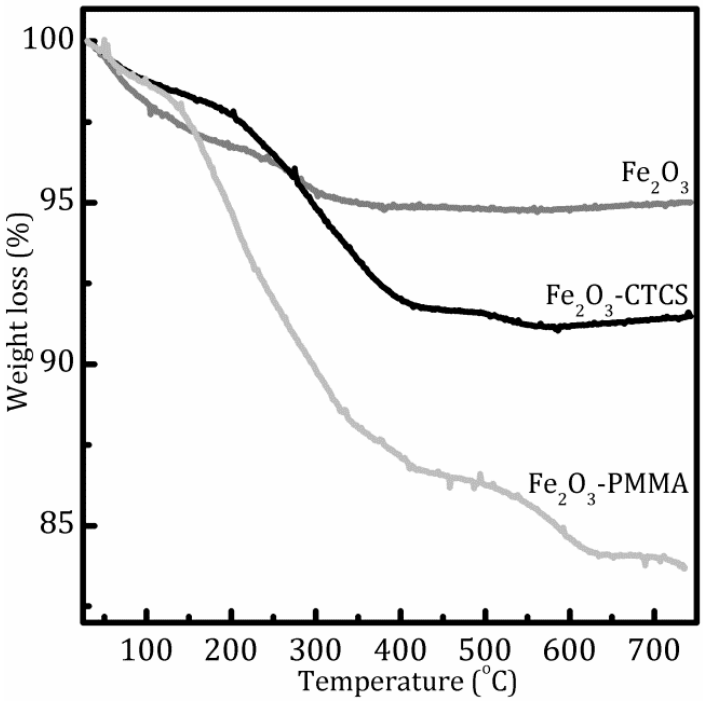

Figure 7.2. TGA thermograms of pristine, silanized and PMMA-modified nanoparticles

The amount of grafted silane has been calculated using Equation 4.1 shown in section 4.3.1 of Chapter 4 (Bartholome et al. 2003). A surface density of 1.1 molecules/nm^2 has been calculated for the initiator. As the hydroxyl group density has been calculated to be 8.1 OH/nm^2 as it has been shown in previous chapters, the yield of silanization process has been calculated to be equal to 13 %. Following the same method, the grafting density of polymer brushes has also been calculated directly from the weight loss of TGA thermogram, obtaining a value of 0.8 chains/nm^2. This grafting density value is in the order of those calculated by other authors (Ohno et al. 2005) following the same method. Moreover, if this grafting density value is compared to that obtained in Chapter 3 by the *grafting to* method (0.04 chains/nm^2), the increase of density is notorious; this may be attributed to the ATRP method adopted for the polymer brush synthesis. When polymer brushes are attached to nanoparticle surface by *grafting to* method, steric hindrance is expected, large polymer chains struggle between them to reach active sites onto nanoparticle surface, what can cause that polymer chains impede the pass to each other, resulting in a lower grafting density. On the contrary, in the

grafting from method, active sites should be reached by small monomer molecules, so much lower steric hindrance can be expected. (Advincula et al. 2004). According to Ferreira et al., as $\sigma\sqrt{N} > 1$, being N the number of monomers in the chains and σ the grafting density, it can be said that nanoparticles are functionalized by dense brushes (Ferreira et al. 1998). Brushes of approximately 1000 g/mol have been obtained, as measured by GPC after cleavage. As it has been mentioned above, the polymerization process has previously been optimized in order to obtain short brushes which lead to a better dispersion within the PMMA domains of the copolymer (Xu et al. 2008).

7.3.2. BCP MORPHOLOGY ANALYSIS

The next step of this work has been the analysis of morphologies obtained for 52/48 and 22/78 block copolymer thin films, in order to select one of them for preparing nanocomposites films with magnetic nanoparticles. To select one of the PI-*b*-PMMA copolymer for preparing organic/inorganic nanocomposites both BCP have been subjected to different annealing treatments, thermal and solvent vapor annealing, and also the as cast morphologies have been analyzed. Thin film morphologies of both BCP have been analyzed by AFM, and the chosen BCP have also been analyzed by TEM and SAXS, in order to better characterize it. Figure 7.3 shows AFM images obtained for copolymer thin films prepared by solvent casting, without any further treatment. Both copolymers phase separate, but while 22/78 copolymer does not show any ordered nanostructure, 52/48 one self-assembles into a lamellar morphology, as it was expected due to its composition (Schalz and Lecommandoux 2010). It should be mentioned that PMMA nanodomains appear brighter than PI ones, due to their higher modulus (Iatrou and Hadjichristidis 1992).

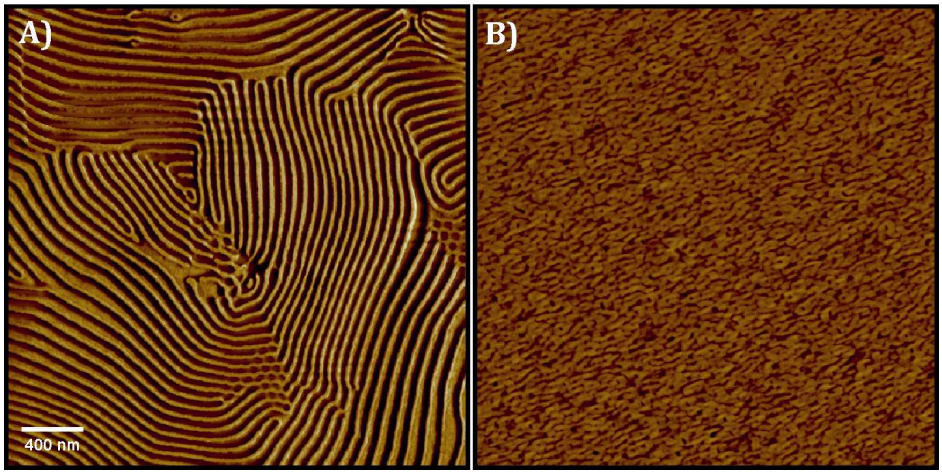

Figure 7.3. AFM phase images of as cast (A) 52/48 and (B) 22/78 copolymer thin films

Next, morphologies obtained for thermal annealed copolymer films have been analyzed. Figure 7.4 shows AFM images obtained for 52/48 copolymer thin film annealed at 120 °C for 1 h. This annealing temperature is above T_g of PI and PMMA (-60 °C and 118 °C, respectively). As it can be seen, the lamellar nanostructuring has been maintained after thermal annealing, creating a long range ordered lamellar structure, with an average interlamellar distance of around 62.6 nm. Very similar morphologies have been obtained for longer annealing times at 120 °C and also for annealing treatments at higher temperatures.

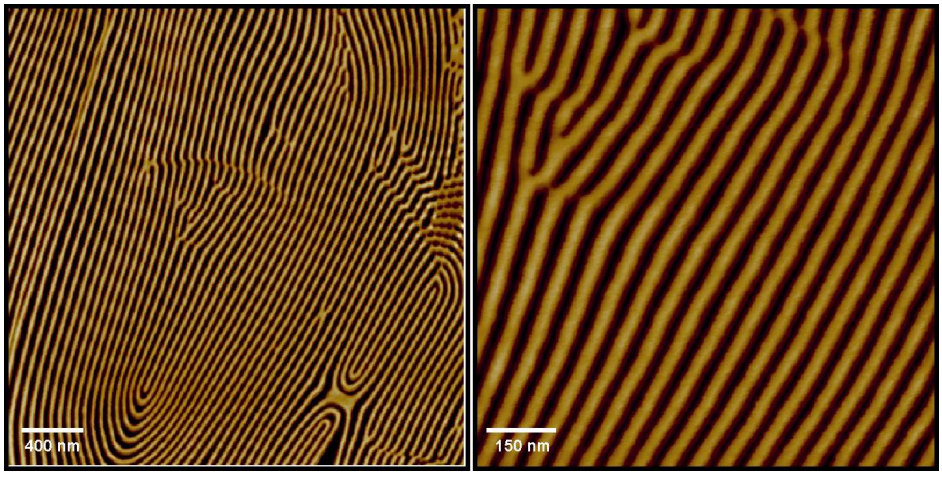

Figure 7.4. AFM phase images with different magnifications for 52/48 copolymer thin film annealed at 120 °C for 1 h

Figure 7.5 shows AFM images obtained for 22/78 copolymer thin film after thermal annealing at 130 °C for 4 h. This annealing temperature is also higher than the T_g of PI and PMMA (-64 °C for PI and 125 °C, respectively). As it can be seen in this AFM phase image, 22/78 copolymer, separates into a worm-like nanostructure, without any ordered orientation. Similar morphologies have been obtained for longer periods at 130 °C and also for thermal annealing treatments carried out at higher temperatures.

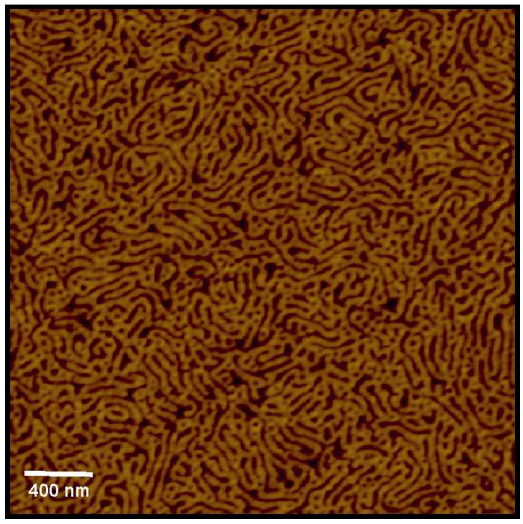

Figure 7.5. AFM phase image of 22/78 copolymer thin film after thermal annealing at 130 °C for 4 h

Nanostructuring of both copolymers has also been carried out by SVA, with acetone as solvent. In Figure 7.6 evolution of 52/48 copolymer morphology with exposure time to acetone vapors can be seen. Acetone is a selective solvent for PMMA block, being χ_{PI}= 0.92 and χ_{PMMA}= 0.5, as calculated from equations 2.1 and 2.2 shown in Chapter 2. When 52/48 copolymer is exposed to acetone vapors, a morphology change from surface-perpendicular lamellar ordering to hexagonally packed cylinders perpendicular to the substrate occurs. Without any treatment, 52/48 copolymer showed lamellar morphology, which changes with exposition to acetone. As it can be seen in Figure 7.6, after 16 h of exposure the lamellar morphology is broken and BCP thin film starts its transformation from lamellar to hexagonally packed cylinder morphology. PMMA lamellae of the as cast copolymer

start to join and PI cylinders start to form. The morphological transformation is completed after 96 h of exposure, without changing for longer exposure times.

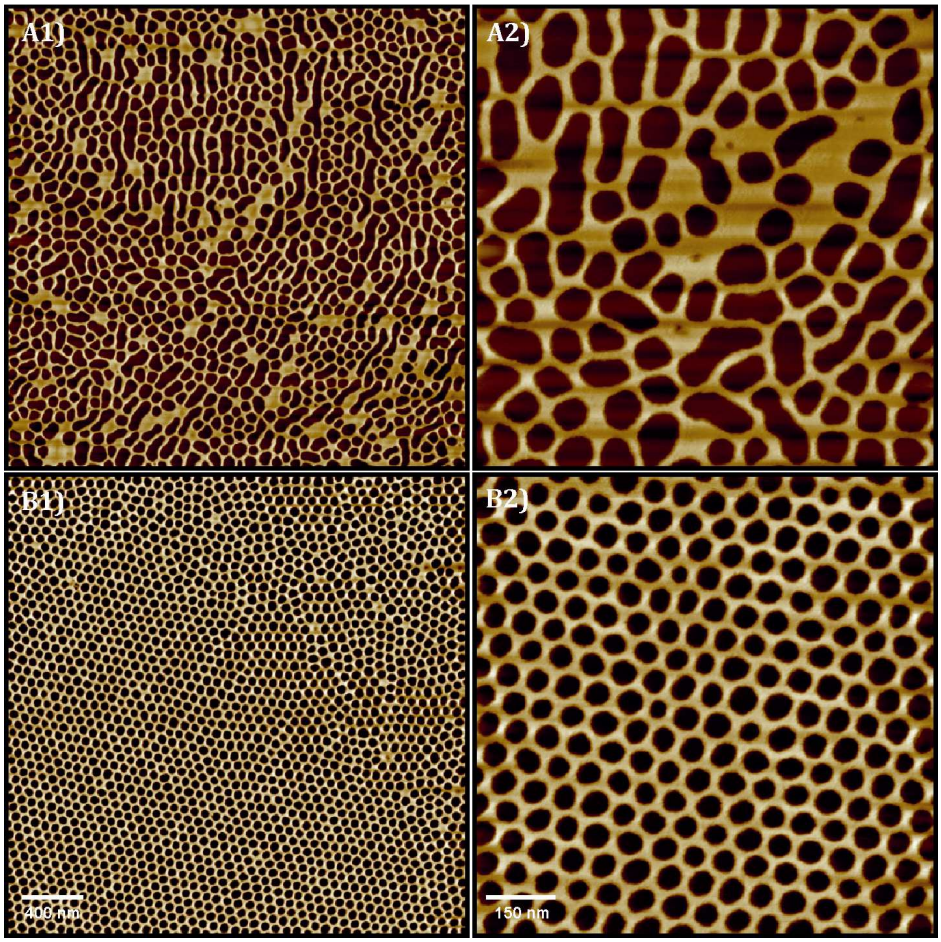

Figure 7.6. AFM phase images at different magnifications for 52/48 copolymer thin films exposed to acetone vapors for A) 16 h and B) 96 h

22/78 copolymer has also been exposed to acetone vapors. Figure 7.7 shows the AFM images obtained for 22/78 copolymer thin films after SVA for 4 h. It can be seen that after 4 h, this copolymer self-assembles into a cylindrical morphology perpendicularly oriented to the substrate, with hexagonally packed cylinders. This could be due to the plasticizing effect of acetone that increases the mobility of PMMA block, favoring the assembly into a nanoordered structure (Park et al. 2009, Marting and Young 2003). The hexagonally packed cylinder morphology is maintained after longer exposure times.

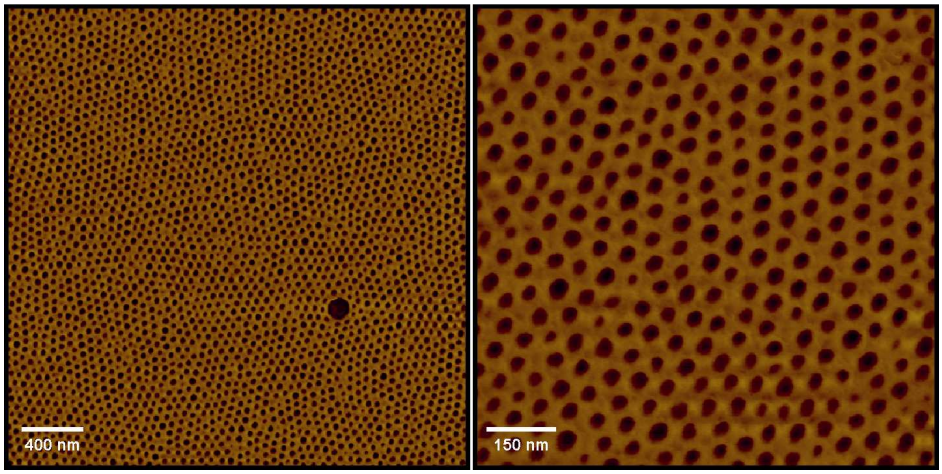

Figure 7.7. AFM phase images at different magnifications for 22/78 copolymer thin films exposed to acetone vapors for 4 h

If the hexagonally packed structure obtained for 22/78 copolymer is compared to that obtained for 52/48 one, the difference is the higher average diameter of PI cylinders for 52/48 copolymer (49.4 nm) when compared with those of 22/78 copolymer (32.5 nm), as expected from its higher PI content. According to its composition (52 % of PI), the stable morphology for 52/48 copolymer should be the lamellar one (Schalz and Lecommandoux 2010), as it has been obtained without any treatment or by thermal annealing. Due to the fact that acetone is a selective solvent for PMMA block, this block could swell with solvent, thus modifying the volume fraction and consequently the stable nanostructure (Park et al. 2009, Huang et al. 2012). According to the results obtained after different treatments for 52/48 and 22/78 BCPs, 52/48 one has been chosen to prepare the nanocomposites, due to its higher versatility to form different nanostructures. From this point forward, when PI-*b*-PMMA is mentioned, it would be in reference to 52/48 copolymer. This BCP has been further characterized by TEM and SAXS measurements. In Figure 7.8 TEM micrograph of the copolymer can be seen. PI domains are represented as dark areas, while PMMA ones correspond to bright ones, due to the higher electron density of the former. From this image, the lamellar nanostructure is confirmed for the neat copolymer.

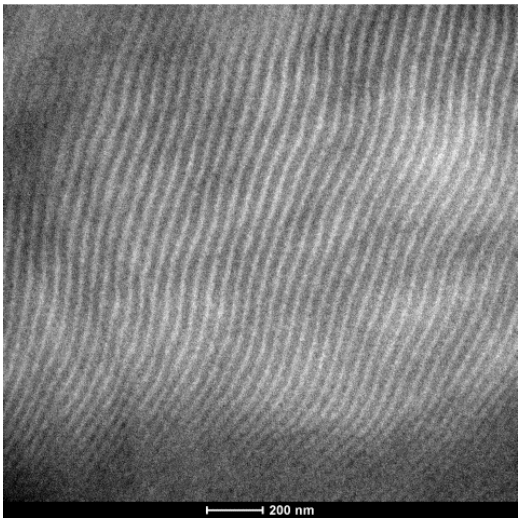

Figure 7.8. TEM micrograph of neat PI-*b*-PMMA copolymer

In Figure 7.9 SAXS patterns of as cast and solvent-annealed PI-*b*-PMMA copolymer thin film can be seen. The presence of the first order peak at q_1= 0.0121 nm^{-1} and the third order peak at q_3= 3·q_1 = 0.0363 nm^{-1} in the as cast BCP pattern are indicative of lamellar nanostructure (Porto et al. 2011). Furthermore, the lack of the second order peak is attributed to the almost symmetric volume fractions (*f*) leading to zero intensity when *n = 2*, according to the Equation 7.1 from which the intensity of each permitted reflection is calculated, for alternating lamellae morphology in a SAXS pattern:

$$I_n \sim \left(\frac{sin(nf\pi)}{n}\right)^2 \qquad (7.1)$$

On the other hand, solvent-annealed neat diblock copolymer first order peak is at q_1= 0.0072 nm^{-1}, second order peak at q_2= $\sqrt{3}$·q_1= 0.0108 nm^{-1} and fourth order peak at q_4= $\sqrt{7}$·q_1= 0.0252 nm^{-1}, which is consistent with the permitted reflections ratio for a hexagonally packed cylindrical nanostructure (Li et al. 2013). The results obtained from the SAXS and TEM measurements agree with the ones obtained with AFM, indicating that the morphology of the surface is the same to the inner nanostructure.

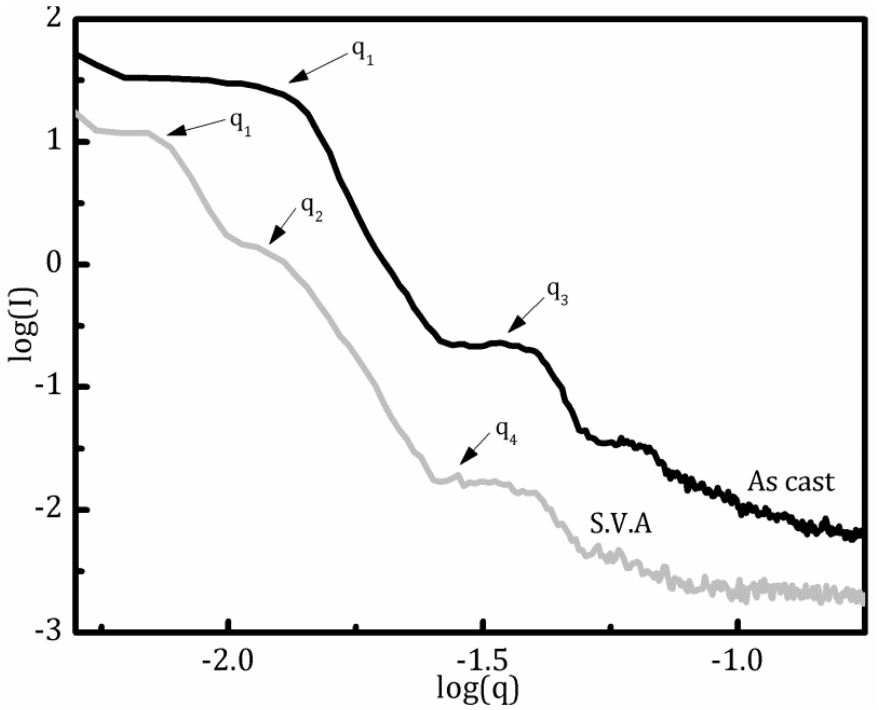

Figure 7.9. SAXS patterns of neat block copolymer and solvent-annealed samples

7.3.3. MORPHOLOGICAL CHARACTERIZATION OF NANOCOMPOSITES

In Figure 7.10 AFM phase images of as cast nanocomposite films with different nanoparticle amounts can be seen. If AFM images of Figure 7.10 are compared with those corresponding to neat block copolymer in Figure 7.3, it can be seen that nanoparticle addition change the orientation of lamellae, resulting in a mixture of perpendicular and parallel ones (Deshmukh et al. 2007). This could be due to nanoparticle addition that could modify the interaction between block copolymer domains and the substrate, evolving an orientation change of the lamellar nanostructure (Xu et al. 2009, Yoo et al. 2011). For the highest nanoparticle concentration some cylinder-forming structures appear between PMMA lamellae, probably due to the selective placement of the PMMA-functionalized nanoparticles within PMMA domains that could lead to an increase of the volume fraction of PMMA domains, the system undergoing a transition from lamellar to cylindrical morphology (Lo et al. 2007).

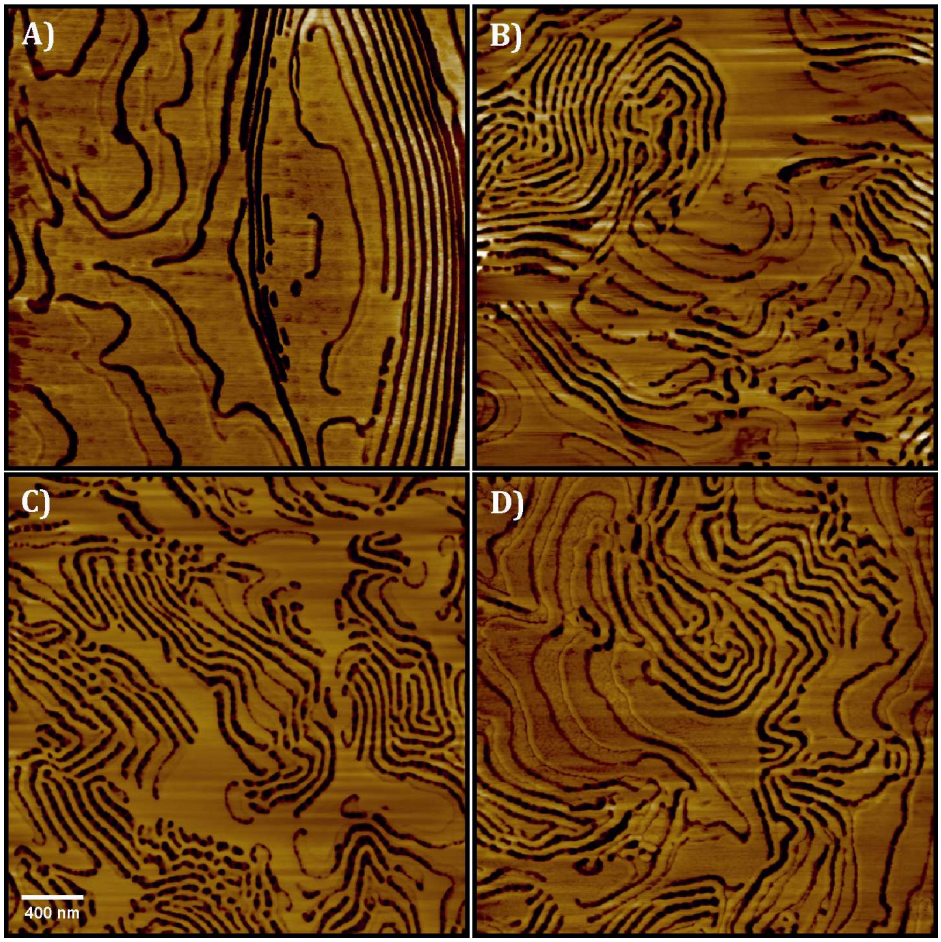

Figure 7.10. AFM phase images of as cast nanocomposite films with A) 0.1, B) 1, C) 2 and D) 5 wt% of nanoparticles

As it has been done for neat BCP, nanocomposite films have also been annealed in acetone vapors. When a BCP thin film is exposed to a solvent, nanostructure could be enhanced, and a long-range orientation order achieved (Park et al. 2009). Figure 7.11 shows the AFM images of solvent-annealed nanocomposites thin films. As it can be seen in these AFM images, the cylindrical morphology obtained for neat copolymer films after solvent annealing (Figure 7.6) is maintained for nanocomposites with 0.1, 1, and 2 wt% nanoparticles, even if some small defects are evident in the nanostructure, probably due to the presence of nanoparticles. For the nanocomposite with the highest nanoparticle content (5 wt%), the cylindrical nanostructure is disrupted and disordered morphology is obtained. It is known that for a block copolymer, the addition of fillers, together with the

solvent treatment, can modify its ODT temperature (Zhao et al. 2009, Hanley et al. 2000). This could be the reason of reaching disordered state with 5 wt% of nanoparticles after exposure to acetone, the combined effect of nanoparticles and solvent exposure that could facilitate the system to reach to a disordered state more easily.

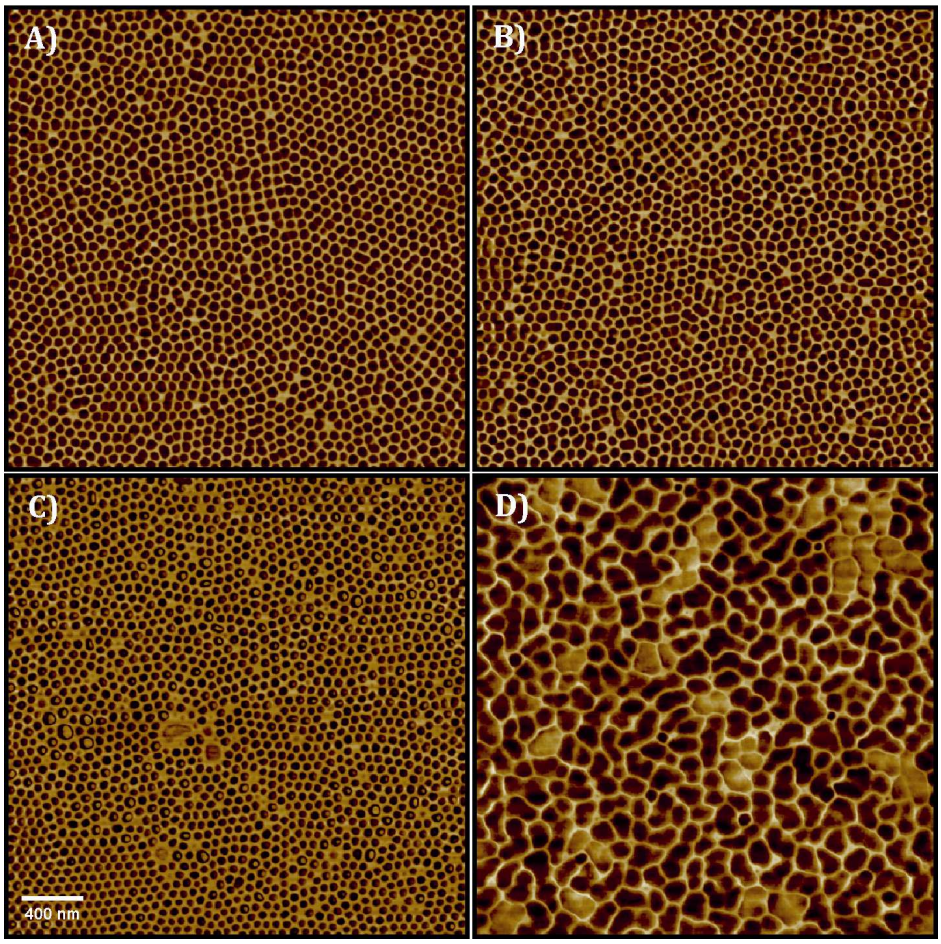

Figure 7.11. AFM phase images of nanocomposite films with A) 0.1, B) 1, C) 2 and D) 5 wt% of nanoparticles, annealed under acetone vapors for 96 h

7.3.4. DEGRADATION BY IRRADIATION WITH UV LIGHT

In order to better visualize the positioning of nanoparticles in PI-*b*-PMMA copolymer, the organic part of as cast film was removed by exposure to UV light irradiation (Peng et al. 2008, Gutierrez et al. 2009). The evolution of block copolymer film morphology with exposure time can be seen at AFM images of Figure 7.12. As it can be appreciated, PMMA block domains are degraded first. After 6 h of exposure lamellar nanostructure of copolymer film is maintained, even if height profile is smoother. This could indicate that PMMA block has been more degraded than PI one. By exposing the copolymer for 48 h, nanostructure totally disappears and both blocks are degraded. Once the degradation of the copolymer film has been reached and exposure time optimized, degradation of nanocomposites film is carried out. When UV light irradiation is applied to the nanocomposites, the organic part is removed, leaving the iron oxide nanoparticles on the silicon surface. Figure 7.13 shows the AFM phase images for the nanocomposites with 1 wt% of nanoparticles as an example, after 48 h of exposure to UV light. As it can be seen, nanoparticles with quite homogeneous size are well dispersed in the nanocomposite. By comparing AFM phase image of nanocomposites with 1 wt% of nanoparticles with that of iron oxide nanoparticles after removing the organic part by UV light irradiation (superposition of images shown in Figure 7.14), it can be seen that the position of the nanoparticles coincides with that of PMMA domains, suggesting that most of them are located within PMMA domains of the nanostructure, due to their increased compatibility given by the functionalization with PMMA brushes. As it was previously pointed out, the lower molar mass of brushes when compared with that of PMMA block, seem to allow the proper wettability of nanoparticles with PMMA domains, reaching to their selective positioning. Very similar results have been obtained after removing the organic part in the rest of nanocomposite films, showing the selective positioning of PMMA-modified nanoparticles in all of them.

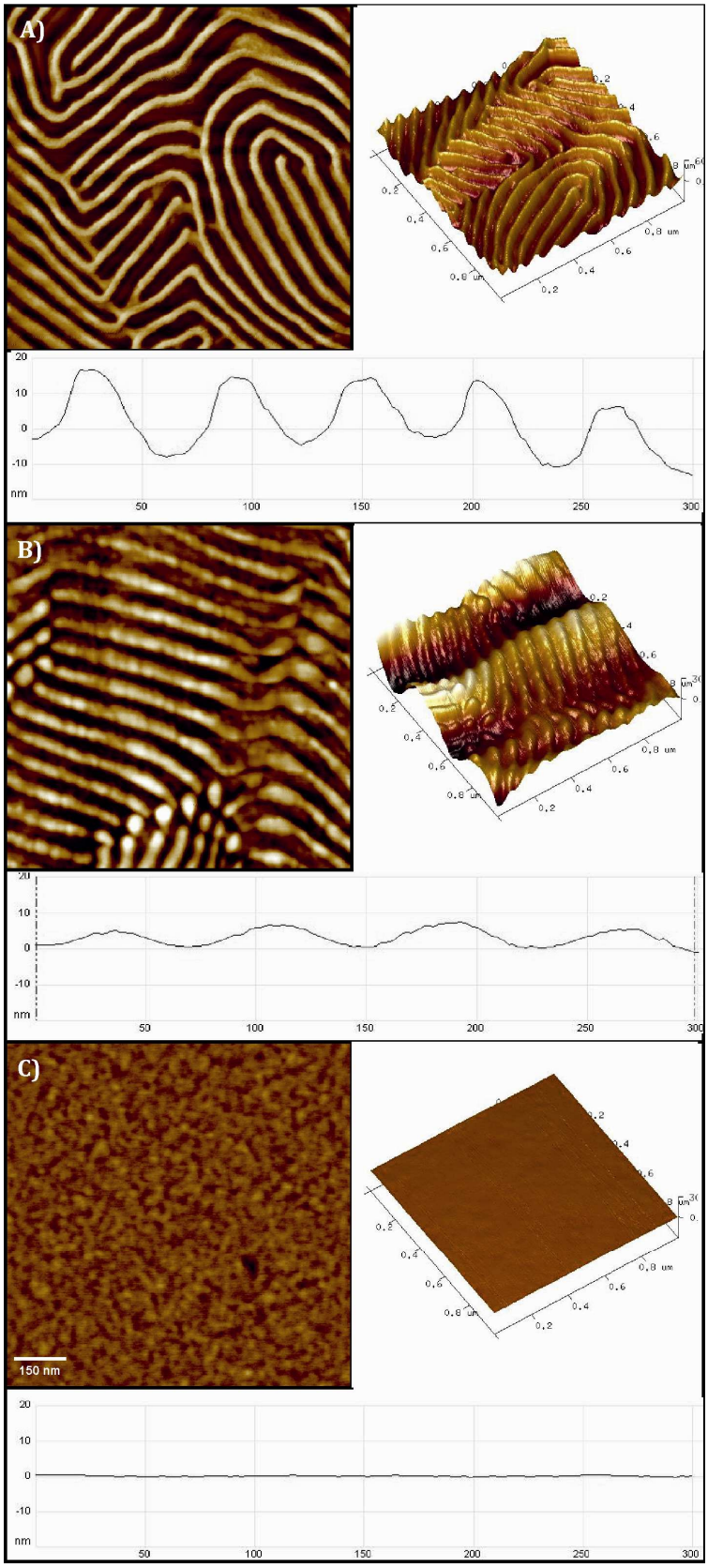

Figure 7.12. AFM phase, 3D height and profile images of A) neat block copolymer film before exposure, and after B) 6 h and C) 48 h of exposure to UV light irradiation

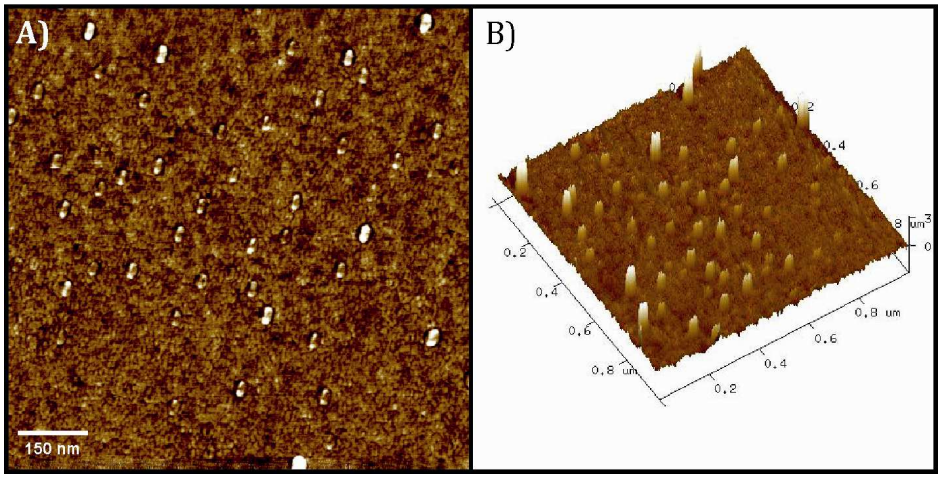

Figure 7.13. AFM (A) phase and (B) 3D height images of nanocomposite with 1 wt% of nanoparticles exposed to UV light irradiation for 48 h

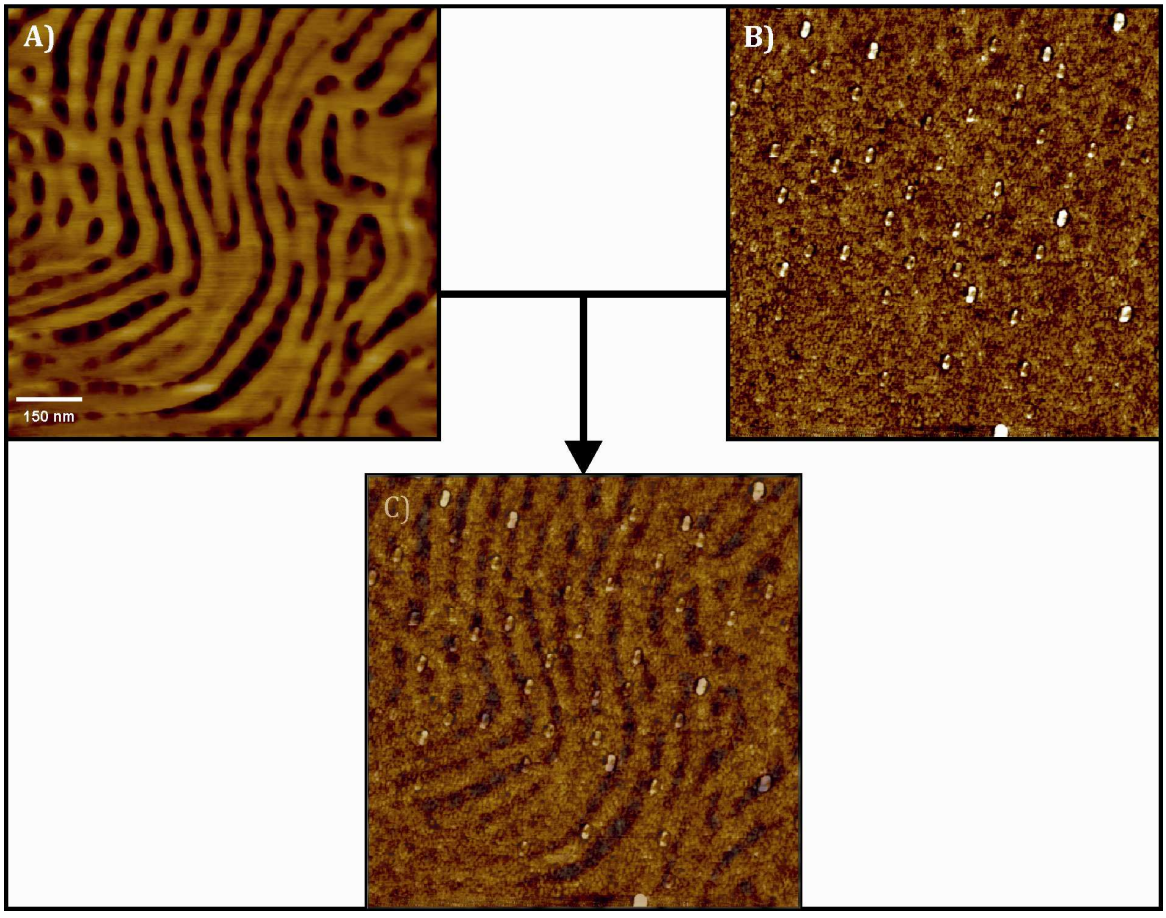

Figure 7.14. AFM phase image of A) as cast nanocomposite film with 1 wt% of nanoparticles, B) nanocomposite film with 1 wt% of nanoparticles exposed to UV light irradiation for 48 h. C) superposition of images A and B

7.3.5. MAGNETIC CHARACTERIZATION

In order to check if magnetic properties of nanoparticles have been transferred to nanocomposites, magnetic characterization has been carried out in terms of both ZFC/FC curves and M *vs* B measurements, performed by SQUID magnetometer and VSM, respectively. Figure 7.15 shows the ZFC/FC curves of as cast nanocomposite films with 2 and 5 wt% of nanoparticles. In a similar way to that shown in previous chapter for other nanocomposite film, both samples exhibit a typical superparamagnetic behavior at room temperature, while at low temperatures it becomes ferromagnetic (Zeng et al. 2006, Bean and Livingston 1959). Below the T_B, FC and ZFC magnetization curves diverge, magnetic moments are singledomain and pinned by anisotropy, while they appear thermally disordered above the T_B. If results obtained from the nanocomposites with 2 and 5 wt% of nanoparticles are compared, it can be seen that the T_B increases with nanoparticle content. As the T_B is related to the size of nanoparticles or formed aggregates (as it can be concluded from Néel-Brown expression, explained in the section 2.4 of Chapter 2), it seems that for higher nanoparticle concentration bigger aggregates are formed. Nevertheless, as it has been seen by degrading the organic part of nanocomposites by irradiating with UV light, nanoparticles are well dispersed through the copolymer, and selectively placed at PMMA domains.

Hysteresis loops have also been measured with VSM at different temperatures of 2, 50 and 150 K, as it is shown in Figure 7.16 for the nanocomposite with 5 wt% of nanoparticles. Below T_B, M *vs* B curves are hysteretic while become non-hysteretic above it. At 2 K the hysteresis is observed with a coercivity of approximately 300 Oe and a remanence of $1.5 \cdot 10^{-5}$ emu, whereas above the T_B both coercivity and remanence become null, demonstrating the superparamagnetic behavior of the nanocomposite (Schulz et al. 2010, Xu et al. 2009). This superparamagnetic behavior was detected for all nanocomposite films, showing the good transference

of magnetic properties from nanoparticles even after their modification with polymer brushes.

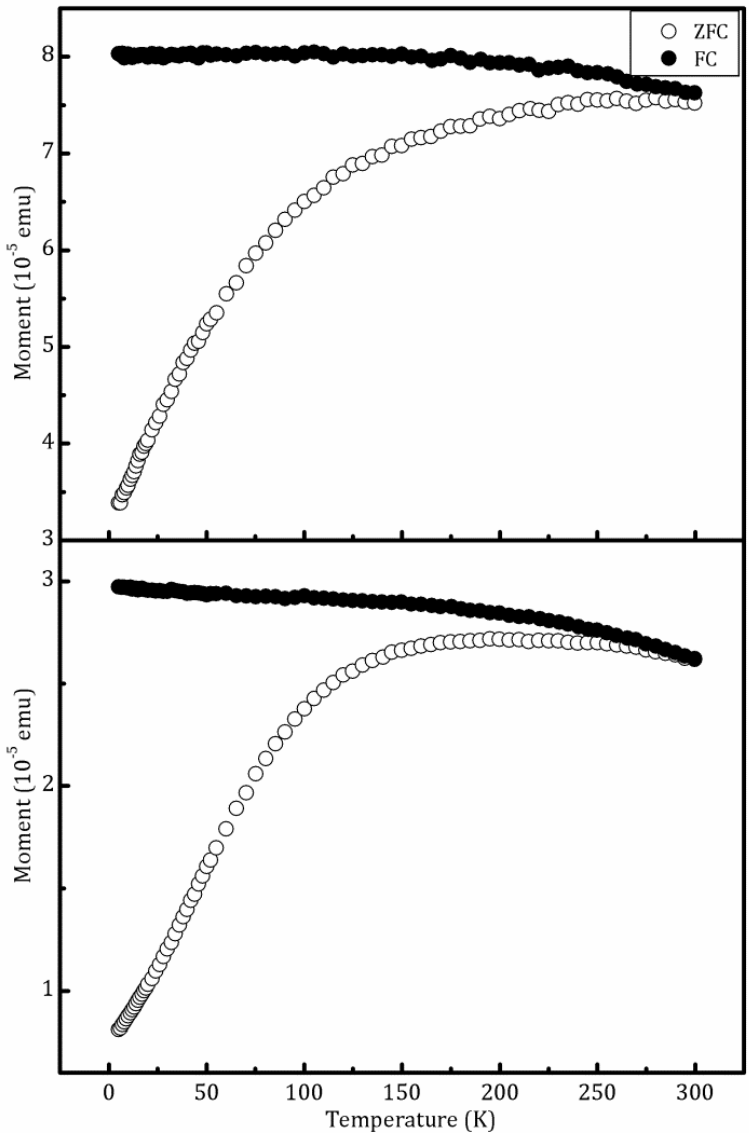

Figure 7.15. ZFC/FC curves at 100 Oe for as cast nanocomposites with 2 and 5 wt% of nanoparticles

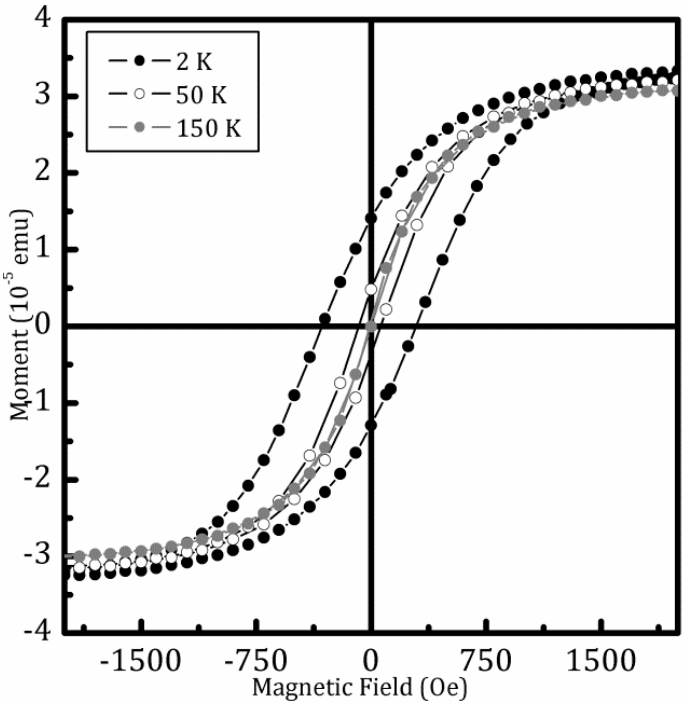

Figure 7.16. M *vs* B curves at 2, 50 and 150 K for the as cast nanocomposite films with 5 wt% of nanoparticles

7.4. CONCLUSIONS

In this chapter it has been demonstrated that *grafting from* technique is an adequate method to modify nanoparticles increasing their compatibility with one of the blocks of a copolymer, selectively dispersing them within desired domains (PMMA ones in this case), obtaining nanostructured hybrid organic/inorganic nanocomposites. Successful grafting of PMMA brushes from the nanoparticle surface with a grafting density of 0.8 chain/nm^2 has been achieved. After analyzing PI-*b*-PMMA copolymer films with different block ratios, subjected to different annealing treatments, the copolymer with f_{PI}= 0.52 and f_{PMMA}= 0.48 has been chosen for preparing nanocomposites films. Functionalization of nanoparticle surfaces by *grafting from* enables a good dispersion of nanoparticles in the polymeric matrix, selectively placing them within PMMA domains. Morphological changes promoted by solvent treatment and nanoparticle addition have also been analyzed. For as cast films nanoparticle addition provokes a

change in the orientation of lamellae at low content, with the formation of some cylinders for the highest content. For solvent-annealed nanocomposites, the nanostructure of neat copolymer is maintained up to 2 wt% of nanoparticles, obtaining disordered morphology for the nanocomposite with the highest nanoparticle content. The selective location of well dispersed nanoparticles within PMMA domains was corroborated removing the organic part of nanocomposites by exposure to UV light irradiation. Moreover, through magnetic measurements the relevant magnetic properties of the nanocomposites were verified, concluding that they were transferred to the nanocomposites from the nanoparticles.

7.5. REFERENCES

Advincula R., Ruehe J., Brittain W. and Caster K., Polymer Brushes. Eds. VCH Wiley, Weinheim, **2004**

Bartholome C., Beyou E., Bourgeat-Lami E., Chaumont P. and Zydowicz N., Nitroxide-Mediated Polymerizations from Silica Nanoparticle Surfaces: "Graft from" Polymerization of Styrene Using a Triethoxysilyl-Terminated Alkoxyamine Initiator. *Macromolecules* **2003**, 36, 7946-7952

Bean C.P. and Livingston J.D., Superparamagnetism. *J. Appl. Phys.* **1959**, 30, S120

Deshmukh R.D., Buxton G.A., Clarke N. and Composto R.J., Nanoscale Block Copolymer Templates Decorated by Nanoparticle Arrays. *Macromolecules* **2007**, *40,* 6316-6324

Esposito L.H., Ramos J.A., Mondragon I. and Kortaberria G., Nanostructured Thermosetting Epoxy Systems Modified with Poly(isoprene-b-methyl metacrylate) Diblock Copolymer and Polyisoprene-Grafted Carbon Nanotubes. *J. Appl. Polym. Sci.* **2013**, Doi: 10.1002/APP.38782

Ferreira P.G., Ajdari A. and Leibler L., Scaling Law for Entropic Effects at Interfaces between Grafted Layers and Polymer Melts *Macromolecules* **1998**, 31, 3994-4003

García I., Tercjak A., Gutierrez J., Rueda L. and Mondragon I., Nanostructuration via Solvent Vapor Exposure of Poly(2-vinyl pyridine-*b*-methyl methacrylate) Nanocomposites Using Modified Magnetic Nanoparticles. *J. Phys. Chem. C* **2008,** *112,* 14343-14347

García I., Zafeiropoulos N.E., Janke A., Tercjak A., Eceiza A., Stamm M. and Mondragon I., Functionalization of Iron Oxide Magnetic Nanoparticles with Poly(methyl methacrylate) Brushes Via Grafting-From Atom Transfer Radical Polymerization. *Journal of Polymer Science: Part A: Polymer Chemistry* **2007**, 45, 925-932

Gutierrez J., Tercjak A., Garcia I. and Mondragon I., The effect of thermal and vapor annealing treatments on the self-assembly of TiO_2/PS-*b*-PMMA nanocomposites generated via the sol-gel process. *Nanotechnology* **2009**, 20, 225603 (9pp)

Hanley K.J., Lodge T.P. and Huang C.-I., Phase Behavior of a Block Copolymer in Solvents of Varying Selectivity. *Macromolecules* **2000**, 33, 5918-5931

Hehn M., Hiller W., Wagner T., Thiel J. and Pasch H., Molar Mass and Microstructure Analysis of PI-*b*-PMMA Copolymers by SEC-NMR. *Macromol. Chem. Phys.* **2012**, 213, 401-410

Huang W.H., Chen P.Y. and Tung S.H., Effects of annealing solvents on the morphology of block copolymer-based supramolecular thin films. *Macromolecules* **2012**, 45, 1562-1569

Iatrou H. and Hadjichristidis N., Synthesis of a model 3-miktoarm star terpolymer. *Macromolecules* **1992**, 25, 4649-4651

Jain P., Dai J., Baker G.L. and Bruening M.L., Rapid Synthesis of Functional Polymer Brushes by Surface-Initiated Atom Transfer Radical Polymerization of an Acidic Monomer. *Macromolecules* **2008**, 41, 8413-8417

Lan Q., Francis L.F. and Bates F.S., Silica Nanoparticle Dispersions in Homopolymer Versus

Block Copolymer. *Journal of Polymer Science: Part B: Polymer Physics* **2007**, 45, 2284-2299

Li H., Gu W., Zhang Y., Russel T.P. and Coughlin E.B., Synthesis of Semicrystalline/Fluorinated Side-Chain Crystalline Block Copolymers and Their Bulk and Thin Film Nanoordering. *Macromolecules* **2013**, 46, 3737-3745

Liu D., Chen Y., Zhang N. and He X., Controlled Grafting of Polymer Brushes on Poly(vinylidene fluoride) Films by Surface-Initiated Atom Transfer Radical Polymerization. *Journal of Applied Polymer Science* **2006**, 101, 3704-3712

Lo C.-T., Lee B., Pol V.G., Dietz Rago N.L., Seifert S., Winans R.E. and Thiyagarajan P., Effect of Molecular Properties of Block Copolymers and Nanoparticles on the Morphology of Self-Assembled Bulk Nanocomposites. *Macromolecules* **2007**, 40, 8302-8310

Lopes S.I.C., Gonçalves da Silva A.M.P.S., Brogueira P., Piçarra S. and Martinho J.M.G., Interfacial Behavior of Poly(isoprene-*b*-methyl methacrylate) Diblock Copolymers and their Blends with Polystyrene at the Air-Water Interface. *Langmuir* **2007**, 23, 9310-9319

Martin T.M. and Young D.M., Correlation of the glass transition temperature of plasticized PVC using a lattice fluid model. *Polymer* **2003**, 44, 4747-4754

Marutani E., Yamamoto S., Ninjbadgar T., Tjii Y., Fukuda T. and Takano M., Surface-initiated atom transfer radical polymerization of methyl methacrylate on magnetite nanoparticles. *Polymer* **2004**, 45, 2231-2235

Ohno K., Morinaga T., Koh K., Tsujii Y. and Fukuda T., Synthesis of Monodisperse Silica Particles Coated with Well-Defined, High-Density Polymer Brushes by Surface-Initiated Atom Transfer Radical Polymerization. *Macromolecules* **2005**, 38, 2137-2142

Park S., Kim B., Xu J., Hofmann T., Ocko B.M. and Russell T.P., Lateral ordering of cylindrical microdomains under solvent vapor. *Macromolecules* **2009**, 42, 1278-1284

Peng J., Knoll W., Park C. and Kim D.H., Two-Dimensional Arrays of Strings of TiO_2 Nanoparticles via Cooperative Block Copolymer Self-Assembly. *Chem. Mater.* **2008**, 20, 1200-1202

Porto L.C., Aissou K., Giacomelli C., Baron T., Rochas C., Pignot-Paintrand I., Armes S.P., Lewis A.L., Soldi V. and Borsali R., Nanostructured Films Made from Zwitterionic Phosphorylcholine Diblock Copolymer Systems. *Macromolecules* **2011**, 44, 2240-2244

Qin S., Qin D., Ford W.T., Resasco D.E. and Herrera J.E., Polymer Brushes on Single-Walled Carbon Nanotubes by Atom Transfer Radical Polymerization of n-Butyl Methacrylate. *J. Am. Chem. Soc*. **2004**, 126, 170-176

Schatz C. and Lecommandoux S., Polysaccharide-containing block copolymers: synthesis, properties and applications of an emerging family of glycoconjugates. *Macromol Rapid Commun* **2010**, 31, 1664-1684

Schillén K., Yekta A., Ni S., Farinha J.P.S. and Winnik M.A., Characterization of Polyisoprene-*b*-Poly(methyl methacrylate) Diblock Copolymer Micelles in Acetonitrile. *J. Phys. Chem. B* **1999**, *103,* 9090-9103

Schulz L., Schirmacher W, Omran A., Shah V.R., Böni P., Petry W. and Müller-Buschbaum P., Elastic torsion effects in magnetic nanoparticle diblock-copolymer structures. *J. Phys.: Condens. Matter* **2010**, 22, 346008 (6pp)

Shanmugharaj A.M., Choi W.S. and Ryu S.H., Synthesis of Well-Defined Polymer Brushes on the Surface of Zinc Antimonate Nanoparticles Through Surface-Initiated Atom Transfer Radical Polymerization. *J Polym Sci Part A: Polym Chem* **2010**, 48, 5092-5099

Sun X.-Y., Yu S.-S., Wan J.-Q. and Chen K.-Z., Facile graft of poly(2-methacryloyloxyethyl phosphorylcholine) onto Fe_3O_4 nanoparticles by ATRP: Synthesis, properties, and biocompatibility. *J Biomed Mater Res Part A* **2013**, 101A, 607-612

Tcherkasskaya O., Ni S. and Winnik M.A., Energy Transfer Studies of Binary Block Copolymer Blends. 1. Effect of Composition on the Interface Area per Chain and the Lamellar Size. *Macromolecules* **1997**, 30, 2623-2632

Wang J. and Matyjaszewski K., Controlled/"Living" Radical Polymerization. Halogen Atom Transfer Radical Polymerization Promoted by a Cu(I)/Cu(II) Redox Process. *Macromolecules* **1995**, 28, 7901-7910

Xu C., Ohno K., Ladmiral V. and Composto R.J., Dispersion of polymer grafted magnetic nanoparticles in homopolymers and block copolymers. *Polymer* **2008**, 49, 3568-3577

Xu C., Ohno K., Ladmiral V., Milkie D.E., Kikkawa J.M. and Composto R.J., Simultaneous Block Copolymer and Magnetic Nanoparticle Assembly in Nanocomposite Films. *Macromolecules* **2009**, 42, 1219-1228

Ye P., Dong H., Zhong M. and Matyjaszewski K., Synthesis of Binary Polymer Brushes via Two-Step Reverse Atom Transfer Radical Polymerization. *Macromolecules* **2011**, 44, 2253-2260

Yoo M., Kim S., Jang S.G., Choi S.-H., Yang H., Kramer E.J., Lee W.B., Kim B.J. and Bang J., Controlling the Orientation of Block Copolymer Thin Films using Thermally-Stable Gold Nanoparticles with Tuned Surface Chemistry. *Macromolecules* **2011**, 44, 9356-9365

Zeng H., Black C.T., Sandstrom R.L., Rice P.M., Murray C.B. and Sun S., Magnetotransport of magnetite nanoparticle arrays. *Physical Reviw B* **2006**, 73, 020402(R)

Zhao Y., Saijo K., Takenaka M., Koizumi S. and Hashimoto T., Order-Disorder Transition of Nanocomposites: Pd Nanoparticles in Polystyrene-*block*-Polyisoprene Microdomain Templates. *Macromolecules* **2009**, 42, 5272-5277

Litina K., Miriouni A., Gournis D., Karakassides M.A., Georgiou N., Klontzas E., Ntoukas E. and Avgeropoulos A., Nanocomposites of polystyrene-b-polyisoprene copolymer with layered silicates and carbon nanotubes. *European Polymer Journal* **2006**, 42, 2098-2107

Porto L.C., Aissou K., Giacomelli C., Baron T., Rochas C., Pignot-Paintrand I., Armes S.P., Lewis A.L., Soldi V. and Borsali R., Nanostructured Films Made from Zwitterionic Phosphorylcholine Diblock Copolymer Systems. *Macromolecules* **2011**, 44, 2240-2244

Li H., Gu W., Li L., Zhang Y., Russell T.P. and Coughlin E.B., Synthesis of Semicrystalline/Fluorinated Side-Chain Crystalline Block Copolymers and Their Bulk and Thin Film Nanoordering. *Macromolecules* **2013**, 46, 3737-3745

Chapter 8

CONCLUSIONS, FUTURE WORK AND PUBLICATIONS

8.1. GENERAL CONCLUSIONS

The main conclusions that can be extracted from the investigation work carried out in this thesis are summarized below.

Maghemite nanoparticles have been successfully functionalized with different polymer brushes by different grafting methods. First, PMMA-*b*-PCL copolymer brushes have been anchored to nanoparticle surface by *grafting to* method; then nanoparticle surface have been modified with PS and PMMA brushes by *grafting through* method; and finally, nanoparticles have been functionalized with PMMA brushes by *grafting from* method. Three methods have demonstrated their validity for nanoparticle functionalization, but some differences among them have been found.

By *grafting to* method low grafting density values have been obtained. Due to this low grafting density, nanoparticles have been mainly placed at the interfaces between different nanodomains of the copolymer nanostructure. In addition, nanoparticles tended to form small aggregates during modification. However, a good dispersion of nanoparticles has been obtained.

One of the inconveniences of *grafting through* method is the impossibility to calculate the grafting density because the cleavage of brushes is not possible. However, it has demonstrated to be an effective method to functionalize nanoparticles with both PS and PMMA brushes. Even if small aggregates of nanoparticles have been formed during dispersion into block copolymer nanostructures, good dispersions have been obtained. Moreover, nanoparticles have been selectively placed into the desired block copolymer domains.

By *grafting from* method nanoparticles have been successfully modified with PMMA brushes. This method enables to calculate the grafting density, as single

polymer chains, grown from nanoparticle surface, can be cleavaged. Considerably higher grafting density values have been obtained when compared with *grafting to* method. Polymerization conditions have been selected for obtaining short polymer chains, facilitating their selective placement at PMMA domains.

Different copolymer matrixes have been used along this work. This fact has given the opportunity to analyze different methods for their nanostructuring, with the obtainment of different nanostructures that can be customized by varying conditions and/or solvents. In this way, for copolymers with high incompatibility among blocks (i.e. PI-*b*-PMMA), as cast method has been enough to obtain lamellar morphology, without further treatments. On the other hand, both thermal and solvent vapor annealing have been successfully used to obtain nanostructured block copolymers. In this way, lamellar morphology was obtained by thermal annealing of PS-*b*-PCL block copolymer. SVA treatment was used to nanostructure PS-*b*-P4VP copolymer, obtaining hexagonally packed morphology with exposure to dioxane vapors (selective for PS block) that evolved to stripped morphology with longer exposure. PS-*b*-PMMA copolymer was also nanostructured by exposing to acetone vapor (selective for PMMA block) obtaining a lamellar morphology. The same PMMA-selective solvent was used to evolve PI-*b*-PMMA copolymer from lamellar to hexagonally packed nanostructure. In the case of ABC-type SBM triblock copolymer lamellar morphology was obtained by casting, without further treatment.

When nanoparticles were added to BCP for nanocomposite generation, it has been observed that they can provoke morphological changes, especially if they are selectively placed in one of the domains. Nanoparticle placement in a copolymer domain provokes its swollen; causing a change in volume ratio among blocks that constitute the BCP, which can lead to a morphological change. Nanoparticle addition can also affect the interaction among blocks, and that between BCP and

substrate, promoting morphology changes or even changes in the nanostructure orientation.

Finally, it has been probed that magnetic properties of nanoparticles have been successfully transferred to nanocomposites even after nanoparticle modification with polymer brushes. Nanocomposites have shown the superparamagnetic behavior of nanoparticles, appearing as suitable for the aforementioned potential applications.

8.2. FUTURE WORK

To continue with this research work, the following future research lines can be proposed:

- Preparation and characterization of nanocomposites in the same way with other kind of nanoparticles that will confer other properties such as electric conductivity to the nanocomposites

- The use of magnetic fields to orient block copolymer domains in which nanoparticles are placed, by using the magnetic properties of nanoparticles.

- Preparation of nanostructured thermosetting systems with magnetic properties by modifying an epoxy matrix with BCP and dispersing functionalized magnetic nanoparticles.

8.3. PUBLICATIONS AND CONFERENCES

The work carried out along this thesis has originated the following papers and contributions to scientific conferences.

8.3.1. PUBLICATIONS

Barandiaran I., Katsigiannopoulos D., Grana E., Avgeropoulos A., Eceiza A. and Kortaberria G., PI-*b*-PMMA diblock copolymers: nanostructure development in thin films and nanostructuring of thermosetting epoxy system. *Colloid and Polymer Science* **2013**, 291, 2173-2180

Barandiaran I., Cappelletti A., Strumia M., Eceiza A. and Kortaberria G., Generation of nanocomposites based on (PMMA-*b*-PCL)-grafted Fe_2O_3 nanoparticles and PS-*b*-PCL block copolymer. *European Polymer Journal* **2014**, 58, 226-232

Barandiaran I. and Kortaberria G., Selective placement of magnetic Fe_3O_4 nanoparticles into the lamellar nanostructure of PS-*b*-PMMA diblock copolymer. *European Polymer Journal* **2015**, 68, 57-67

Barandiaran I. and Kortaberria G., Synthesis and characterization of nanostructured PS-*b*-P4VP/Fe_2O_3 thin films with magnetic properties prepared by solvent vapor annealing. *RSC Advances* **2015**, 5, 95840-95846

Barandiaran I., Grana E., Katsigiannopoulos D., Avgeropoulos A. and Kortaberria G., Nanocomposites based on nanostructured PI-*b*-PMMA copolymer and selectively placed PMMA-modified magnetic nanoparticles: Morphological and magnetic characterization. *European Polymer Journal* **2016**, 75, 514-524

Barandiaran I. and Kortaberria G., Hybrid organic/inorganic nanocomposites with magnetic properties based on nanostructured SBM triblock copolymer and selectively placed magnetic nanoparticles. *European Polymer Journal*, *Under revision*

Posocco P., Mohammed Y., **Barandiaran I.**, Laurini E., Sweyer M., Baldini G., Fermeglia M., Galder Kortaberria G. and Pricl S., Combined mesoscale/experimental study of selective placement of magnetic nanoparticles in diblock copolymer films via solvent vapour annealing. *The Journal of Physical Chemistry, Part C, Under revision*

8.3.2. CONFERENCES

Barandiaran I, Eceiza A. and Kortaberria G., PI-*b*-PMMA diblock copolymers: Nanostructure development in thin films and nanostructuring of epoxy thermosetting systems. **Poster**, ImagineNano 2013, Bilbao (Spain), 04/2013

Barandiaran I., Cappelletti A., Strumia M. and Kortaberria G., Fe_2O_3 magnetic nanoparticle modification with PMMA-*b*-PCL copolymer, and nanoparticle dispersion into PS-*b*-PCL block copolymer. **Poster,** NanoPortugal 2014, Porto (Portugal), 02/2014

Barandiaran I., Cappelletti A., Strumia M. and Kortaberria G., PS-*b*-PCL blokezko kopolimeroan eta Fe_2O_3 nanopartikuletan oinarrituriko nanokonpositeen prestaketa eta karakterizazioa. **Oral comunication**, II Materialen Zientzia eta Teknologia Kongresua, Donostia (Spain), 07/2014

Barandiaran I., Cappelletti A., Strumia M. and Kortaberria G., Generation of nanocomposites based on block copolymer and Fe_2O_3 nanoparticles modified by grafting to method with PMMA-*b*-PCL copolymer. **Oral communication**, International Conference on Modification, Degradation and Stabilization of Polymers, Portoroz (Slovenia), 09/2014

Posocco P., Mohammed Y., **Barandiaran I.**, Laurini E., Sweyer M., Baldini G., Fermeglia M., Galder Kortaberria G. and Pricl S., Thinking small is not easy: an attempt to disperse magnetic nanoparticles in lamellar PS-*b*-PMMA block copolymer. **Poster**, EUROFILLER 2015, Montpellier (France), 04/2015

Barandiaran I. and Kortaberria G., Selective placement of surface-modified magnetic nanoparticles on nanostructures generated by self-assemblyof a PS-*b*-PMMA diblock copolymer. **Oral communication**, 2nd International Conference on Chemical and Environmental Sciences, Istanbul (Tukey), 05/2015

Kortaberria G. and **Barandiaran I.**, Nanocomposites Based on Block Copolymer Templates and Nanoparticles with Polymeric Brushes. **Oral communication**, The 31st International Conference of the POLYMER PROCESSING SOCIETY, Jeju (Republic of Korea), 06/2015

Barandiaran I. and Kortaberria G., PI-*b*-PMMA and iron oxide nanoparticle based nanocomposite preparation and morphological changes. **Poster**, 12th

International Conference on Materials Chemistry, York (United Kingdom), 07/2015

Barandiaran I. and Kortaberria G., Selective placement of magnetic Fe_2O_3 nanoparticles into the lamellar nanostructure of PS-*b*-PMMA diblock copolymer. **Oral communication**, 1st French-Spanish Joint Congress for Young Researchers in Polymers, Donostia (Spain), 09/2015

Posocco P., Mohammed Y., **Barandiaran I.**, Laurini E., Sweyer M., Baldini G., Fermeglia M., Galder Kortaberria G. and Pricl S. Still looking for the magic spot: dispersing modified nanoparticles into lamellar PS-b-PMMA diblock copolymer by vapor solvent annealing. **Poster**, 15th Aiche Conference, Salt Lake City (USA), 11/2015

Barandiaran I. and Kortaberria G., Selective placement of magnetic nanoparticles on nanostructures generated by self-assembly of PS-b-PMMA diblock copolymer. Magnetic characterization. **Poster**, 14th Pacific Polymer Conference, Kauai, Hawaii (USA), 12/2015

Appendix

1. LIST OF SCHEMES

2. LIST OF TABLES

3. LIST OF FIGURES

4. LIST OF EQUATIONS

Equation 2.1

$$\chi \approx 0.34 + \frac{V}{RT}(\delta_P - \delta_S)^2$$

Equation 2.2

$$\delta = \sqrt{\frac{E_{coh}}{V}} = \sqrt{\frac{\Delta H_V - RT}{V}}$$

Equation 2.3

$$\tau = \tau_0 exp\left(\frac{K_{eff}V}{k_B T}\right)$$

Equation 4.1

$$silane(mol/m^2) = \frac{\frac{\Delta m_{120-750}}{100 - \Delta m_{120-750}} \cdot 100 - \Delta m_{OH120-750}}{PM_{MPTS} \cdot SSA \cdot 100}$$

5. LIST OF ABBREVIATIONS

^{57}Fe	Iron 57 isotope
AB	Linear diblock copolymer composed with A and B blocks
ABA	Linear triblock copolymer composed with A and B blocks
ABC	Linear triblock copolymer composed with A, B and C blocks
AFM	Atomic force microscopy
Ag	Silver
AIBN	2,2'-azobisisobutyronitrile
APTS	3-aminopropyl tryethoxysilane
ATRP	Atom transfer radical polymerization
Au	Gold
B	Applied magnetic field
$BaTiO_3$	Barium titanate
BBCP	Brush block copolymer
BCC	Body centered cubic
BCP	Block copolymer
Bi	Bismuth
Bip	Bipyridine
BSM	Polybutadiene-*block*-polystyrene-*block*-poly(methyl methacrylate)
BSV	Polybutadiene-*block*-polystyrene-*block*-poly(2-vinylpyridine)
CaH_2	Calcium hydride
CdSe	Cadmium selenide

***Cl*-PMMA-*b*-PCL**	Poly(methyl methacrylate)-*block*-poly(ε-caprolactone) with terminal chlorine group
CM	Contact mode
Co	Cobalt
$CoPt_3$	Cobalt platinum
CRP	Controlled radical polymerization
CTCS	2-(4-chlorosulfonylphenyl) ethyl trichlorosilane
CuBr	Copper (I) bromide
$CuBr_2$	Copper (II) bromide
DC	Direct current
DCM	Dichloromethane
DMF	Dimethylformamide
DSC	Differential scanning calorimetry
FC	Field-cooled
Fe	Iron
Fe^{2+}	Divalent iron
Fe^{3+}	Trivalent iron
FeO	Wüstite
FePt	Iron platinum
FTIR	Fourier transform infrared spectroscopy
GPC	Gel permeation chromatography
HF	Hydrogen fluoride
In	Indium

JCPDS	Joint Committee on Powder Diffraction Standards
MNP	Magnetic nanoparticles
mPEO-SH	Thiol-ended poly(ethylene glycol) methyl ether
MPTS	3-methacryloxypropyl trimethoxysilane
MRI	Magnetic resonance imagining
MWCNT	Multi-walled carbon nanotube
N_2	Nitrogen
***n*-BuLi**	*n*-butyllithium
NMP	Nitroxide-mediated polymerization
NP	Nanoparticles
ODT	Order disorder transition
OFETs	Organic field-effect transistors
-OH	Hydroxyl group
P(PEGMA)-*co*-PNIPAAm	Poly(ethylene glycol) monomethacrylate and N-isopropylacrylamide monomer
P2VP-*b*-PMMA	Poly(2-vinyl pyridine)-*block*-poly(methyl methacrylate)
P4VP	Poly(4-vinyl pyridine)
PAA	Poly(acrylic acid)
PAA-*b*-PEDOT	Poly(acrylic acid)-*block*-poly(3,4-ethylenedioxythiophene)
Pb	Lead
PbTe	Lead telluride
PCA	Poly(carboxylic acid)
PCL	Poly(ε-caprolactone)

PEDOT	Poly(3,4-ethylenedioxythiophene)
PEGMA	Poly(ethylene glycol) monomethacrylate
PEO	Poly(ethylene oxide)
PEP-*b*-PEO-*b*-PHMA	Poly(ethylene-*alt*-propylene-*block*-ethylene oxide-*block*-*n*-hexyl methacrylate)
PI	Polyisoprene
PI-*b*-PMMA	Polyisoprene-*block*-poly(methyl methacrylate)
PMMA	Poly(methyl methacrylate)
PMMA-*b*-PS	Poly(methyl methacrylate)-*block*-polystyrene
P*n*BA	Poly(*n*-butyl acrylate)
POSS	Polyhedral oligomeric silsesquioxane
PPE	Poly(2,6-dimethyl-1,4-phenylene ether)
PPMS	Physical properties measurement system
PS	Polystyrene
PS-*b*-P2VP	Polystyrene-*block*-poly(2-vinyl pyridine)
PS-*b*-P4VP	Polystyrene-*block*-poly(4-vinyl pyridine)
PS-*b*-PAA	Polystyrene-*block*-poly(acrylic acid)
PS-*b*-PCL	Polystyrene-*block*-poly(ε-caprolactone)
PS-*b*-PEO	Polystyrene-*block*-poly(ethylene oxide)
PS-*b*-PLLA	Polystyrene-*block*-poly(*L*-lactide)
PS-*b*-PMMA	Polystyrene-*block*-poly(methyl methacrylate)
PS-*b*-PNIPAM	Polystyrene-*block*-poly(N-isopropylacrylamide)
PS-*b*-QP4VP	PS-*block*-quaternized P4VP

RAFT	Reversible addition-fragmentation chain transfer
RF	Radio frecuency
RIPS	Reaction induced phase separation
SAN	Polystyrene-*co*-polyacrylonitrile
SAXS	Small angle X-ray scattering
SBM	Polystyrene-*block*-polybutadiene-*block*-poly(methyl methacrylate)
SBS	Polystyrene-*block*-polybutadiene-*block*-polystyrene
SBT	Polystyrene-*block*-polybutadiene-*block*-poly(*tert*-butyl methacrylate)
SBV	Polystyrene-*block*-polybutadiene-*block*-poly(2-vinyl pyridine)
SEBM	Polystyrene-*block*-poly(ethylene-*co*-butylene)-*block*-poly(methyl methacrylate)
***sec*-BuLi**	*sec*-butyl lithium
SEC-NMR	Size exclusion chromatography-nuclear magnetic resonance
SFM	Scaning force microscopy
Si	Silicon
SIS	Polystyrene-*block*-polyisoprene-*block*-polystyrene
Sn	Tin
SQUID	Superconducting quantum interference device
SSA	Specific surface area
SVA	Solvent vapor annealing
SWCNT	Single-walled carbon nanotube
TEM	Transmission electron microscopy

TGA	Thermogravimetric analysis
THF	Tetrahydrofuran
TiO_2	Titanium dioxide
TM	Tapping mode
UV	Ultra violet
VSM	Vibrating sample magnetometer
XRD	X-ray diffraction
ZFC	Zero-field-cooled
ISO	Polyisoprene-*block*-polystyrene-*block*-poly(ethylene oxide)
He	Helium
Fe_2O_3-*g*-(PMMA-*b*-PCL)	PMMA-*b*-PCL grafted iron oxide nanoparticles
α-Fe_2O_3	Hematite
β-Fe_2O_3	β-phase iron oxide
γ-Fe_2O_3	Maghemite
ε-Fe_2O_3	ε-phase iron oxide
$CoFe_2O_4$	Cobalt ferrite
$MgFe_2O_4$	Magnesium ferrite
$MnFe_2O_4$	Manganese ferrite
Fe_3O_4	Magnetite
1D	One dimension
2D	Two dimensions
3D	Three dimensions

6. LIST OF SYMBOLS

$\mathbf{A}$	Exchange constant
$\mathbf{D_c}$	Diameter of spherical particle
$\mathbf{E}$	Magnetic anisotropy energy per particle
$\mathbf{E_{coh}}$	Cohesive energy
$\mathbf{E_{dw}}$	Domain-wall energy
$\boldsymbol{f}$	Copolymer composition
$\boldsymbol{f}_{\mathbf{PCL}}$	Poly(ε-caprolactone) fraction
$\boldsymbol{f}_{\mathbf{PMMA}}$	Poly(methyl methacrylate) fraction
$\boldsymbol{f}_{\mathbf{PS}}$	Polystyrene fraction
$\mathbf{H_C}$	Coercivity
$\mathbf{k_B}$	Boltzmann's constant
$\mathbf{K_{eff}}$	Anisotropy constant
$\boldsymbol{l}$	Thickness of lamellar domains
$\mathbf{M}$	Magnetic moment
$\mathbf{M_n}$	Number average molecular weight
$\mathbf{M_R}$	Remanence
$\mathbf{M_s}$	Saturation magnetization
$\mathbf{M_w}$	Weight average molecular weight
$\boldsymbol{N}$	Polymerization degree
$\mathbf{PM_{MPTS}}$	Molecular weight of MPTS
$\mathbf{T}$	Temperature

$\mathbf{T_B}$	Blocking temperature
$\mathbf{T_g}$	Glass transition temperature
$\mathbf{V}$	Volume
$\boldsymbol{\delta}$	Solubility parameter
$\mathbf{\Delta E_{MS}}$	Magnetostatic energy
$\mathbf{\Delta Hv}$	Vaporization enthalpy
$\mathbf{\Delta m_{120\text{-}750}}$	Weight loss between 120 and 750 °C
$\mathbf{\Delta m_{OH120\text{-}750}}$	Weight loss between 120 and 750 °C of the pristine nanoparticles
$\boldsymbol{\theta}$	Angle between axis
$\boldsymbol{\mu_0}$	Vacuum permeability
$\boldsymbol{\tau}$	Relaxation time
$\boldsymbol{\chi}$	Flory Huggins interaction parameter
$\boldsymbol{\chi_{P4VP}}$	Flory Huggins interaction parameter of P4VP
$\boldsymbol{\chi_{PI}}$	Flory-Huggins interaction parameter of PI
$\boldsymbol{\chi_{PMMA}}$	Flory Huggins interaction parameter of PMMA
$\boldsymbol{\chi_{PMMA/PB}}$	Flory Huggins interaction parameter between PMMA and PB
$\boldsymbol{\chi_{PMMA/PS}}$	Flory Huggins interaction parameter between PMMA and PS
$\boldsymbol{\chi_{PS}}$	Flory Huggins interaction parameter of PS
$\boldsymbol{\chi_{PS/PB}}$	Flory Huggins interaction parameter between PS and PB